ISBN 978-82-326-1444-8 (printed version)
ISBN 978-82-326-1445-5 (electronic version)
ISSN 1503-8181

NTNU
Norwegian University of
Science and Technology

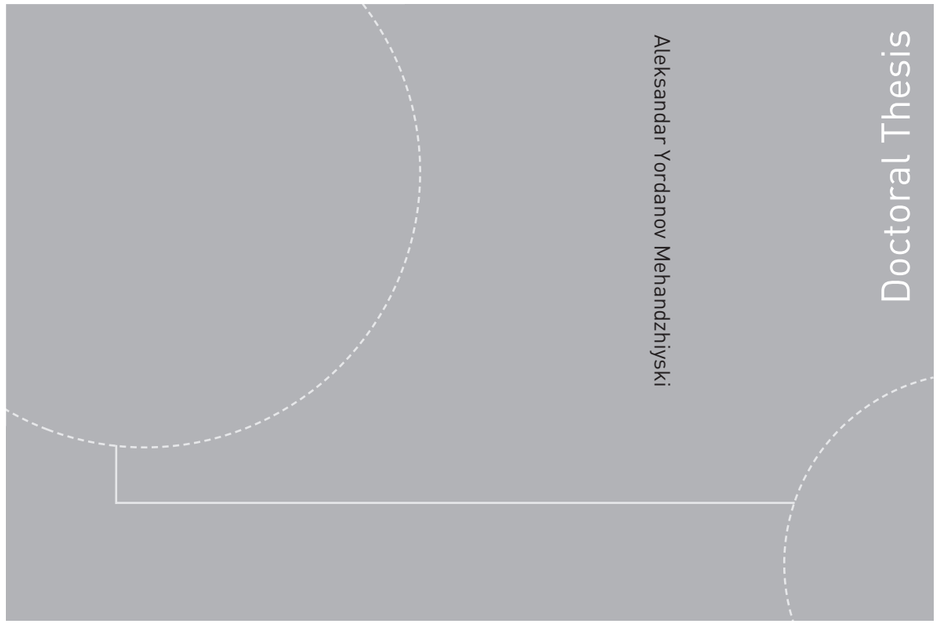

Doctoral theses at NTNU, 2016:53

Aleksandar Yordanov Mehandzhiyski

Multiscale Modelling of the Calcium Naphthenate Precipitation Reaction in Petroleum Processing

Doctoral theses at NTNU, 2016:53

NTNU

NTNU
Norwegian University of
Science and Technology
Faculty of Natural
Sciences and Technology
Department of Chemical Engineering

NTNU
Norwegian University of
Science and Technology

Aleksandar Yordanov Mehandzhiyski

Multiscale Modelling of the Calcium Naphthenate Precipitation Reaction in Petroleum Processing

Thesis for the degree of Philosophiae Doctor

Trondheim, March 2016

Norwegian University of Science and Technology
Faculty of Natural
Sciences and Technology
Department of Chemical Engineering

NTNU
Norwegian University of
Science and Technology

NTNU
Norwegian University of Science and Technology

Thesis for the degree of Philosophiae Doctor

Faculty of Natural
Sciences and Technology
Department of Chemical Engineering

ISBN 978-82-326-1444-8 (printed version)
ISBN 978-82-326-1445-5 (electronic version)
ISSN 1503-8181

Doctoral theses at NTNU, 2016:53

Printed by Skipnes Kommunikasjon as

Preface

This thesis is submitted in partial fulfilment of the requirements for the degree of Philosophiae Doctor (Ph.D.) at the Norwegian University of Science and Technology (NTNU) and consists of four papers. The work was carried out in the chemical engineering department of NTNU, supervised by associate professor Brian A. Grimes and co-supervised by associate professor Titus S. van Erp from the department of chemistry at NTNU. The project has been funded by the research Council of Norway and the Faculty of Natural Science and Technology of NTNU as part of the project *From Molecules to Process Applications*.

I have completed my Master of Science in chemistry with specialization in Computational Chemistry in Sofia University in October 2012. I have been accepted as a Ph.D. candidate in the chemical engineering department in January 2013.

Acknowledgement

I would like to acknowledge the following people without the completion of this thesis would not be possible.

First of all I would like to express my deepest gratitude to my supervisor associate professor Brian Grimes for giving me the opportunity to participate in this interesting project. Thank you for your patience and absolutely professional guidance throughout the whole project!

I would like to thank my co-supervisor associate professor Titus van Erp for having an active role in my project and always available for fruitful discussions.

I am very thankful to Dr. Enrico Riccardi for having many interesting discussions concerning my project and also giving me very helpful tips about programming.

I also am very grateful to all the great people here in K5 and PFI for the nice working atmosphere and very interesting discussions during our lunch breaks. Thank you Thomas, Birgitte, Jens, Meysam, Sebastian, Diego, Albert, Bartek, Camilla, Bicheng and many more who joined the lab later on.

Last but certainly not least, I want to thank my beloved Veselina for always being there for me when I needed her the most and sharing the whole experience here with me. I love you!

Abstract

The formation of calcium naphthenate precipitates occurring in the petroleum industry is both an undesirable side reaction and can introduce costly shutdowns and cleaning processes. Although the reaction has been studied by experimental techniques, the exact mechanism of reaction and precipitation is still under debate.

In the present work, we apply a multiscale approach to study the formation of calcium naphthenate precipitates. To systematically study this otherwise complex reaction influenced by many factors, we first have applied density functional theory (DFT) calculations on the interaction energies between carboxylate anion(s) and calcium and sodium cations. The influence of the multibody effects have been determined by DFT and their impact on the commonly used OPLS-AA force field is assessed. It has also been indicated that the calcium ion can coordinate up to four carboxylate molecules. The lowest interaction energy has been reached when calcium interacts with 3 carboxylates. A comparison between DFT and OPLS-AA shows satisfactory representation of the carboxylate - calcium interactions by the force field, which has been further used to study the calcium naphthenate precipitation reaction.

The calcium naphthenate reaction has been shown to be very selective and calcium is the most abundant cation in the precipitates amongst all the divalent cations. To address this observation *ab initio* molecular dynamics simulations have been performed to understand the basic mechanism of the carboxylate - metal ion dissociation in water. By thermodynamic integration we have evaluated the free energy of interaction between propanoate anion and the divalent Mg^{2+}, Ca^{2+}, Sr^{2+} and Ba^{2+} cations. This study revealed that the strongest interactions of the carboxylate anion are with magnesium followed by calcium, strontium and barium, which partially explains the selectivity. However, magnesium shows also the strongest interactions with the solvent molecules, which has affected their dynamics. The dynamics of the solvent molecules together with the self-diffusion of the divalent ions infer that calcium most likely will bind with the carboxylate rather than magnesium.

The preferred binding with calcium has been further complimented by calculating the probability for reaction between two carboxylates and one divalent metal cation as a function of the distance separating the carboxylates. That has been achieved by performing molecular dynamics (MD) simulations together with umbrella sampling. The probability of reaction has been finally used as a constituent function in the method development for recreating the interfacial density of tetracarboxylic acid (TA) molecules to calcium naphthenate precipitation. This method involves MD simulations of TA molecules at an oil-water interface for obtaining

different probability distributions from the simulation trajectories describing their molecular orientation and structuring. Then the MD simulated probabilities are used to recreate the interfacial density in a coarse-grain manner from which we have determined the fractional conversion of TA molecules to calcium naphthenate precipitation as a function of the interfacial concentration ($f_p(\Gamma_{TA})$). The $f_p(\Gamma_{TA})$ is shown to increase non linearly with the increase of interfacial concentration.

Contents

List of Tables

List of Figures

List of Symbols

a_0, a_x, a_c - empirically fitted parameters

a - acceleration

A - interfacial area

$\triangle$ *A* - Helmholtz free energy

AIMD - *Ab initio* Molecular Dynamics

BOMD - Born-Oppenheimer Molecular Dynamics

D - self-diffusion coefficient

DFT - Density Functional Theory

$E_0[\rho]$ - ground state energy as a function of the density

$E_{xc}[\rho]$ - exchange-correlation energy

$E_{xc}^{LDA}[\rho]$ - exchange-correlation energy in the local density approximation

$E_{Ne}[\rho]$ - nuclear-electron interaction energy

$E_{xc}^{GGA}[\rho]$ - exchange-correlation energy in the generalized gradient approximation

E_{xc}^{hyb} - hybrid exchange-correlation energy

$E(r)_{inter}$ - total interaction energy

$E(r)_{pair-inter}$ - pair-interaction energy

$E(r)_{complex}$ - energy of the carboxylate-ion complex

$E(r)_{ion}$ - energy of an ion

$E(r)_{acid}$ - energy of a carboxylic acid

$E_N(r)$ - energy of the system in absence of a metal ion

$\triangle E$ - successive water binding energy

$E\{M(H_2O_n^{2+})\}$ - energy of a metal ion - water complex

E_{H_2O} - energy of a water molecule

$f_p(\Gamma_{TA})$ - fractional conversion of tetra-carboxylic acids to calcium naphthenate precipitates as a function of the interfacial concentration of tetra acids

$F[\rho]$ - functional

F - force

F_j - free energy

H_e - electronic Hamiltonian

$J[\rho]$ - Coulomb potential

k_i - force constant

k_b - Boltzmann constant

$l_i, l_{i,0}$ - bond length and equilibrium bond length

m - mass

M_I - nuclear mass

MD - Molecular Dynamics

n - periodicity constant for torsion angle potential

N - number of particles

N_w - number of windows

N_{TA} - number of TA molecules

$\langle N_{cl}(\Gamma_{TA})\rangle$ - average cross-linked sites

n_i, n_j - simulation window

$P(\xi)_{un}$ - unbiased probability distribution

$p(\xi)_i^{bias}$ - biased probability distribution

q - charge

$Q(N, V, T, \lambda)$ - partition function

r - position

$\ddot{R}_I(t)$ - second derivative of the coordinates of the nuclei with respect to time

$T[\rho]$ - kinetic energy of electrons

$T_s[\rho]$ - Kohn-Sham kinetic energy

t - time

T - temperature

U - potential energy

u - mobility coefficient

$V_{ext}(r)$ - external potential

$V_{ee}[\rho]$ - electron-electron interaction potential

$V_{xc}(r)$ - potential due to the exchange-correlation energy

V_n - torsion angle force constant

v - velocity

$V_L^{n,m}$ - arm vector length

$X_{COO^-}^{n,m}, Y_{COO^-}^{n,m}$ - xy-position of the COO^- group of the mth arm of the nth TA molecule

X_{cn}^n, Y_{cn}^n - xy-position of the molecule center

$Z_{COO^-}^{n,m}$ - z-position of the COO^- group of the mth arm of the nth TA molecule

Z_{cn}^n - z-position of the molecular center

Z_A - nuclear charge

Greek letters

β - inverse temperature

γ - phase shift angle

Γ_{TA} - interfacial concentration of tetra-carboxylic acid molecules

$\gamma^{n,m}$ - horizontal orientation angle of the arms

Γ_{max} - maximum interfacial concentration

ϵ_0 - vacuum permittivity constant

ϵ_{xc} - exchange-correlation energy per particle of an uniform electron gas

ϵ_{ij} - energy minimum of the potential well in the Lennard-Jones potential

$\Theta_i, \Theta_{i,0}$ - valence angle and equilibrium valence angle

$\Theta^{n,m}$ - vertical orientation angle of the TA molecule arm

λ - coupling parameter

Λ - thermal de Broglie wavelength

π - the number pi

ρ - electron density

ρ_0 - ground state electron density

$\tilde{\rho}(r)$ - trial electron density

σ_{ij} - interatomic distance where the potential is zero in the Lennard-Jones potential

ψ_i - molecular orbital

Ψ_0 - wave function

ω - torsion angle

$\omega_j(\xi)$ - umbrella potential

List of Publications

Paper 1

Aleksandar Y. Mehandzhiyski, Enrico Riccardi, Titus S. van Erp, Henrik Koch, Per-Olof Åstrand, Thuat T. Trinh, Brian A. Grimes. *Density Functional Theory Study on the Interactions of Metal Ions with Long Chain Deprotonated Carboxylic Acids*. *J. Phys. Chem. A*, **2015**, 119 (40), 10195-10203

Paper 2

Aleksandar Y. Mehandzhiyski, Enrico Riccardi, Titus S. van Erp, Thuat T. Trinh, Brian A. Grimes. *Ab Initio Molecular Dynamics Study on the Interactions between Carboxylate Ions and Metal Ions in Water*. *J. Phys. Chem. B*, **2015**, 119, 10710-10719

Paper 3

Aleksandar Y. Mehandzhiyski, Brian A. Grimes. *Calculation of the Probability for Ionic Association and Dissociation Reactions by Molecular Dynamics and Umbrella Sampling*. Accepted for publication in *Mol. Phys.*, **2016**

Paper 4

Aleksandar Y. Mehandzhiyski, Brian A. Grimes. *Coarse-Grain Interface Surfactant Density Maps for the Calculation of the Fractional Conversion of Tetra-Carboxylic Acids to Calcium-Naphthenate Precipitates*. Submitted to Industrial & Engineering Chemistry Research, December **2015**

Additional publications

Enrico Riccardi, Karina Kovalchuk, Aleksandar Y. Mehandzhiyski, Brian A. Grimes. *Structure and Orientation of Tetracarboxylic Acids at Oil-Water Interfaces*. *J. Disp. Sci. Tech.*, **2014**, 35, 1018-1030

Karina Kovalchuk, Enrico Riccardi, Aleksandar Y. Mehandzhiyski, Brian A. Grimes.

Aggregates of Poly-Functional Amphiphilic Molecules in Water and Oil Phases. *Colloid Journal*, **2014**, 76 (5), 564-575

Thomas Tichelkamp, Aleksandar Y. Mehandzhiyski, Meysam Nourani, Enrico Riccardi, Brian A. Grimes, Gisle Øye. *Effect of Calcium/Sodium Ratio on Hydrocarbon-Water Interfacial Tension in the Presence of Anionic Surfactants*. Manuscript in preparation **2015**

Gurvinder Singh, P. Anil Kumar, Aleksandar Y. Mehandzhiyski, Sulalit Bandhopadhay, Roland Mathieu, Davide Peddis, Erik Wahlstøm, Brian A. Grimes, Wilhelm R. Glomm. *Importance of Sodium Oleate in the Synthesis of Shaped Controlled Magnetic Nanoparticles*. Manuscript in preparation **2015**

Conference contributions

Talk at the 20th International Symposium on Surfactants in Solution (SIS 2014)

Aleksandar Y. Mehandzhiyski, Karina Kovalchuk, Enrico Riccardi, Brian A. Grimes. Multiscale Modelin of Interfacial Mass Transport in Liquid-Liquid Dispersions: Application to Calcium Naphthenate Precipitation in Petroleum Transport Process. Coimbra, Portugal, June 2014

Talk at the 20th International Workshop on Quantum Systems in Chemistry, Physics and Biology

Aleksandar Y. Mehandzhiyski, Enrico Riccardi, Titus S. van Erp, Thuat T. Trinh, Brian A. Grimes. Ab Initio Molecular Dynamics Study on the Interactions between Carboxylate Ions and Metal Ions in Water. Varna, Bulgaria, September 2015

Chapter 1

Introduction

1 Crude oil

Crude oil is a complex fluid mixture of thousands of various hydrocarbons and other organic compounds.[1] The complex nature of crude oil is a result of the complicated pathways which led to its formation and from the various precursors involved in the process. The most widely accepted theory is the biogenic [1] origin of crude oil. The biogenic theory suggests that crude oil originated from aquatic plants and animals that lived and died hundreds of millions of years ago. The organic matter left after their death has been gradually decomposed over the geologic timescale which eventually led to the formation of crude oil or to its precursor. Then the crude oil moved from its initial sedimentation basins to adjacent rock layers. There became trapped into porous rocks and the reservoirs have formed.

Although the precursors of crude oil vary widely, the proportions of the constituting chemical elements vary in a narrow limit.[1] The main elemental constituents of crude oil are carbon, hydrogen, nitrogen, oxygen, sulfur and traces of some metal elements as vanadium and nickel. The elemental composition [1] of crude oil is presented in Table 1.1.

Table 1.1: Elemental composition of crude oil

Chemical element	Appearance
Carbon	83.0% - 87.0%
Hydrogen	10.0% - 14.0 %
Nitrogen	0.1% - 2.0%
Oxygen	0.05% - 1.5%
Sulfur	0.05% - 6.0%
Metals	<1000 ppm

The chemical (molecular) composition of crude oil on the other hand is very complex and the chemical structure of all of its components can not be determined. Although, much work [2–4] has been done to analyse specific chemical compounds from crude oil with mass spectroscopy, it is tedious and difficult and still difficult to identify specific chemical structures. However, the chemical compounds can be divided into different fractions by their solubility, aromaticity and polarity. The SARA fractionation [5–8] divides the components of crude oil into four groups: Saturates, Aromatics, Resins and Asphaltenes. A general scheme[9] of the process is given in Figure 1.1

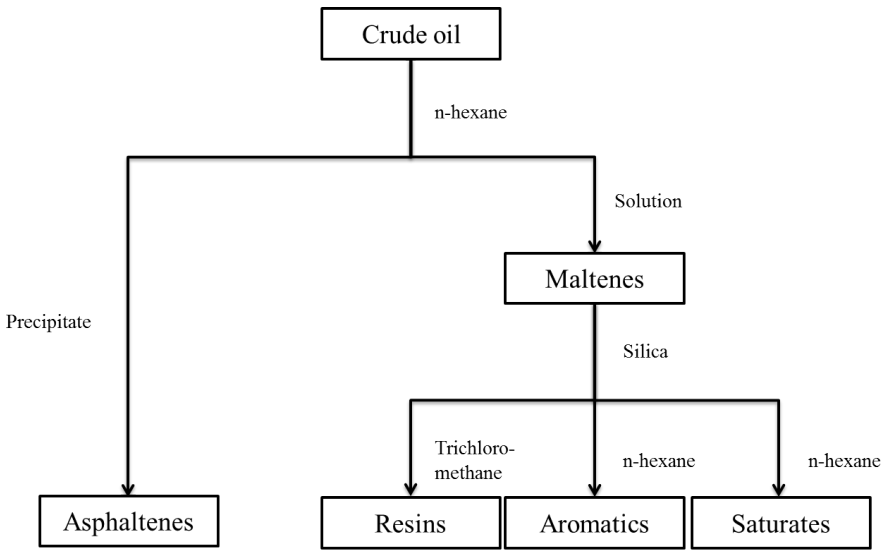

Figure 1.1: SARA fractionation

1.1 Saturates

Saturates (aliphatic) are non-polar, straight-chain and branched hydrocarbons (alkanes) and they are the lightest fraction of crude oil. Cycloalkanes (naphthenes) also belong to the group of saturates as well as waxes (paraffins). Waxes are long-chain alkanes with chain lengths typically between 20 and 30 carbon atoms. The saturates have very low interfacial activity.

1.2 Aromatics

The aromatic compounds in crude oil contains benzene and its structural derivatives. They are classified as mono-, di-, tri- or polyaromatic where several benzene rings present in the molecular structure. In addition to the aromatic rings, often alkyl chains and cycloalkane rings are substituted in the benzene moieties. The aromatics have low interfacial activity.

1.3 Resins

Resins are the fraction of crude oil defined as soluble in light alkanes, such as pentane and heptane, but insoluble in liquid propane. Resins contain in their structure heteroatoms (O, N, S) and have higher molecular weight than saturates and aromatics. Resins are structurally similar to asphaltenes, but have lower molecular weight and higher H/C ratio of 1.2 - 1.7 compared to asphaltenes with 0.9 - 1.2. Within the resin fraction, naphthenic acids are also commonly classified. The resins have high interfacial activity.

1.4 Asphaltenes

Asphaltenes are the heaviest fraction of crude oil and they are defined as the insoluble fraction of crude oil in light alkanes, such as pentane and heptane from which they precipitate. They have a similar structure as resins, but have much higher molecular weight and lower H/C ratio. Asphaltenes contain the largest percentage of heteroatoms (O, N, S) in the crude oil. The asphaltenes have high interfacial activity.

2 Flow assurance

Flow assurance refers to the successful and most cost-effective multiphase transport of the produced hydrocarbons from the reservoir to the receiving facility or to the point of sale. With increasing numbers of more remote oil fields and deeper and colder water, the transportation of crude oil will become more and more challenging. Several undesirable problems that can obstruct pipelines and block the flow can occur during the transportation of crude oil. For instance, the formation of gas hydrates [10, 11], wax [12, 13] and asphaltenes [14] deposits as well as scale

deposits [15] and calcium naphthenate precipitation [16–18] can cause blockage and/or shutdowns. The main scope of the present study is in the framework of calcium naphthenate precipitation. Therefore, the following section presents the problem of calcium naphthenate precipitation in grater detail.

3 Calcium naphthenate precipitation

3.1 Naphthenic acids

Naphthenic acids are natural components of crude oil (within the resins fraction) and are a complex mixture of alkyl-substituted acyclic and cycloaliphatic carboxylic acids where the carboxylic acid group is attached to the aliphatic side chain of the cycloaliphatic ring. They are non-volatile, chemically stable and act as surfactants. Naphthenic acids are often found in immature heavy crude oil and considered products of biodegradation of petroleum hydrocarbon in the reservoir.[18] Naphthenic acids have the general formula $C_nH_{2n+Z}O_2$, where n indicates the total number of carbon atoms and Z is specifying the hydrogen deficiency arising from the ring formation. The value of Z can be zero or a negative even integer. The absolute value of Z divided by 2 gives the total number of rings in the chemical structure. The rings can be fused or bridged. The structure of naphthenic acids is shown in Figure 1.2. [19]

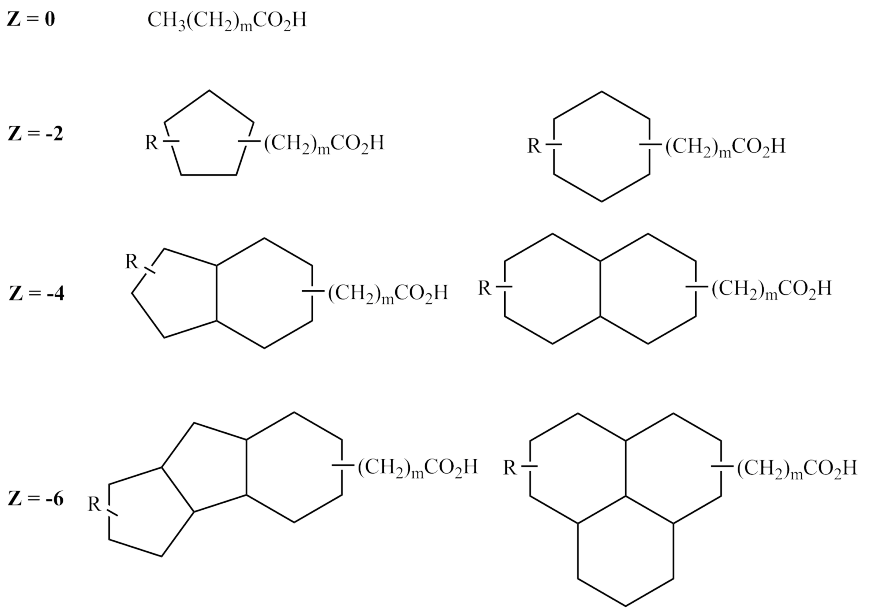

Figure 1.2: Naphthenic acid structures where Z is the hydrogen deficiency, R is alkyl chain and m is the number of CH_2 groups.

The standard way of quantifying the content of acids in crude oil is the Acid Standard Test Method (ASTM). The acid content is represented by the Total Acid Number (TAN). This test method involves titration of dissolved sample with potassium hydroxide (KOH) and the TAN is given by milligrams of KOH able to neutralize 1 gram of the sample (mg KOH/g). High acidic crude oils are considered to be crude oils with TAN > 1.0. There is an increase of the production of crude oils with high TAN number in the recent years. Some oil fields in the Norwegian continental shelf, North Sea, West Africa, South America and South East Asia are considered to produce crude oil with high TAN. The high content of acids in the crude oil can lead to several technical difficulties during the production and transportation of the oil, such as formation of tight emulsions (sludge), increased salt content in the exported crude oil, difficulty of treating the produced water because of dissolved acids, corrosion and formation of naphthenate precipitates.

3.2 Tetrameric carboxylic acids

The formation of calcium naphthenate deposits during the production of oil have been observed at several different locations around the world. Calcium naphthenate deposits were first observed on the Norwegian continental shelf in the Heidrun oilfield in 1996, but also found in oilfields in United Kingdom, West Africa, Brazil and China. It was not before 2005 when Baugh et al. [16] identified the main constituent of these deposits to be a new class of tetra-carboxylic acids and given them the generic name - ARN acids. The ARN acids have molecular weights in the range of 1227-1237 g/mol. These acids possess four carboxylic acid groups attached to a mono- or bi- cyclopentane moiety and are linked together through long hydrocarbon chains [18]. The molecular structure of ARN acid with a molecular weight 1231 g/mol and the empirical formula $C_{80}H_{142}O_8$ is used to represent a typical tetra-acid structure and is shown in Figure 1.3.

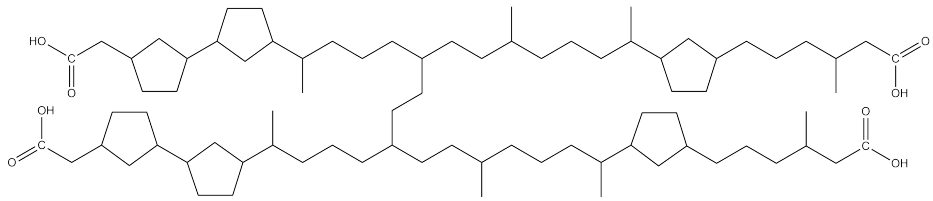

Figure 1.3: Molecular structure of ARN tetra-carboxylic acid.

The indigenous ARN tetra-carboxylic acids are difficult to purify to the extent that they can be used for quantitative laboratory experiments in order to understand the interfacial behaviour of these molecules. Thus, a synthetic analogue of the indigenous compounds has been developed [20, 21] to mimic the interfacial behaviour

of the naturally occurring acids. The synthetic analogue named BP10 is shown in Figure 1.4.

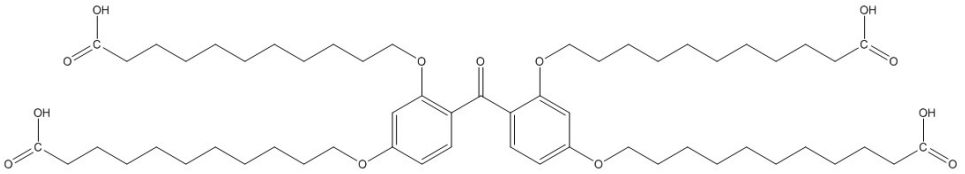

Figure 1.4: Molecular structure of the synthetic BP10 tetra-carboxylic acid.

3.3 Formation of calcium naphthenate precipitates

The calcium naphthenate deposits are adhesive, difficult to remove and can form in various process equipment, such as hydrocyclones, separators, coalescers, pipes, pumps etc. The precipitates can obstruct the process equipments and flow assurance problems could occur. Their removal leads to costly shut-down, cleaning, and restart processes. Calcium naphthenate precipitates formed inside [18] and retrieved [22] from a coalescer are shown in Figures 1.5(a) and 1.5(b), respectively.

(a) Calcium naphthenate deposit formed inside a coalescer

(b) Calcium naphthenate deposit retrieved from a coalescer

Figure 1.5: Calcium naphthenate precipitates formed in a coalescer

The exact reaction mechanism of the formation of calcium naphthenate precipitates is not yet completely known. However, the most widely accepted mechanism includes formation of a cross-linked network of tetra acid ARN molecules at the oil-water interface. This hypothesis includes several factors.

- During the extraction of crude oil from the reservoir, the pressure decreases significantly, which leads to the release of the CO_2 gas solvated in the water.

This leads to increase of the pH of the water.

- The naphthenic acids migrate to the oil-water interface and adsorb. *This leads to a dense grouping of carboxylic groups at the interface.*
- The increase in pH then leads to the dissociation of the carboxylic groups of the naphthenic acids. *The interfacial activity and water solubility of the naphthenic acids are increased due to their dissociation.*
- At the oil-water interface the tetra-carboxylic acids react with the dissolved in the water metal ions. *This leads to precipitates.*

The molecular structure of the tetra acids allows carboxylic groups from different TA molecules to react with one divalent metal ion, particularly calcium.[17] In that way a cross-linked network of tetra acid molecules can be formed at the oil-water interface, as depicted in Figure 1.6. The high molecular weight polymeric salt structure formed in this reaction is insoluble in both water and oil and therefore stays at the interface between the two phases. Eventually, the precipitates start to deposit on different metal surfaces of the process equipment.

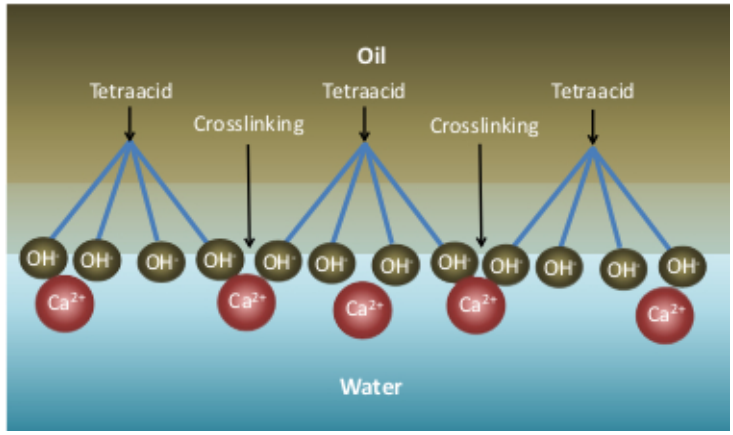

Figure 1.6: Cross-linked network of tetra-acid molecules at an oil-water interface.

The interfacial and bulk behaviour of tetra acids has been extensively studied experimentally [17, 20, 21, 23–31]. These studies are based on the tetra acid molecule BP10 since ARN has not been able to be purified to the desired quality. However, BP10 has been designed to have similar interfacial behaviour as ARN, as it was mentioned above, therefore the conducted experiments should in principle be valid for ARN as well.

The tetra-carboxylic acid - metal ion reaction is shown [17] to be very selective and calcium is the most reactive amongst the divalent ions with the following selectivity - $Ca^{2+} > Sr^{2+} \approx Ba^{2+} > Mg^{2+}$. The precipitates obtained from the field also include primarily calcium. The affinity of binding divalent ions has been explained [17] by the shielding density of solvation molecules and the size of the cations. However, the experimental confirmation of this explanation was beyond the scope of the study and the odd selectivity behaviour of metal ions remained an open question.

Molecular dynamics (MD) simulations [32] of tetra-carboxylic acids at the oil-water interface have been performed and demonstrated that carboxylic groups from different molecules could be cross-linked due to the presence of metal ions dissolved in the water phase. The extent of cross-linking is dependent on the interfacial concentration of TAs - Γ_{TA}. Consequently, a multiscale framework [33, 34] employing MD simulations and continuum modelling has been developed for liquid-liquid dispersions to predict Γ_{TA} on the process scale, which could provide quantitative results for the mass of calcium naphthenate precipitates produced per unit process volume. An important constituent function in this multiscale approach is the fractional conversion ($f_p(\Gamma_{TA})$) of tetra-carboxylic acids to calcium naphthenate precipitates as a function of the interfacial concentration of tetra acids. Since the functionality of the fractional conversion is not known, Kovalchuk et al.[34] assumed $f_p(\Gamma_{TA})$ to have a sigmoidal shape. However, the exact functionality of $f_p(\Gamma_{TA})$ has not been determined experimentally or by simulations.

3.4 Scope and main objectives of the work

The present study, as it was mentioned above, is within the scope of the study of the calcium naphthenate precipitation problem occurring in the petroleum industry. The main objectives covered in the present work could be divided into three main parts:

- Obtaining explanation for the observed experimental selectivity behaviour of the divalent metal ion reaction with carboxylic acids.
- Calculating the probability for reaction of two carboxylic groups with one divalent metal ion as a function of the distance between the carboxylic groups.
- Calculating the fractional conversion ($f_p(\Gamma_{TA})$) of tetra-carboxylic acids to calcium naphthenate precipitates as a function of the interfacial concentration of tetra acids.

To accomplish these goals and to model the desired interaction we have used a combination of Density Function Theory (DFT), Molecular Dynamics (MD) and

ab initio Molecular Dynamics (AIMD). Based on the results of this work, four manuscripts have been prepared, from which two have been already published. In the first paper we have investigated the interactions between deprotonated carboxylic acids (propanoate ions) with calcium and sodium metal ions in the gas phase. Emphasis in this paper has been put on testing and validating the force field (OPLS-AA) used later on the MD simulations and on the multibody effects when more carboxylate ions interact with one metal ion. The second paper deals mainly with the ion selectivity discussed above, where we have studied the interactions between a propanoate ion and divalent metal cations via AIMD in solution. In the third paper we have calculated the probability for reaction of two carboxylate groups with one divalent metal ion as a function of the distance between the carboxylate groups via umbrella sampling and MD. For the final, fourth, paper we have performed full-atomistic MD simulation of ARN and BP10 and have obtained different probability distribution functions describing the molecular geometries and structuring of the molecules at an oil-water interface. Then, we have used the probability distributions to recreate in a coarse-grain manner the interfacial region and to calculate the fractional conversion ($f_p(\Gamma_{TA})$) of tetra-carboxylic acids to calcium-naphthenate precipitates as a function of the interfacial concentration of tetra acids. Details of the methods used here and the main results can be found in the following sections.

Chapter 2

Models and methods

1 Density Functional Theory - DFT

Density functional theory (DFT) is one of the most widely used computational quantum chemistry methods. DFT calculates the energy and describes the electronic structure of atoms and molecules based on the electron density. The work of Hohenberg and Kohn [35] has been considered as the foundation of modern DFT. According to their work [35], there is only one unique functional F[ρ] describing the electron state of a many-body system and this functional delivers the ground state of the system only if the input density is the true ground state density ρ_0. In other words, DFT is variational with respect to the energy and any trial density $\tilde{\rho}(r)$ will deliver an upper boundary of the true ground state energy E_0. The ground state energy of the system can be calculated from:

$$E_0[\rho] = \int \rho(r) V_{ext}(r) dr + F[\rho] \tag{2.1}$$

where

$$F[\rho] = T[\rho] + V_{ee}[\rho] \tag{2.2}$$

V_{ext} is the external potential in which the electrons are moving, $V_{ee}[\rho]$ is the electron-electron interaction and $T[\rho]$ is the kinetic energy of the electrons. In principle, DFT is exact if F[ρ] could be known. In that case E_0 can be obtained from the variational principle. Kohn and Sham [36] have proposed the following form of the functional $F[\rho]$:

$$F[\rho] = T_s[\rho] + J[\rho] + E_{xc}[\rho] \tag{2.3}$$

where $J[\rho]$ is the Coulomb potential, $E_{xc}[\rho]$ is the exchange-correlation energy and $T_s[\rho]$ is the kinetic energy of the non-interacting system given by:

$$T_s[\rho] = -\frac{1}{2}\sum_{i}^{N}\langle\psi_i|\nabla^2|\psi_i\rangle \tag{2.4}$$

where ψ_i is a molecular or atomic orbital. $T_s[\rho]$ is different from $T[\rho]$ and the difference between them is included in $E_{xc}[\rho]$. Now the energy functional can be written as:

$$\begin{gathered} E_0[\rho] = T_s[\rho] + J[\rho] + E_{xc}[\rho] + E_{Ne}[\rho] = \\ -\frac{1}{2}\sum_{1}^{N}\langle\psi_i|\nabla^2|\psi_i\rangle + \frac{1}{2}\sum_{i}^{N}\sum_{j}^{N}\iint|\psi_i(r_1)|^2\frac{1}{r_{12}}|\psi_j(r_2)|^2 dr_1 dr_2 \\ + E_{xc}[\rho] - \sum_{i}^{N}\int\sum_{A}^{M}\frac{Z_A}{r_{1A}}|\psi_i(r_1)|^2 dr_1 \end{gathered} \tag{2.5}$$

Where r_{12} is the distance between electrons, r_{1A} is the electron-nuclear distance and Z_A is the nuclear charge.

$E_{xc}[\rho]$ basically contains everything which is unknown. By applying the variational principle [37, 38] the resulting Kohn-Sham equations are:

$$\left(-\frac{1}{2}\nabla^2 + \left[\int\frac{\rho(r_2)}{r_{12}} + V_{xc}(r_1) - \sum_{A}^{M}\frac{Z_A}{r_{1A}}\right]\right)\psi_i = \left(-\frac{1}{2}\nabla^2 + V_s(r_1)\right)\psi_i = \epsilon_i\psi_i \tag{2.6}$$

$$V_s(r_1) = \int\frac{\rho(r_2)}{r_{12}} + V_{xc}(r_1) - \sum_{A}^{M}\frac{Z_A}{r_{1A}} \tag{2.7}$$

$V_{xc}(r_1)$ is the potential due to the exchange-correlation energy $E_{xc}[\rho]$. Since $E_{xc}[\rho]$ is not known, also $V_{xc}(r_1)$ is unknown and is simply defined as the functional derivative of $E_{xc}[\rho]$ with respect to ρ:

$$V_{xc} \equiv \frac{\delta E_{xc}}{\delta\rho} \tag{2.8}$$

The accuracy of DFT depends completely on the accuracy of the exchange-correlation functional and on the basis set. The quest for finding the best exchange-correlation functional is the greatest challenge in DFT. Kohn and Sham [36] have introduced the first approximation for the exchange-correlation functional named the *local density approximation* - LDA. LDA is based on the assumption of uniform electron gas, where the electrons move on a positive background charge distribution.

This model represents to a very good extent a simple metals as for example sodium. $E_{xc}^{LDA}[\rho]$ is given by:

$$E_{xc}^{LDA}[\rho] = \int \rho(r)\epsilon_{xc}(\rho(r))dr \tag{2.9}$$

where ϵ_{xc} is the exchange-correlation energy per particle of an uniform electron gas of density $\rho(r)$, which is weighted with the probability $\rho(r)$ that there is an electron at this position in space. Furthermore, $\epsilon_{xc}(\rho(r))$ can be split into exchange and correlation contributions, where they can be evaluated separately:

$$\epsilon_{xc}(\rho(r)) = \epsilon_x(\rho(r)) + \epsilon_c(\rho(r)) \tag{2.10}$$

However, LDA has only limited application and in general does not give good results for molecules, where the electron density varies considerably. An intuitive extension of LDA is to take into account the gradient of the charge density $\nabla\rho(r)$. This approximation is known as the *generalized gradient approximation* - GGA. The GGA functionals can be generally written as:

$$E_{xc}^{GGA}[\rho] = \int f(\rho, \nabla\rho)dr \tag{2.11}$$

where like in LDA the functional can be separated to exchange and correlation part and approximations for them can be applied individually.

Another approach for having the appropriate form of the exchange-correlation energy is the approach for hybrid functionals proposed by Becke. [39] The hybrid functionals incorporates combination of pure density functional for exchange and a portion of the exact Hartree-Fock exchange [39, 40]:

$$E_{xc}^{hyb} = E_{xc}^{LDA} + a_0(E_x^{HF} - E_x^{LDA}) + a_x(E_x^{GGA} - E_x^{LDA}) + a_c(E_c^{GGA} - E_c^{LDA}) \tag{2.12}$$

where the different a parameters are empirically fitted values.

2 Molecular Dynamics - MD

Molecular dynamics (MD) is a method which traces the dynamical evolution of a many-body molecular system by integrating Newton's laws of motion. This results in a phase-space trajectory describing how the positions and velocities evolve in time. The trajectory is obtained by solving the following differential equation given by Newton's second law:

$$F = ma = m\frac{dv}{dt} = m\frac{d^2r}{dt^2} \tag{2.13}$$

where F is the force acting between particles, m is mass, a is acceleration, v - velocity, r - position and t is the time. The forces in MD simulations are calculated from the negative gradient of the potential energy:

$$F(r) = -\frac{dU}{dr} \tag{2.14}$$

The potential energy, (U), is given by the sum of the intra- and inter-molecular potential energies:

$$U = U_{intra} + U_{inter} \tag{2.15}$$

The intra-molecular potential energy has three contributions: bond stretching, angle bending and bond rotation (torsion) also referred as bonded interactions. The inter-molecular or non-bonded interactions are given by the sum of the van der Waals and electrostatic interactions. All of these interactions combined together are known as a *force field*, which generally is given by [41]:

$$U(r) = \sum_{bonds} \frac{k_i}{2}(l_i - l_{i,0})^2 + \sum_{angles} \frac{k_i}{2}(\Theta_i - \Theta_{i,0})^2 + \sum_{torsions} \frac{V_n}{2}(1 + \cos(n\omega - \gamma)) + \sum_{i=1}^{N} \sum_{j=i+1}^{N} \left(4\epsilon_{ij} \left[\left(\frac{\sigma_{ij}}{r_{ij}} \right)^{12} - \left(\frac{\sigma_{ij}}{r_{ij}} \right)^{6} \right] + \frac{q_i q_j}{4\pi\epsilon_0 r_{ij}} \right) \tag{2.16}$$

Where the first term on the right is the bond stretching, the second is the angle bending, the third is the torsion potential, the fourth is the Lennard-Jones potential and the final term is the Coulomb potential.

Many force fields have been developed and parametrized for different systems, from which some of the most widely used are AMBER [42], CHARMM [43], OPLS-AA [44], GROMOS [45] etc. In this work we have used the OPLS-AA force field to carry out the necessary MD simulations in the GROMACS [46] simulation package.

3 *Ab initio* Molecular Dynamics - AIMD

Ab initio molecular dynamics (AIMD) can be viewed as a combination of the two methods (DFT and MD) described in the previous sections. Like in the classical MD, AIMD predicts the time evolution of the system. Unlike classical MD, the forces in AIMD are calculated by *ab initio* methods, usually DFT. There are three approaches for AIMD: Ehrenfest MD [47], Born-Oppenheimer MD (BOMD) and Car-Parrinello MD [48]. In this work we have used BOMD, which has been included in the CP2K simulation package [49] and we shall give a brief description of the method.

In Born-Oppenheimer MD, the electronic and nuclear degrees of freedom are separated and the nuclear coordinates are propagated in time according to classical dynamics. The electrons are following the dynamics of the much heavier nuclei, thus they do not possess their own dynamics. On every MD step, the time-independent Schrödinger equation is solved for the electronic part of the system for a given fixed positions of the nuclei at this particular moment of time. The total energies obtained in a specific electronic state yield directly the forces and the equations of motion of the BOMD method are given by [50]:

$$M_I \ddot{R}_I(t) = \nabla_I min\{\langle \Psi_0 | H_e | \Psi_0 \rangle\} \tag{2.17}$$

$$E_0 \Psi_0 = H_e \Psi_0 \tag{2.18}$$

where for every MD step the minimum of $\langle H_e \rangle$ has to be reached.

4 Calculation of free energy of interaction and probability of reaction

The interactions between deprotonated carboxylic group(s) (carboxylate anion(s)) and divalent metal cations are identified as the dominant interactions influencing the calcium naphthenate precipitation behaviour. Therefore, the carboxylate-metal ion interactions, in the context of the calcium naphthenate precipitation phenomena are extensively studied in this work. The TA molecules ARN and BP10 possess more then 150 atoms, which would require a substantial amount of computational power and time, if one considers the whole molecules in a DFT calculation or AIMD simulation. Moreover, the main interactions are between the carboxylate groups and the metal ions, as was mentioned above, and the rest of the molecule would not have much effect on these interactions. Therefore, we have used a short chain mono-acid molecule (propanoate anion), to represent a general carboxylate group interacting with divalent metal ions. To wit, we have calculated the interaction free energies and probability for reaction using the thermodynamic integration and umbrella sampling methods described below. However, it should be noted that full-atomistic MD simulations on the TAs have also been carried out.

4.1 Thermodynamic integration

The method of thermodynamic integration (TI) allows the free energy difference between two states of a system to be calculated from a molecular simulation. A system with a potential energy function U is coupled with a coupling parameter λ, which varies between 0 and 1, such that for $\lambda = 0$ if the system is in one state (U_I) and for $\lambda = 1$ is in different one (U_{II}) [51]:

$$U(\lambda) = (1 - \lambda)U_I + \lambda U_{II} = U_I + \lambda(U_{II} - U_I) \tag{2.19}$$

The slow variation of λ between 0 and 1 is connecting the two states of the system and the partition function of this system is given by:

$$Q(N,V,T,\lambda) = \frac{1}{\Lambda^{3N}N!}\int e^{-\beta U(\lambda)} \tag{2.20}$$

The derivative of the free energy with respect to λ can be written by:

$$\begin{aligned}\left(\frac{\partial A(\lambda)}{\partial\lambda}\right) &= -\frac{1}{\beta}\frac{\partial}{\partial\lambda}\ln Q(N,V,T,\lambda) = -\frac{1}{\beta Q(N,V,T,\lambda)}\frac{\partial Q(N,V,T,\lambda)}{\partial\lambda} \\ &= \frac{\int dr^N(\partial U(\lambda)/d\lambda)\exp[-\beta U(\lambda)]}{\int dr^N \exp[-\beta U(\lambda)]} = \left\langle\frac{\partial U(\lambda)}{\partial\lambda}\right\rangle_\lambda\end{aligned} \tag{2.21}$$

By integrating Equation 2.21, one can obtain the free energy difference between states II and I:

$$\triangle A(\lambda) = \int_{\lambda=0}^{\lambda=1}\left\langle\frac{\partial U(\lambda)}{\partial\lambda}\right\rangle_\lambda d\lambda \tag{2.22}$$

In this work, we have used BOMD simulations and TI to calculate the free energy profiles of the propanoate-divalent metal ions interactions in water. This has been done by varying the distance between the carboxylate group and the metal ion, and calculating the force between them. Then by integrating the force, the free energy of interaction has been calculated.

4.2 Umbrella sampling

The umbrella sampling is another method to sample the configuration space between two states (I and II) of a system from which one can obtain the free energy difference between them. In umbrella sampling, the states I and II are biased with an umbrella potential (often harmonic potential), the respective states are sampled and the probability for finding the system in state I and II is obtained. Thus, states which are difficult to be sampled otherwise and therefore remain inaccessible in the potential energy surface become accessible. That is particularly helpful when studying chemical reactions.

In this work, we have used umbrella sampling to find the probability for reaction as a function of the distance between two carboxylates molecules, providing the requirement that a metal ion is interacting with both carboxylates at the same time. To accomplish that, we have applied umbrella potentials to different separation distances between the two carboxylates in the presence of a metal ion. Then we have used the Weighted Histogram Analysis Method (WHAM) [52, 53] to unbias the obtained probability. The set of equations needed to solve in order to unbias the probability distributions are:

$$P(\xi)_{un} = \frac{\sum_{i=1}^{N_w} n_i p(\xi)_i^{bias}}{\sum_{j=1}^{N_w} n_j e^{-[\omega_j(\xi)-F_j]/k_bT}} \tag{2.23}$$

$$e^{-F_i/k_bT} = \int e^{-\omega_j(\xi)/k_bT} P(\xi)^{un} \tag{2.24}$$

where $P(\xi)_{un}$ is the unbiased probability distribution, N_w is the number of simulation windows, n_i and n_j are the respective simulation window, $p(\xi)_i^{bias}$ is the biased probability distribution, $\omega_j(\xi)$ is the umbrella potential, F_j is a free energy, k_b is the Boltzmann constant and T is the temperature. The equations can be solved iteratively.

Subsequently, the probability for reaction has been used for the generation of coarse-grain interface maps described in the following section. The unbiased probability distribution in Equation 2.23 is the actual probability for reaction as a function of the reaction coordinate ξ, which respectively is the distance between the carboxylate groups. The highest probability in the distribution function would correspond to the most probable distance where the carboxylate are located and are bound to the divalent metal ion.

5 Generation of random interface COO$^-$ density maps

In order to generate a coarse-grained representation of the density of the carboxyalte groups of the TA molecules at the oil-water interface we have used various probability distributions [32] obtained from MD simulations and presented in Figures 3.13 and 3.14. To wit, we can randomly place a large number of TA molecules on an interface at a given concentration Γ_{TA} and use these distribution functions to recreate the interfacial distribution of all the COO$^-$ groups at the interface in a Monte Carlo approach. By generating a substantial amount of random COO$^-$ interface maps for a fixed value of Γ_{TA}, the fractional conversion of the tetra-carboxylic acid to calcium-naphthenate precipitates could be calculated as a function of the interfacial concentration by evaluating the mutual displacement of the COO$^-$ groups with respect to the probability of binding (Section 4.2) to determine if the COO$^-$ groups are corss-linked. The main algorithm for generating the random density maps is shown in Figure 2.1. First, the input parameters have been passed to the main program. The necessary input parameters are the interface map dimensions (A) and the interfacial concentration of the tetra-carboxylic acids - Γ_{TA}. The condition on A is that it should be large to accommodate a large number of TA molecules. Based on the values of Γ_{TA} and A, the number of TA molecules, N_{TA}, in simulation is given by:

$$N_{TA} = \Gamma_{TA} A \tag{2.25}$$

where Γ_{TA} is given in molecules/nm^2.

For the specified interfacial concentration, lateral dimensions (x and y) of the N_{TA} molecule centers have been randomly placed on a plane representing the interface region and the probability distributions from Figure 3.13 have been used to generate the positions of the COO^- groups based on arm lengths, orientation angles and vertical displacement from an arbitrary "dividing" surface as done by Ricardi et al. [32] Once the intermolecular distances between the COO^- groups have been determined, the fractional conversion of tetra-carboxylic acids to calcium-naphthenate precipitation can be obtained from the binding probability in Figure 3.14. More detailed algorithms for generating the coordinates of molecular centers and COO^- groups are presented in Figures 2.2 and 2.3, respectively.

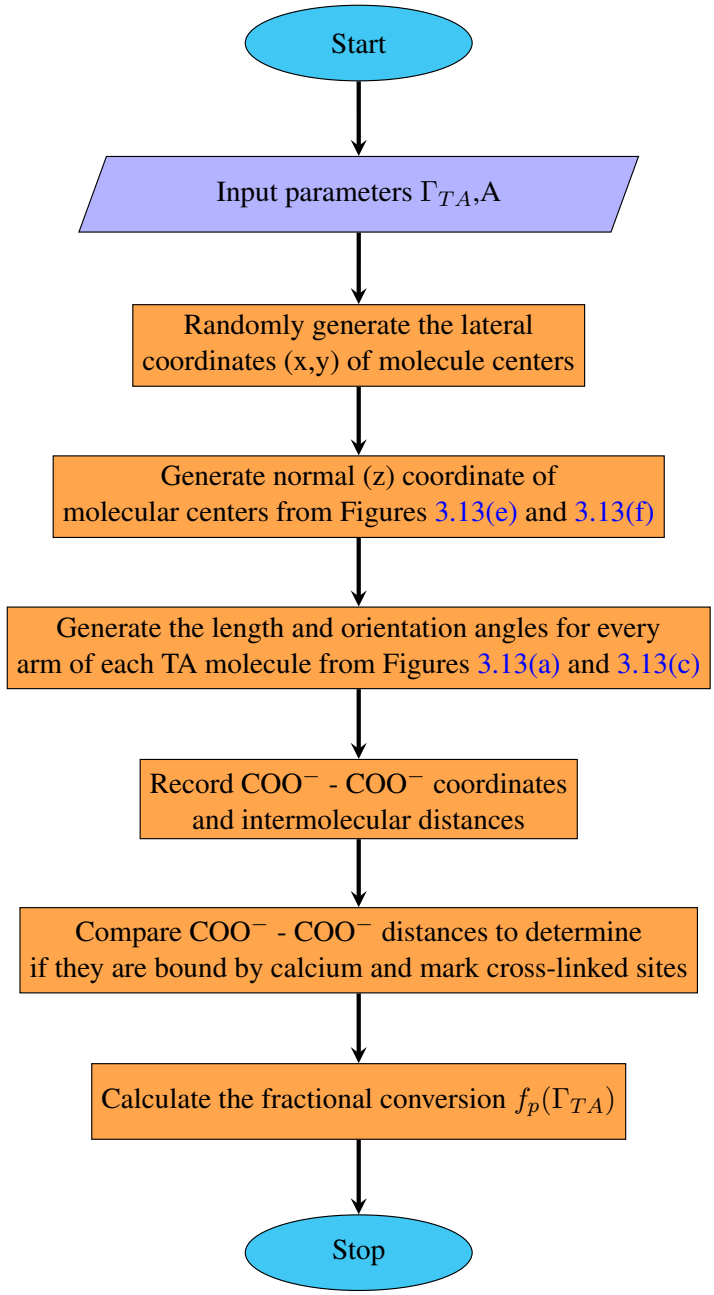

Figure 2.1: Main algorithm for generating the interface maps based on the probability distributions obtained from MD simulations

In Figure 2.2, the algorithm for randomly generating the molecular centers is

presented. The molecular center of BP10 is composed of a benzophenone core and the center of ARN is comprised of the central hydrocarbon moiety connecting the four carboxylate groups. The molecular centers are placed randomly on a plane with dimensions of 100 $\times$ 100 nm using PBC. We have set the interfacial concentrations of the TAs in the range of 0.0007 - 0.1387 molecules/nm^2. Kovalchuk et al.[33] have calculated the minimum interfacial area per molecule to be 7.21 nm^2 for BP10, which for Γ_{TA} gives a maximum value Γ_{max}=0.1387 molecules/nm^2. Γ_{max} for ARN is not available, therefore we have used the same value as for BP10, although it might slightly differ. After the first random assignment of molecule centers, we check to see if the required value of Γ_{TA} is reached. Specifically, when a new molecule center is placed, the program checks if there is overlap with the previously placed TA molecule. If the distance between the new molecule and any previously placed TA is smaller than a certain threshold the new molecule is rejected. The molecular center distance threshold has been set to 1.4 nm and 1.0 nm for ARN and BP10, respectively. These values represent roughly the molecule center diameter. The random assignment of molecule centers continues until the desired value of Γ_{TA} is reached.

If the threshold is satisfied the molecule center coordinates are saved and the program generates the z position of the respective molecule center according to a cumulative distribution function (CDF). The CDF is constructed based on the probability distribution function (PDF) for the molecular center obtained from the MD simulations, Figures 3.13(e) and 3.13(f). To assign the z-coordinate, a random number generator (RNG) has been used to generate a random number between 0 and 1. Since both the CDF and the random number are between 0 and 1, the random number will correspond to a value for the z-coordinate from the CDF. Then the assigned z-coordinate is compared to the PDF obtained from the MD simulation and is checked to determine if it falls within the boundaries of the PDF. If the condition is not satisfied, a new z-coordinate is generated, until the new z-coordinate is accepted according to the criteria discussed above.

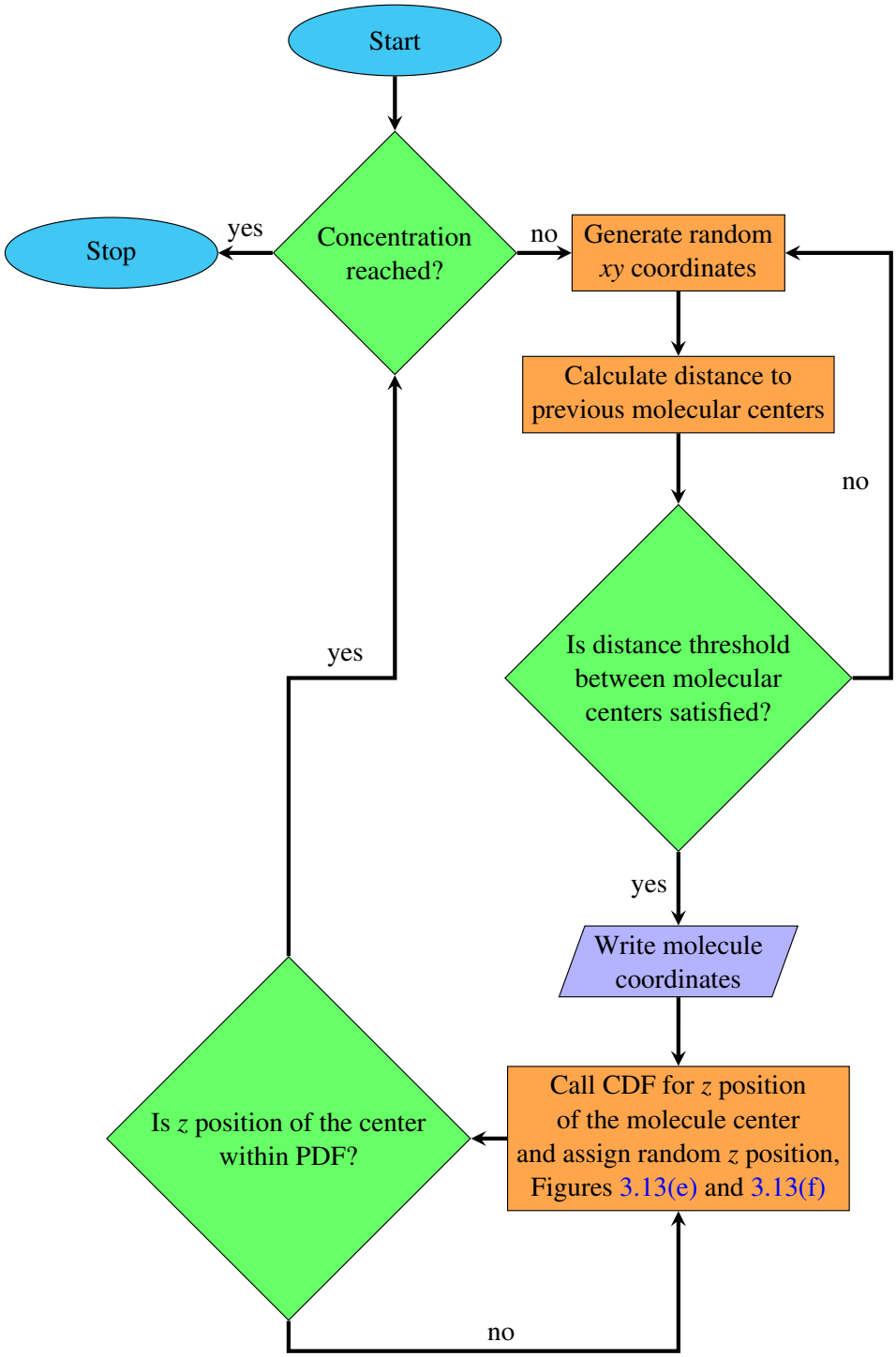

Figure 2.2: Algorithm for generating the coordinates of the molecule centers

Once all the coordinates of the molecular centers are determined, four arm groups must be assigned to each molecular center. The algorithm for generating the length and orientation angles of the four long hydrocarbon chains on each TA molecule, referred as "arms", is depicted in Figure 2.3. For each molecule center we generate four arms where in the first step of the algorithm, four lengths are generated in accordance with the PDF in Figure 3.13(a) of the arm vector lengths. After that, the vertical orientation angle of each of the 4 the molecule arms relative to the interface has been generated using the PDF in Figure 3.13(b). Then the z-position of each COO^- group for the respective arm is calculated by:

$$Z_{COO^-}^{n,m} = Z_{cn}^{n} + V_L^{n,m} \sin \Theta^{n,m} \tag{2.26}$$

$Z_{COO^-}^{n,m}$ is the z-position of the COO^- group of the m^{th} arm of the n^{th} TA molecule, Z_{cn}^{n} is the z-position of the n^{th} molecular center, $V_L^{n,m}$ is the arm vector length, $\Theta^{n,m}$ is the vertical orientation angle of the arm, n and m are the indexes for molecule center and COO^- group, respectively. Afterwards, the generated z-position is checked to determine if it is within the PDF obtain from the MD simulation shown in Figures 3.13(e) and 3.13(f) for ARN and BP10, respectively. Once all vertical orientation angles are determined, a horizontal orientation angle of the molecular arm is generated according to Figure 3.13(c). Then the arm xy-position is calculated by:

$$X_{COO^-}^{n,m} = X_{cn}^{n} + V_L^{n,m} \cos \gamma^{n,m} \tag{2.27}$$

$$Y_{COO^-}^{n,m} = Y_{cn}^{n} + V_L^{n,m} \sin \gamma^{n,m} \tag{2.28}$$

$X_{COO^-}^{n,m}$ and $Y_{COO^-}^{n,m}$ are the respective xy-positions of the COO^- group, X_{cn}^{n} and Y_{cn}^{n} are the respective xy-position of the molecule center and $\gamma^{n,m}$ is the horizontal orientation angle of the arms. In the next step, the distances between the intra-molecular carboxylate groups as well as the distance of the carboxylate group with the molecular centers are checked, if they overlap or fall into the acceptable region of the PDF for the case of the intra-molecular COO^- - COO^- distance in Figure 3.13(d). If the conditions are satisfied the coordinates are saved and a new cycle begins, otherwise 4 new arms are generated until the required conditions are met. At this point an interface map is generated in terms of knowing all the x,y,z coordinates of the molecular centers, and their 4 corresponding COO^- groups and now we have to evaluate how many TA molecules are cross-linked by evaluating the probability of reaction based on the relative distances between the carboxylate groups.

In order to calculate the fractional conversion of TA to calcium-naphthenate precipitates, we have evaluated how many possible cross-linked sites exist. This has been done by calculating the distances between the inter-molecular carboxylate groups and evaluating the probability to place a calcium ion between them according to Figure 3.14. We have used the probability distribution for checking the probability for reaction of two carboxylate groups with one calcium ion. The probability of reaction is constructed to represent the probability of two carboxylate groups to be associated to one calcium ion as a function of the separation distance between them. Then we generate random numbers and check if this number is within the probability. If the random number is smaller then the PDF of reaction, the site is marked as cross-linked and if it is larger there is no cross-linking possibility. The fractional conversion $f_p(\Gamma_{TA})$ is calculated by Equation 2.29 where $\langle N_{cl}(\Gamma_{TA})\rangle$ is the average number of cross-linked sites for a given Γ_{TA} and Γ_{max} is the maximum interfacial concentration, which was given above and equals $\Gamma_{max} = 0.1387$ molecules/nm^2. $f_p(\Gamma_{TA})$ is scaled so the highest value equals 1.

$$f_p(\Gamma_{TA}) = \frac{\langle N_{cl}(\Gamma_{TA})\rangle}{\Gamma_{max}} \tag{2.29}$$

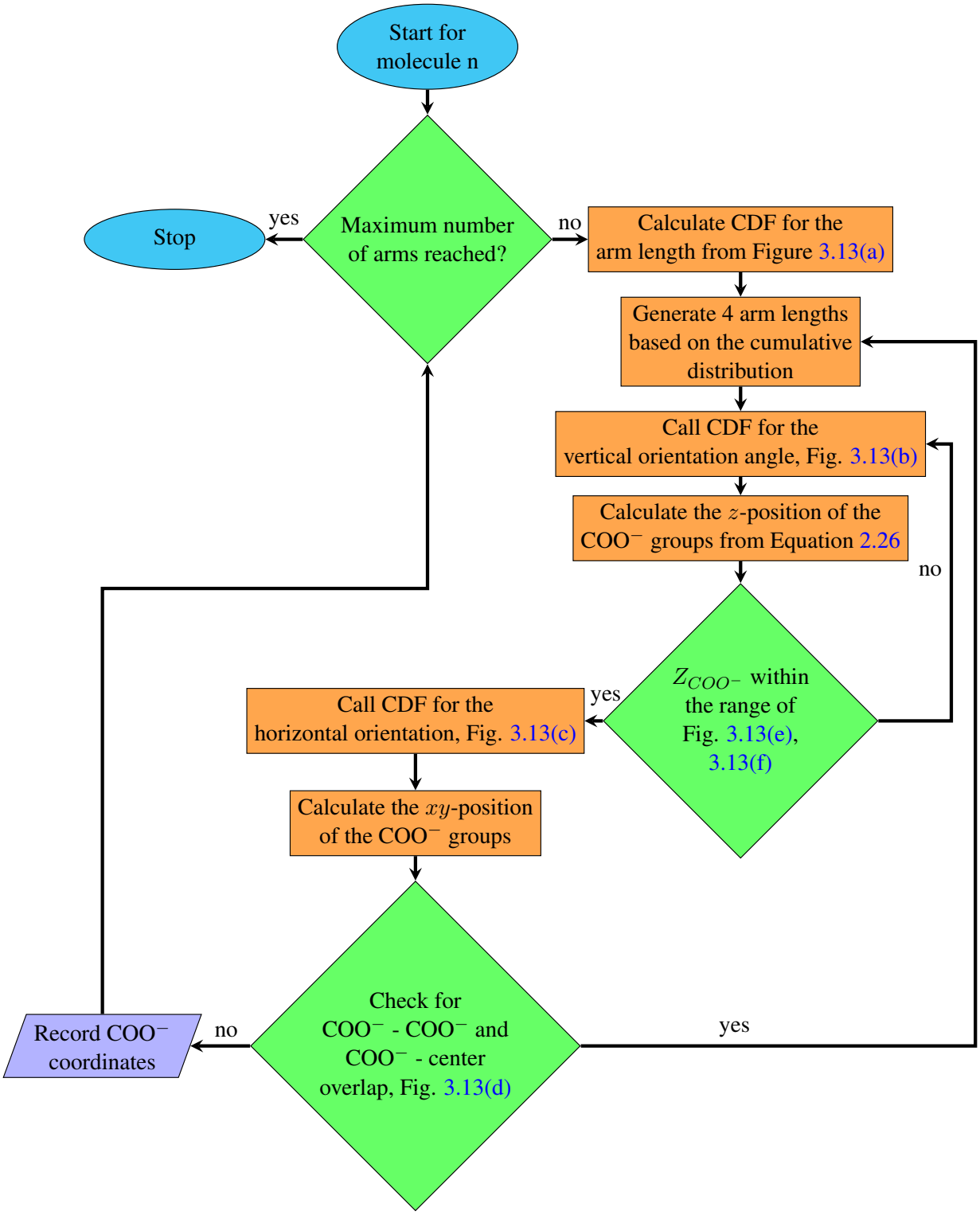

Figure 2.3: Algorithm for generating the coordinates of the COO^- groups at the terminus of the TA arms.

Chapter 3

Main results

The present section highlights the main results obtained in this study. For a more comprehensive discussion of the results the reader is encouraged to see the attached manuscripts.

1 DFT gas phase calculations

The interactions between one to four carboxylate anions with calcium and sodium metal cations in the gas phase have been first investigated by DFT. The geometries of the four anion-cation complexes are depicted in Figure 3.1. The total interaction energy and the pair-interaction energy of these complexes have been calculated by Equations 3.1 and 3.2, respectively.

$$E(r)_{inter} = E(r)_{complex} - E_{ion} - NE_{acid} \tag{3.1}$$

$$E(r)_{pair-inter} = \frac{E(r)_{complex} - E_{ion} - E_N(r)}{N} \tag{3.2}$$

$E(r)_{complex}$ is the total energy of the multibody complex at different carboxylate - ion distances, *r*, E_{ion} is the energy of the metal ion, E_{acid} is the energy of the carboxylate and *N* is the number of propanoates considered in the system. $E_N(r)$ is the energy of the system in absence of the metal ion, which is the energy of the complex of carboxylates. The total interaction energy provides an estimation of the most stable and, respectively, more probable molecular geometry and orientation of the carboxylate acids around the metal ions. The pair-interaction energy on the other hand evaluates the average relative strength of the ionic interaction between a single carboxylate acid group and the metal ion in the presence of the other carboxylate acid pair interactions. In that way, this is an estimation of the influence of the multibody effects on the ionic interactions in the complex.

Carboxylate anions can have numerous chain lengths, thus a suitable model must be chosen to mimic many chains in general. Therefore, we initially consider carboxylates with chain lengths of 2 - 6 carbon atoms. For these molecules we have calculated and presented in Table 3.1 the Mulliken [54] partial charges in order to determine the effect on the charge distribution of the COO^{-}. It can be observed that the prolongation of the carbon-hydrogen tail beyond 3 carbons minimally affects the charge distribution of the carboxyl group. It should be noted that either the propanoate or butanoate ion could be a possible model molecule for the following calculations since the charge distribution on the oxygens on both ions is nearly identical. That indicates that an explicit comparison of the interaction energy is needed. Thus, calculations of the interaction energies have been carried out for both, propanoate and butanoate, and presented in Figure 3.2. It can be seen that they give similar results and, therefore, the propanoate ion has been selected as the best compromise between computational efficiency and effects of the chain length on the carboxyl group charge distribution. Therefore, the results presented afterwards are only for the propanoate ion.

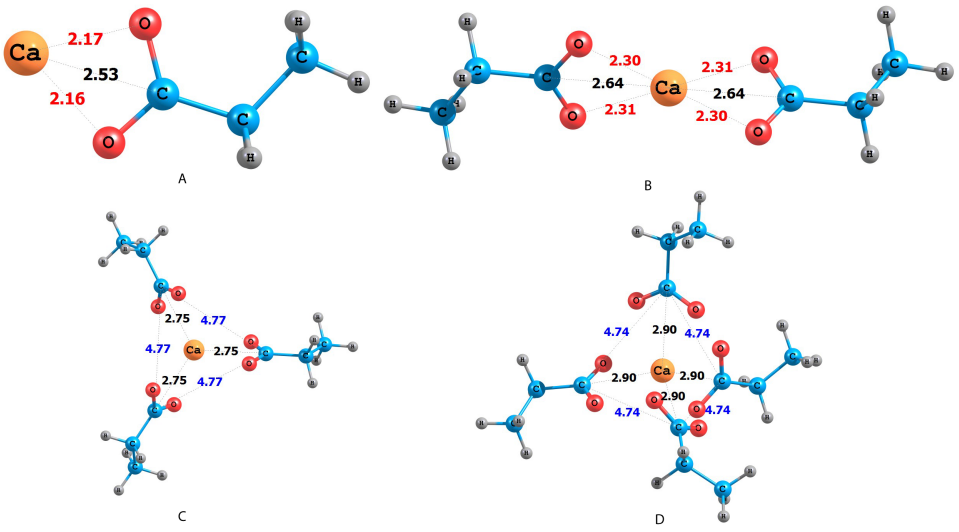

Figure 3.1: Optimized geometries of the complexes with 1 (A), 2 (B), 3 (C) and 4 (D) carboxylates and 1 Ca^{2+}. Distances are given in Å, in black are the distances between Ca^{2+} and C from (COO^{-}) group, in red-Ca^{2+} and O from (COO^{-}) group and in blue-between the carbon atoms of the carboxylate groups.

Table 3.1: Mulliken partial charges (e^-) of the carboxylate group and its constituent atoms for different carboxylate ions

Number of carbon atoms	COO^-	O	O	C
2 (acetate)	-0.847	-0.498	-0.498	0.148
3 (propanoate)	-0.896	-0.480	-0.499	0.083
4 (butanoate)	-0.869	-0.474	-0.498	0.103
5 (pentanoate)	-0.872	-0.473	-0.491	0.092
6 (hexanoate)	-0.881	-0.472	-0.487	0.077

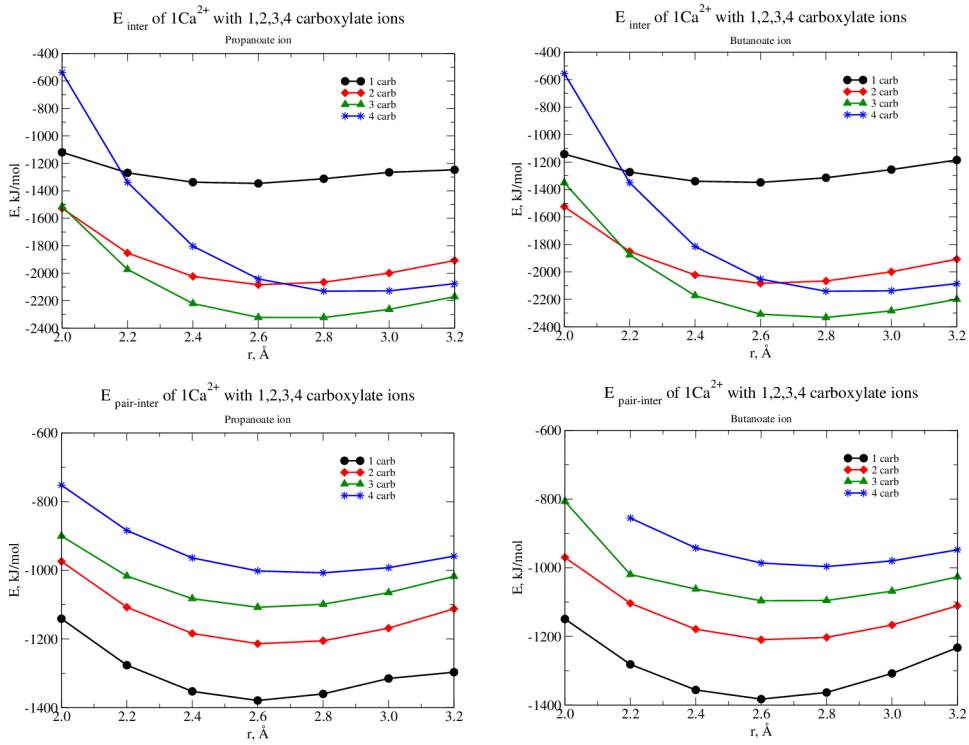

Figure 3.2: Comparison between the total interaction energies, $E(r)_{inter}$, according to Equation 3.1 and pair-interaction energy, $E(r)_{pair-inter}$, according to Equation 3.2 between the propanoate ion(s) and Ca^{2+} (left) and butanoate ion(s) and Ca^{2+} (right).

Beside quantifying the carboxylate-metal ion interactions, we have also made a comparison and validated the fit of the interactions with the OPLS-AA force field [44] and a modification of OPLS-AA made by Yan et al. [55], where the force field

parameters are presented in Table 3.2. The multibody effects are also evaluated by Equation 3.2 and presented in Figure 3.3.

Both Figures 3.1 and 3.3 demonstrate that increasing the number of carboxylate groups increases the equilibrium distance between Ca^{2+} and the carbon in the carboxylate group. The distance varies from 2.5 Å for 1 carboxylate to 2.9 Å for 4 carboxylates as shown in Figure 3.1. Figure 3.3 reports how the total interaction energy varies as a function of distance for different numbers of carboxylate acid groups. It appears that the lowest total interaction energy (Equation 3.1) for the investigated systems can be reached when 3 carboxylates are surrounding the metal ion. That has been shown to be valid for both DFT and MM interaction energies, implying that the MM results are qualitatively in agreement with DFT. Although, MM reproduces the same ordering of the potential curves as DFT, it fails to predict the equilibrium distance in the complexes of 2 and 3 carboxylates, where they have shifted with 0.04 Å and 0.15 Å compared to DFT, respectively, towards shorter distances. In DFT, the placement of more negatively charged carboxylates would promote more charge transfer to the positively charged calcium, which decreases the total interaction energy in Figure 3.3. Then one could expect that by placing more carboxylates, the interaction energy would decrease, because that would imply more charge transfer to the calcium, as it is shown from the partial charges determined by the natural bond orbital method [56, 57] in Table 3.3. However, the complex with the lowest interaction energy is the one with 3 carboxylates, not 4 as one could expect. This observation could be explained by a) reaching a case where the charge transfer difference is decreasing significantly upon addition of extra carboxylate and b) the mutual orientation of the carboxylates relative to each other. When more carboxylates are placed around the ion the mutual distance between them decreases, as seen from Figure 3.1, which destabilizes the complex (decreases the interaction energy) since they are negatively charged and tend to repel each other. The balance between the effect which stabilizes the complex (charge transfer from the carboxylate group to the metal ion) and the effect destabilizing it (the repulsion between the carboxylates) determines the trends of the potential curves in Figure 3.3. From Figure 3.3, it can also be seen that the MM calculated energies, for the equilibrium geometries underestimate the interaction energy compared to DFT for the case with 1 and 2 carboxylates by 92 kJ/mol and 210 kJ/mol, respectively. In contrast, the MM interaction energies for 3 and 4 carboxylates are overestimated by 195 kJ/mol and 250 kJ/mol, respectively. This observation clearly highlights the importance of the multibody interactions in the cases where two or more carboxylates interact with the calcium.

The pair interaction energies (Equation 3.2) calculated with the two methods for different numbers of acid molecules interacting with the metal ion are reported

in the bottom plot of Figure 3.3. The strongest carboxylate-calcium interaction as indicated by the pair-interaction energy is formed when one carboxylate group interacts with the metal ion, as shown by both DFT and MM. However, the pair-interaction energy computed via MM is higher in energy by 125 kJ/mol compared with DFT. The pair-interaction energy for the cases of more than 1 carboxylate ion computed by DFT increases nearly linearly with the addition of more acids to the complex and it is highest with 4 acids. That could be explained by the fact that as more molecules share the interaction energy with the ion, the energy per acid-ion pair in the complexes of more than one carboxylate ion becomes weaker. Another effect would also be the mutual orientation and repulsion between the carboxylates as explained in the previous paragraph. In the case of MM, the pair-interaction energy for all the cases is similar, as one would expect. Not only is the energy different, but also the trend does not match the DFT derived potentials. The strongest pair-interaction is again with 1 carboxylate, but in this case followed by 3, then 4, and then 2. Also the equilibrium distances obtained with MM, in all of the complexes except for 1 carboxylate, moved to shorter distances compared to DFT. These observations also point out the importance of the multibody interactions in the examined complexes which are not represented in simple pair potentials.

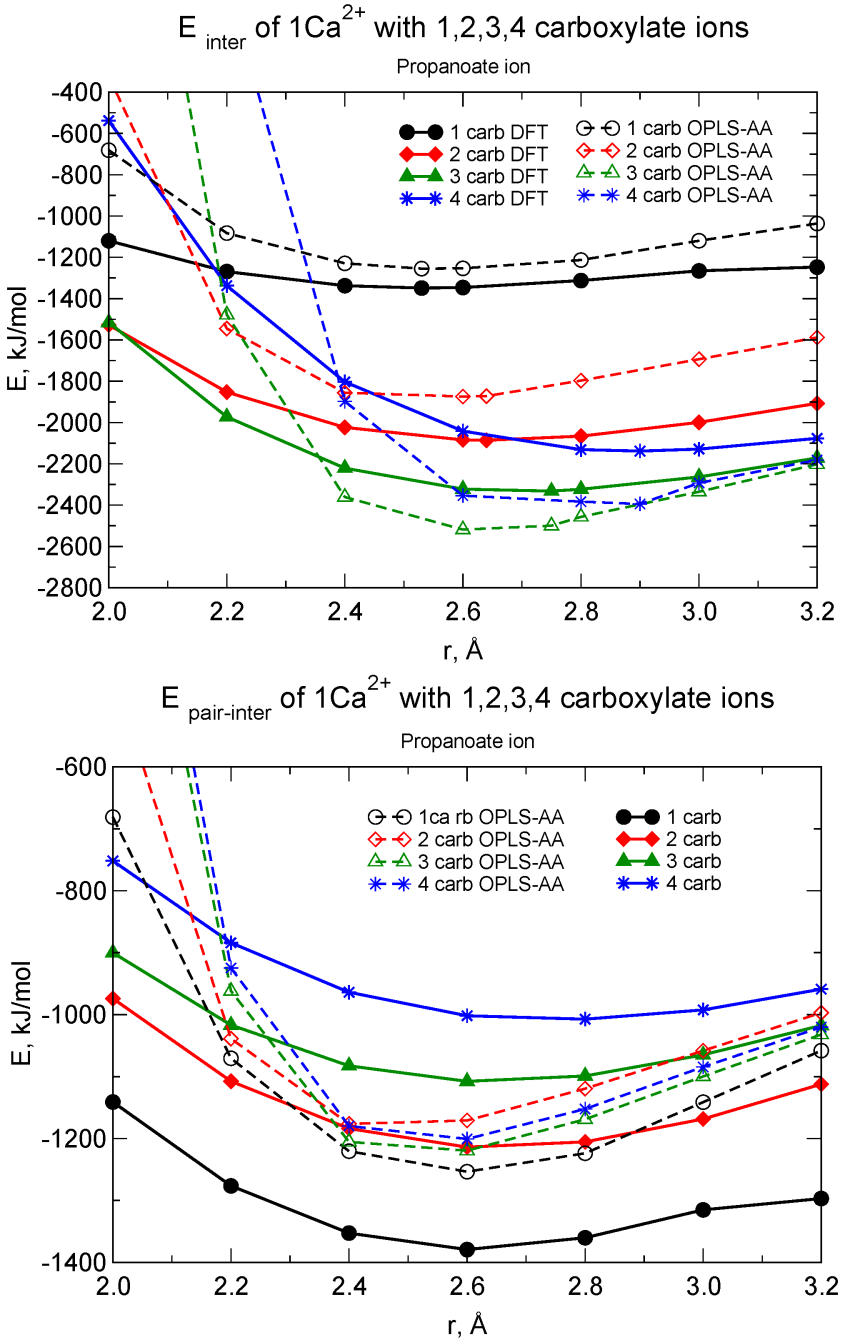

Figure 3.3: Comparison between the DFT (solid lines) and the MM (dashed lines) total interaction energies, $E(r)_{inter}$, (top) according to Equation 3.1 and pair-interaction energies, $E(r)_{pair-inter}$, according to Equation 3.2 (bottom) between complexes with 1 (black), 2(red), 3(green), 4(blue) carboxylate groups and Ca^{2+}.

Table 3.2: Molecular mechanics parameters, Lennard-Jones and electrostatic interactions.

Atoms	(i) and (ii)		OPLS-AA (i)	Yan [55] (ii)
	σ (nm)	ϵ (nm)	q (e^-)	q (e^-)
C (in -CH_3)	0.350	0.27614	-0.18	-0.18
C (in -CH_2-)	0.350	0.27614	-0.22	-0.12
H	0.250	0.12552	0.06	0.06
C (in -COO^-)	0.375	0.43932	0.70	0.91
O (in -COO^-)	0.296	0.87864	-0.80	-0.84
Na^+	0.333	0.01160	1.00	1.00
Ca^{2+}	0.241	1.88130	2.00	2.00

Table 3.3: Partial atomic charges calculated with Natural Bond Orbital (NBO) analysis method.

	Complex with 1 carboxylate	Complex with 2 carboxylates	Complex with 3 carboxylates	Complex with 4 carboxylates
Ca^{2+}	1.76	1.68	1.56	1.49
COO^-	-0.84	-0.84	-0.80	-0.77
C (from -COO^-)	0.82	0.79	0.78	0.76
O (from -COO^-)	-0.83	-0.82	-0.79	-0.76

The potential curves for 1 and 2 carboxylates with Ca^{2+} and Na^+ have been calculated for separation distances between 2 and 20 Å and are presented in Figures 3.4 and 3.5 along with the molecular geometries at selected separation distances. In the plots, the red star symbol (*) implies that the potential curves are derived with the relaxed scan procedure - optimizing the geometry of the complex for every step while the distance between the ion and the carbon atom in the carboxylate group are kept constant. The results suggest that near the equilibrium distance, the charge transfer favors the stabilization of the complex and, thus, lowers the total interaction energy. On the other hand, at distance around 6 Å the DFT and the MM potential curves start to diverge and the interaction energy does not converge to 0 in the case of DFT as seen from Figure 3.4(a). It has been found that due to the DFT gas phase calculations, the charge on the calcium ion for separation distances above 6 Å is +1, which leads to different dissociation of the charges than the liquid systems we want to investigate. The carboxylate - calcium complex in water solution dissociates to the following partial charges: -1 located on the carboxylate and +2 on the calcium ion, respectively, and since the OPLS-AA force field is parameterized for liquid simulations we constrain the charges to mimic dissociation in a liquid phase. In order to reproduce exactly the dissociation of the charges in

the complex at longer distances and to compare the tail of the interaction energy directly with molecular mechanics, constrained density functional theory (CDFT) [58, 59] calculations have been carried out. In CDFT, the electron population of the calcium and sodium ions has been constrained so their charge has been kept fixed during the optimization of the complex and, thus, the charge transfer between the ions and the carboxylate group has not been allowed. That could consequently affect the potential curves as can be seen later, in the sense that the potential curves converge to 0 at high separation distances. The calcium and sodium charges have been constrained to +2 and +1, respectively. The black circles (o) in Figures 3.4 and 3.5 represent the CDFT potential functions. By blocking the charge transfer between the carboxylate group and the counter ion, the potential curve asymptotically converges to 0. However, at the equilibrium distance, an underestimation of the potential well of about 200 kJ/mol has been recorded with a shift of the equilibrium distance towards higher distances - from 2.53 Å to 2.71 Å in the complex with 1 carboxylate and 1 Ca^{2+}; from 2.64 Å to 2.78 Å in the case with 2 carboxylates and 1 Ca^{2+}; from 2.5 Å to 3.1 Å for the complex with 1 carboxylate and 1 Na^{+} and from 2.65 Å to 3.26 Å in the case of 2 carboxylates and 1 Na^{+}.

The MM potential should accurately represent the interactions around the equilibrium distance as well as at higher separations. Around the equilibrium distance, the MM potential should be compared with the relaxed scan curve (*), where the charge transfer is allowed and for longer separation distances it should match the CDFT curve. In the cases with 1 carboxylate, the original OPLS-AA potential is shown to be the closest to the obtained DFT potential curves. This potential shows an underestimation of the interactions of about 100 kJ/mol at the equilibrium distances (the minimum in the potential well), while using the parameters from Reference [55] showed an even greater discrepancy - about 300 kJ/mol. On the other hand the tail of the potential curve (high separation distance) is well matched by the OPLS-AA FF. For the case of 2 carboxylates and 1 calcium, the original parameters of OPLS-AA once again matched the DFT calculated interactions better. However, the difference in the depth of the potential well between DFT and MM is slightly more, about 200 kJ/mol, compared to the case of 1 carboxylate. The tail of the potential has shifted to lower energies. The parameters of Yan et al.[55] are shown to shift the whole potential to higher interaction energies compared to the original ones.

The potential curve for sodium and 1 carboxylate, Figure 3.5(a), is perfectly matched by the original parameters of OPLS-AA for the whole range between 2 Å and 20 Å. The MM potential overlaps with the DFT derived one for short separation distances and with the CDFT for long separation distances. The Yan et al.[55] parameters underestimated the potential depth by approximately 100 kJ/mol. The equilibrium

distance of the complex with 1 carboxylate as depicted in Figure 3.5(a) is 2.5 Å, for both DFT and MM. For the case of 2 carboxylates, the DFT potential falls between the two MM potentials where the OPLS-AA parameters overestimate the interaction energies by 50 kJ/mol and the Yan et al.[55] parameters underestimate the interaction energies by 50 kJ/mol. The equilibrium distance of the complex with 2 carboxylates is 2.65 Å, for both DFT and MM.

In the cases with calcium at distance around 3.4 Å, the ion coordinates itself to only one of the oxygens, which gives a little plateau and changes the potential curves around that distance. This is observed for both the constrained and unconstrained DFT potential functions. At longer separation distances above 10 Å, the coordination of the counter ion has been found to be the same as near the equilibrium distance - directly opposite to the carbon atom and at equal distance to the oxygen atoms. The same coordination phenomenon has also been observed in the cases for the sodium ion. However, due to a weaker interaction, the impact on the shape of the potential function is not so significant compared to calcium. In the case of 1 acid and 1 Na^+, the change of the coordination of the sodium to only one of the oxygens does not affect the shape of the potential curve as much as compared to calcium. In the case of 2 acids and 1 Na^+, the difference in the coordination seems not to affect the shape of the potential curve at all and the observed plateau in the previous cases does not exist.

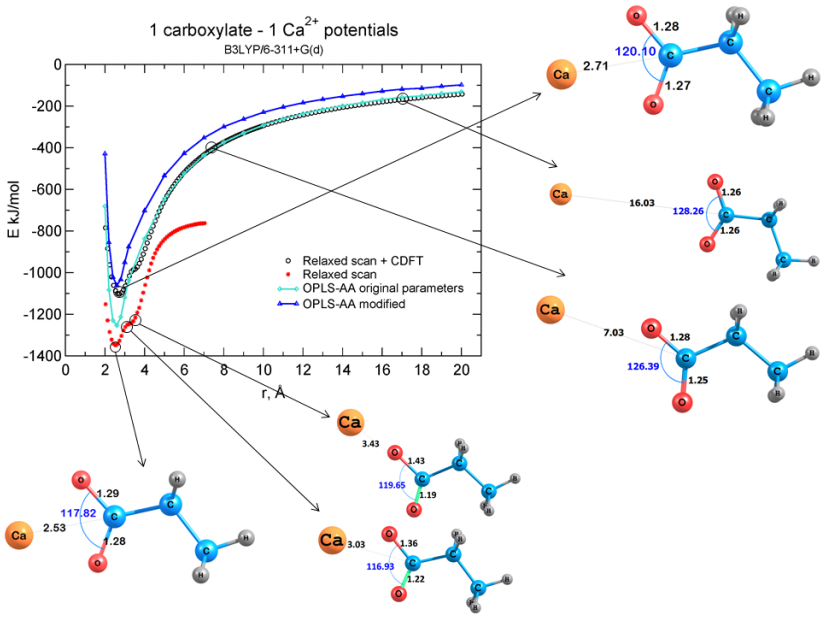

(a) 1 carboxylate - 1 Ca^{2+}

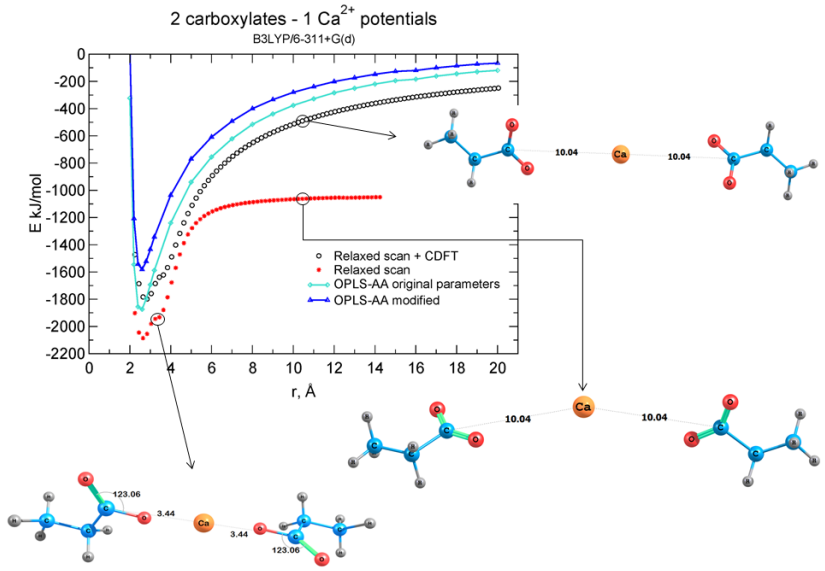

(b) 2 carboxylates - 1 Ca^{2+}

Figure 3.4: Potential energy curves and molecular structures of 1 carboxylate-1 Ca^{2+}. DFT curves, red stars - relaxed scan, black circles - relaxed scan with CDFT B3LYP/6-311+G(d). MM curves - OPLS-AA original set of parameters, OPLS-AA modified

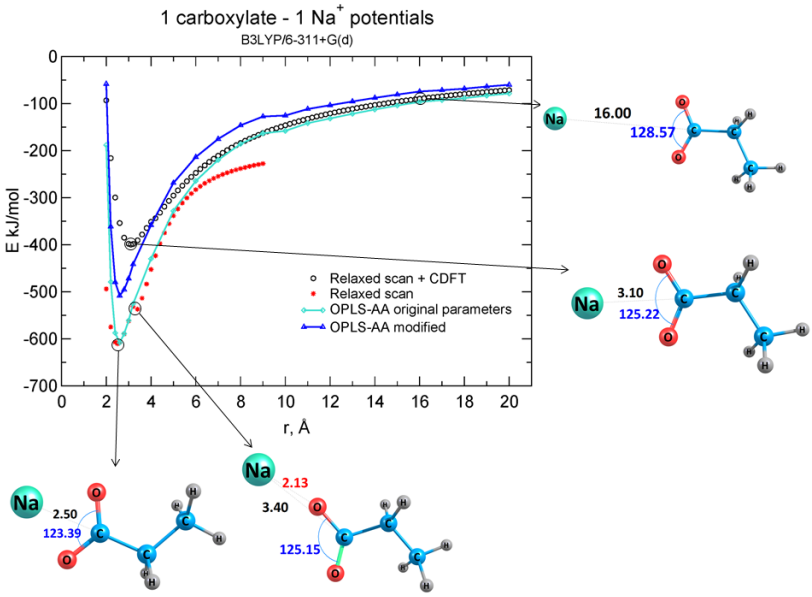

(a) 1 carboxylate - 1 Na^+

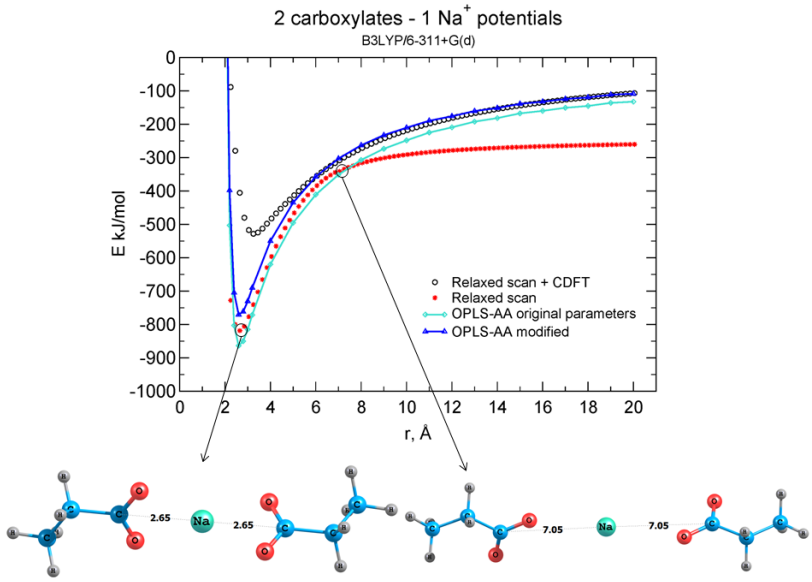

(b) 2 carboxylates - 1 Na^+

Figure 3.5: Potential energy curves and molecular structures of 1 carboxylate-1 Na^+. DFT curves, red stars - relaxed scan, black circles - relaxed scan with CDFT B3LYP/6-311+G(d). MM curves - OPLS-AA original set of parameters, OPLS-AA modified

2 BOMD calculations in water phase

The interactions between 1 carboxylate and 1 divalent metal ion in water are further investigated by performing BOMD simulations. We have calculated the interaction energies between 1 propanoate and 1 Mg^{2+}, Ca^{2+}, Sr^{2+} and Ba^{2+} by thermodynamic integration. Furthermore, we have carried out extensive analysis of the simulation trajectories in order to obtain more detailed mechanism of the interactions. That includes, calculation of the water binding energies, self-diffusivity and mobility of ions, radial distribution functions and water coordination numbers and exchanges of water molecules in the first solvation shell of the ions during the simulations. The water binding energy is depicted in Figure 3.6 and is calculated by:

$$\triangle E = E\{M(H_2O^{2+}_{n-1})\} + E(H_2O) - E\{M(H_2O^{2+}_{n})\} \tag{3.3}$$

The first term on the right is the energy of the metal ion-water complex with $(n-1)$ water molecules, the second is the energy of an isolated water molecule and the third term is the energy of the metal ion-water complex with n water molecules.

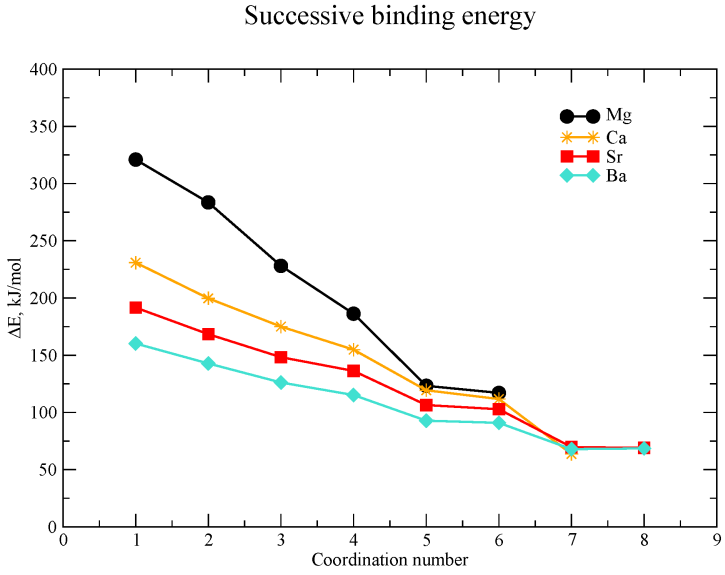

Figure 3.6: Successive water binding energy as a function of the coordination number.

From Figure 3.6, it can be seen that the magnesium ion has the highest successive binding energies with water amongst the studied ions, followed by calcium,

strontium and barium. The highest change in the successive binding energy by adding more water molecules to the first solvation shell is for the magnesium ion, which can be seen from the most negative magnitude of the average slopes of the curves in Figure 3.6. The average slope represents the average change in energy for adding or removing water molecules. For the calcium ion the magnitude of the average slope is 41% lower compared to magnesium, while the slope is 57% lower for strontium and 67% lower for barium compared to magnesium, respectively. The first water molecule successive binding energies differ amongst the different ions. The values for Mg^{2+}, Ca^{2+}, Sr^{2+} and Ba^{2+} are 320.9, 230.9, 191.6 and 160.2 kJ/mol, respectively. The successive binding energies of the fifth, sixth and, especially, the seventh and eight water molecules binding energies are almost the same. It appears that the binding energies follow the group trend and the smaller ions from the second group in the periodic table have higher binding energies. Therefore, the smaller 2^{nd} group ions appear to form stronger complexes with the water molecules. The slopes of the curves in Figure 3.6 combined with the water binding energies imply that the magnesium ion attracts the water molecules more strongly.

The metal ion - water radial distribution functions (RDF) without and with presence of the carboxylate ion have been calculated and presented in Figure 3.7. he RDF is denoted as $g(r)$ and constructed based on the separation distance between the metal ion and the oxygen atom of the water molecule. The magnesium ion has the most compact solvation shell which can be seen from the distance at which the first solvation shell peak appears. The peak magnitude is highest for Mg^{2+} and lowers in the order $Ca^{2+} > Sr^{2+} > Ba^{2+}$. Beside the magnitude, the first peak is also narrower for the small ions and it becomes wider for the larger ions. The coordination number of water molecules increases with increasing ionic radius. These observations imply that the smaller ions have stronger interactions with the water molecules, as seen also from the magnitude in Figure 3.6, and also that the structure of the first solvation shell around the small ions is more compact compared to the larger ones. It can also be seen from Figures 4a) and b) that when the metal ion is in a complex with carboxylate, its water coordination number is lower. It is also apparent from Figure 4b) that the first solvation shell for Ca^{2+} became more compact and the peak has moved to shorter distances in the presence of the carboxylate, which means that its hydrodynamic radius [60] has decreased.

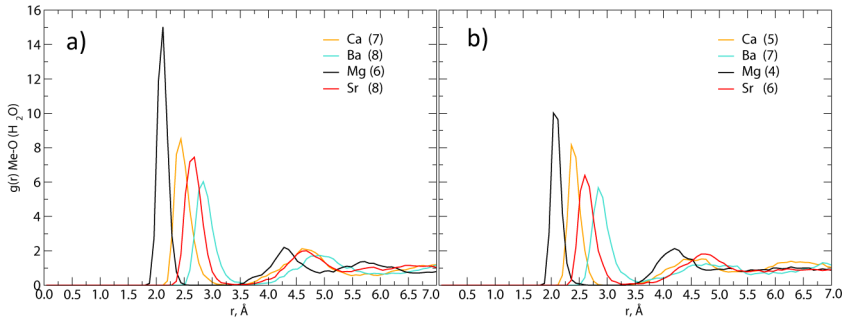

Figure 3.7: Radial distribution functions between a given metal ion and the oxygen from the water molecules a) without carboxylate, b) in the presence of carboxylate. In the legend, the coordination number of the respective ions is given in parenthesis.

The self-diffusion, mobility coefficients and number of exchanges of solvent molecules in the first solvation shell of the metal ions have been calculated and presented in Table 3.4. The self-diffusion coefficients have been calculated by the mean square displacement and the Einstein relation:

$$D = \lim_{t \longrightarrow \infty} \frac{1}{6Nt} \left\langle \sum_{i=1}^{N} [r_i(t) - r_i(t_0)]^2 \right\rangle \tag{3.4}$$

where N is the number of molecules, t is time, $r_i(t)$ are the spatial coordinates at time t and $r_i(t_0)$ are the coordinates at time t_0. The ion mobilities are calculated from the self-diffusion coefficients by:

$$u = \frac{Dq}{k_b T} \tag{3.5}$$

where k_b is the Boltzmann constant, T is the temperature and q is the charge of the ion. The values of D and u for the ions decrease with the ionic radius from Ba^{2+} to Mg^{2+} , as seen from Table 3.4. The same trend for the self-diffusion coefficients of the divalent ions in water at 298.15 K has been reported by Buffle et al. [61] When the metal ions are in the complex with the carboxylate, the self-diffusion and the mobility coefficients decrease, except in the case of Ca^{2+}, which has increased. The increase of the self-diffusion and the mobility coefficients can be associated with the decrease of the hydrodynamic radius observed in Figure 3.7 in the presence of carboxylate, since the hydrodynamic radius is inversely proportional to the diffusion coefficient.

It can also be observed from Table 3.4 that the smaller ion, Ca^{2+} and Mg^{2+}, have significantly less exchanges in their first solvation shell. That is consistent with

the results for the successive binding energies presented in Figure 3.6, where the smaller ions (Ca^{2+}, Mg^{2+}) have higher binding energies and the water molecules are strongly bound to them. That implies that the interchange of water molecules in the first solvation shell is easier and happens relatively more frequently for the larger ions.

Table 3.4: Calculated self-diffusion coefficients, mobility, and number of exchanges of the water coordination shell for the metal ions with and without carboxylate.

	Ion without COO^-				Ion with COO^-			
	Ba^{2+}	Ca^{2+}	Mg^{2+}	Sr^{2+}	Ba^{2+}	Ca^{2+}	Mg^{2+}	Sr^{2+}
$D(10^{-10}m^2/s)$	6.59	2.16	0.68	2.84	4.52	5.17	0.0003	1.73
$u(10^{-8}m^2/Vs)$	5.10	1.69	0.53	2.19	3.49	3.99	0.0002	1.34
Change in coordination	11	2	0	8	31	0	0	16

In Figure 3.8 and Table 3.5, the interaction free energies and free energy barriers between the carboxylate group and a given metal ion are presented. The free energy profiles have been obtained by calculating the force by keeping the distance between the carbon atom from the carboxylate group and the metal ion fixed between 2 and 6 Å at intervals of 0.25 Å. Then the force has been integrated according Equation 2.21. The highest interaction energy is with Mg^{2+} followed by Ca^{2+}, Sr^{2+} and Ba^{2+}. The free energy barrier also increases in the same order. These observations of the potential curves could partially explain the selectivity of the reaction for calcium-naphthenate precipitation. Since the free energy barrier is higher for Sr^{2+} and Ba^{2+}, the possibility of reaction with carboxylate ions is much lower compared to Ca^{2+} and Mg^{2+} and, therefore, the formation of precipitates with Sr^{2+} and Ba^{2+} should not be very likely. As seen from the potential curves, the magnesium interaction free energy is 4 times greater than the calcium interaction free energy and, moreover, there is no free energy barrier, which suggests that the carboxylate preferably would undergo a reaction with magnesium rather than with calcium, which contradicts the experimental findings.

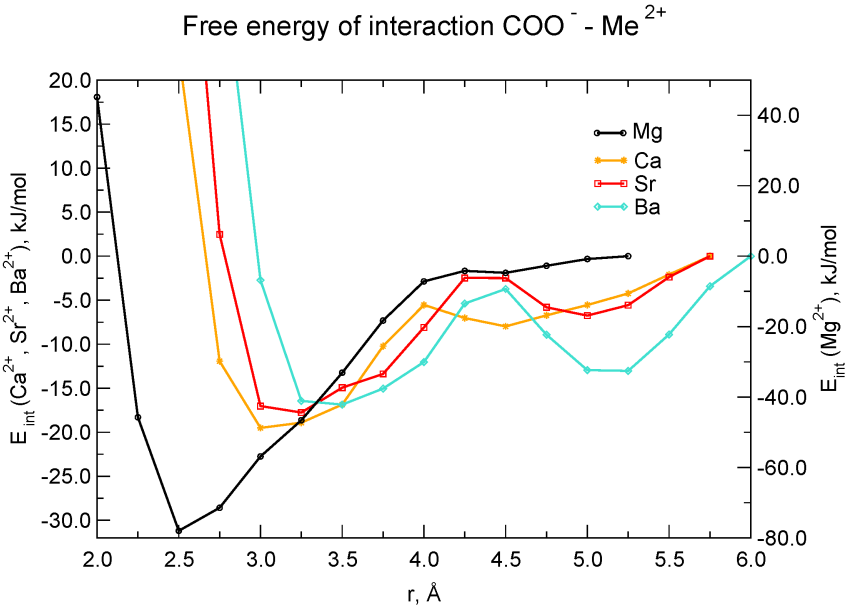

Figure 3.8: Helmholtz free energy, E_{int}, curves of the metal ion - carboxylate ion complex in solvent. The distance in the abscissa is given in Å and represents the distance between the metal ion and the carbon atom from the COO^- group. Along the right ordinate axis the interaction free energy with the magnesium ion is given and along the left ordinate axis the interaction free energy with the other ions is given.

Table 3.5: Calculated Helmholtz free energy and free energy barriers for the carboxylate - metal ion interaction.

Ion	Free energy, kJ/mol	Free energy barrier, kJ/mol
Mg^{2+}	-77.99	0.56
Ca^{2+}	-19.50	2.43
Sr^{2+}	-17.76	4.26
Ba^{2+}	-16.86	9.30

In Table 3.6, the number of exchanges of water molecules in the first solvation shell has been reported for separation distances from 2 Å to 6 Å. For the divalent ions, most exchanges are found for the bigger ions, Ba^{2+} and Sr^{2+} , compared with the small ones (Mg^{2+} and Ca^{2+}). The magnesium does not exchange water molecules (for the present simulation time) except for at separation distances of 3 Å and 3.25 Å, where only 1 and 2 exchanges have been observed, respectively.

The calcium ion has exchanged water molecules significantly more often compared to magnesium. The strontium and barium ions exchange water molecules in their first solvation shell more frequently, which can also be correlated with the successive hydration energy, although it has been derived for 0 K and the molecular dynamics simulations are performed at 300 K. Since the successive water binding energy between Mg^{2+} and water is strongest and decreases in the order of Ca^{2+}>Sr^{2+}>Ba^{2+} it is expected to see an increase of water exchanges going in the opposite direction Ba^{2+}>Sr^{2+}>Ca^{2+}>Mg^{2+}, which can be observed in Table 3.6. The reluctance of Mg^{2+} to exchange water molecules could suggest that there is a lower probability that the metal ion will be associated with a second carboxylate group. The magnesium needs to lose some of the water molecules coordinated around it in order to be able to coordinate an additional carboxylate group. As we also can see from Figure 3.6, the change in the coordination to a lower number of water molecules is not energetically favourable compared with the other divalent ions, because of the steepest average slope of the curve. Moreover, the ionic radius of the magnesium is the smallest of all the divalent ions studied here and sterically it cannot sustain the possibility to coordinate many functional groups with bigger van der Waals radii. The mobility coefficient of the magnesium is also lower in magnitude compared with the calcium, especially in the presence of COO^{-}. All of the above observations suggest that the calcium ion could have more binding potential than the magnesium. That could explain the experimentally observed selectivity towards a reaction of the tetracarboxylic acids anions with calcium and the formation of naphthenate precipitates preferably with calcium and not with the other divalent ions.

Table 3.6: Number of exchanges of water molecules in the first coordination shell of the different metal ions. The constrained separation distance between the metal ion and the carbon from the COO^- group is given in the first column. Every distance in the first column represents different 12 ps simulations, respectively.

r, Å	Ba^{2+}	Ca^{2+}	Mg^{2+}	Sr^{2+}
2.00	-	0	0	-
2.25	-	0	0	-
2.50	8	0	0	8
2.75	25	0	0	0
3.00	3	8	1	0
3.25	18	1	2	8
3.50	21	10	0	10
3.75	4	1	0	15
4.00	1	0	0	2
4.25	0	4	0	34
4.50	12	0	0	25
4.75	35	1	0	13
5.00	30	8	0	6
5.25	18	12	0	2
5.50	37	18	0	21

In Figure 3.9, the above results are schematically summarized in an attempt to explain the specific ion selectivity. It should be noted that the scaling in the figure does not represent the true values and it is made just for clarity of illustration. The reported selectivity of the reaction between divalent metal ions with carboxylic groups shown in Figure 3.9 can be interpreted by considering that an increasing arrow indicates an increased value of the property which it describes. First, the factors determining the selectivity can be roughly divided into two groups: (i) the first group contains properties which promote the interaction between the metal ions and the COO^- group(s), such as the interaction free energy between the metal ion and the COO^- group along with the self-diffusion coefficient, and (ii) the second group contains the properties which weaken the interaction between the metal ion and the COO^- group, such as the interaction energy of the metal ion with the solvent molecules, the number of exchanges of solvent molecules and the energy free barrier for the Me^{2+} - COO^- reaction. The preference of binding Ca^{2+} instead of Sr^{2+} and Ba^{2+} could be explained by the fact that Ca^{2+} has a higher interaction free energy and lower free energy barrier for a reaction with COO^-. On the other hand, taking into account only those two properties suggest that Mg^{2+} would have higher binding probability when compared to Ca^{2+}. Thus,

a more detailed examination of the ion - solvent interactions must be considered in order to understand the experimental and simulation results for Ca^{2+} and Mg^{2+}. First, the successive binding energy of water molecules to the ion was examined, showing that Mg^{2+} has a much higher binding energy with water than Ca^{2+}. This potentially could affect the ion - water dynamics. That is exactly what has been shown from the number of exchanges for both ions, since Mg^{2+} has higher interaction energy with the water molecules, it has a lower amount of exchanges of water into its first solvation shell. This observation could become important when a second COO^{-} group is in close proximity to the ion, since with more exchanges of solvent molecules there is a higher probability for this second COO^{-} group to bind with the ion. Finally, the self-diffusion coefficient of Ca^{2+} is higher than that of Mg^{2+}, which in solution indicates that Ca^{2+} is a more mobile ion compared to Mg^{2+}. This means that when the two metal ions (Ca^{2+}, Mg^{2+}) are present in solution, most likely Ca^{2+} will be able to diffuse faster to any available COO^{-} groups, especially for tetracarboxylic acids adsorbed at an oil-water interface where transport dynamics should affect the selectivity. However, it should be pointed out that some of the estimated features, such as the interaction free energy and the free energy barrier or the water binding energies and number of exchanges of water molecules, are strongly interrelated, so conclusions about one of them naturally applies to the others.

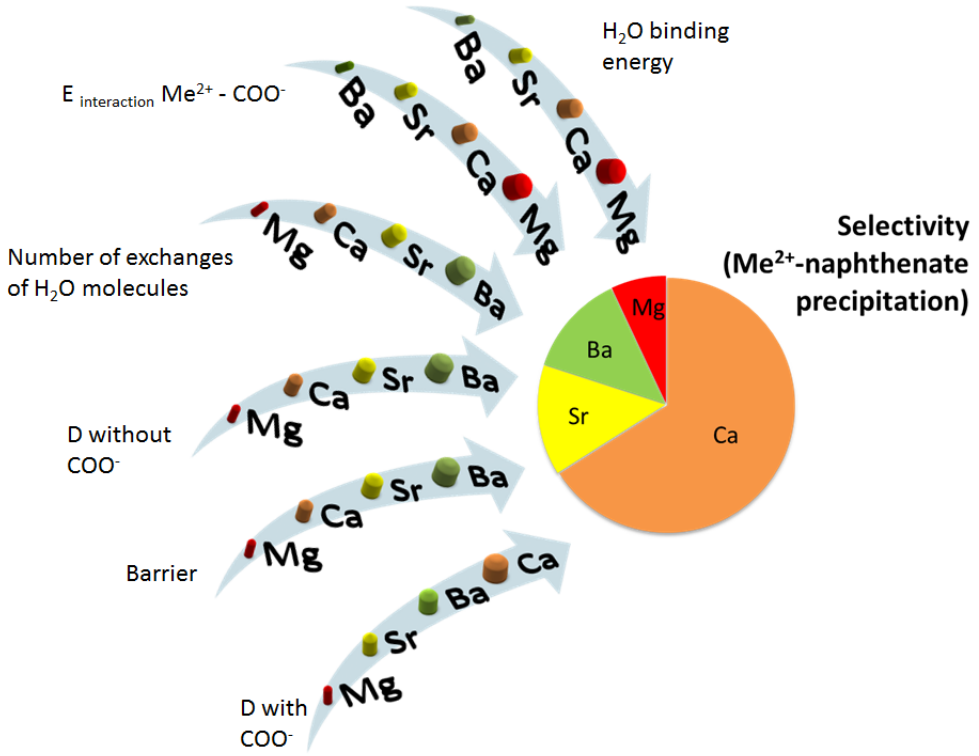

Figure 3.9: Schematic summary of the Me^{2+} - COO^{-} selectivity. The scaling does not represent the true values.

3 Calculation of the probability of reaction with umbrella sampling

The probability of reactions between two carboxylate groups with one metal ion as a function of the distance between the carboxylates have been calculated by umbrella sampling. We already saw that OPLS-AA represents well the potential functions in terms of equilibrium distances between carboxylates and divalent metal ions. Therefore, we have used it to obtain the probability for reaction. The initial configuration for the umbrella sampling is shown in Figure 3.10. In the initial configuration of the complex, the carboxylates are in opposite position with respect to each other with point group symmetry C_{2h}. The complex is centred in the geometrical centre of the simulation box and the coordinates of the metal ion have been frozen. Umbrella potentials have been imposed at the centre of mass (COM) of the two carboxylate groups by employing a harmonic potential with a force constant of 2000 kJ/mol. We have performed 14 simulations per ion where

every simulation has been 1.2 ns long from which the last 1.0 ns has been used for the production run. The umbrella windows have been separated by 0.25 Å starting from 2 Å as depicted in Figure 3.10. In that way we have initial separation distances between the carboxylates of 4.0, 4.5, 5.0, 5.5, 6.0, 6.5, 7.0, 7.5, 8.0, 8.5, 9.0, 10.0, 12.0 and 14.0 Å. By imposing the umbrella potentials on the COM of the carboxylate groups and starting from opposite positions of the two carboxylates, we have assumed that the distance between the carboxylates would be double the distance between one carboxylate and the metal ion. By using the above assumption as well as the frozen position of the metal ion, we have assured that the two carboxylates are sampling equally the distances around the metal ion. In that way, we are avoiding the probability of only one of the carboxylates to interact preferentially with the metal ion, since the main objective is to find the probability for reaction as a function of the distance between the carboxylates, providing the requirement that the metal ion is interacting with both carboxylates at the same time.

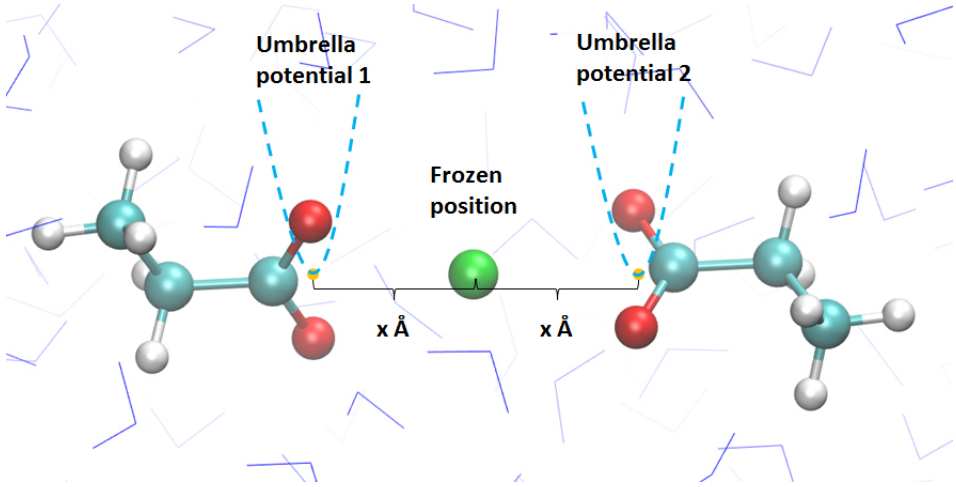

Figure 3.10: Initial configuration of the system. The initial distance between the two carboxylate groups has been set to 2 x Å and umbrella potentials have been applied to the centre of mass of both carboxylate groups. The carbon atoms are depicted in cyan, oxygen in red, hydrogen in white, the metal ion in green and the water molecules are depicted as blue sticks.

The probability of reaction as a function of the separation distance between the centre of masses of the carboxylate group is depicted in Figure 3.11. First it should be noted that the probability of reaction has been rescaled such that the highest peak takes the value of 1, because of its convenience for further use for the generation of the interface density maps discussed above. In both cases for Ca^{2+} and

Mg^{2+}, the probability of reaction has three distinct peaks with highest probability located at 4.53 Å and 3.65 Å, respectively. The probability of reaction for Ca^{2+} spans the region between 4.3 Å to almost 7 Å, while the probability of reaction for Mg^{2+} is located between 3.5 and 6.1 Å. However, the probability for calcium never quite goes to zero between the peaks, whereas the probability function for magnesium clearly goes to zero between the peaks in the regions between 3.8 - 4.2 Å and 5.0 - 5.7 Å. It can also be observed that the peaks for Mg^{2+} are narrower compared to Ca^{2+}, which has a wider probability distribution in all regions. According to a previous study magnesium has much higher interaction free energy and more tightly coordinated 1^{st} solvation shell compared to calcium which could also be a reason for the narrower distribution. That would mean the carboxylates would be more strongly attracted to the magnesium and most likely within shorter distances. However, from Figure 3.11 it can be seen that for calcium, the carboxylates have higher probability of binding to it, because of the non-zero values between the peaks and the broader span of the probability. Additionally from Figure 3.11, it can be inferred that the complexes are dissociated when the distance between the COM of the carboxylate groups is larger than 6.9 Å and 6.1 Å for calcium and magnesium, respectively. The probability of reaction also compliments the results showed above concerning the selectivity of the metal ions to react with carboxylate groups. The higher mobility, shown in the previous section implies that Ca^{2+} will diffuse faster to any available carboxylate groups compared to Mg^{2+}. Moreover, not only will diffuse faster, but also will bind the carboxylates when the distance between them is higher, because of the probability of binding is higher and spans to higher separation distances shown in Figure 3.11.

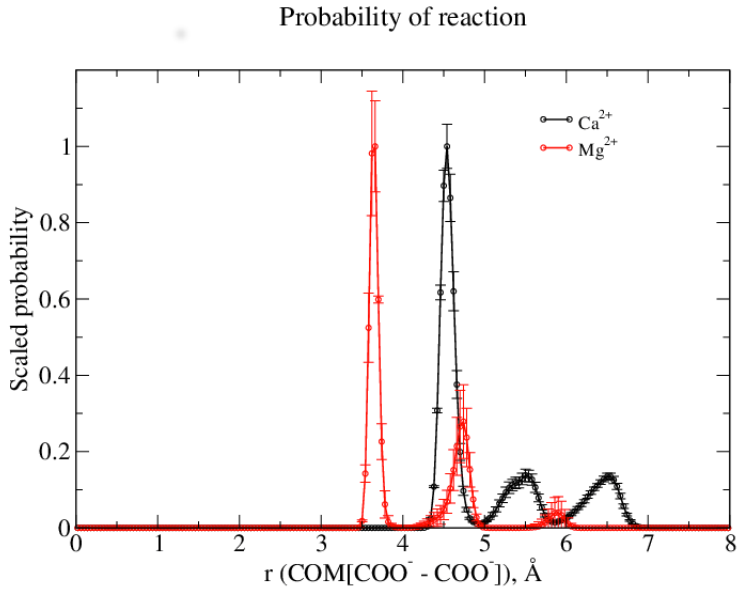

Figure 3.11: Probability of reaction as a function of the separation between the centres of masses of the carboxylate groups.

4 MD simulations and coarse-grain interface density maps

We have performed MD simulations of ARN and BP10 at an oil-water interface in the presence of calcium ions in the water phase. Then based on MD generated structural probabilities of ARN and BP10, we have constructed a coarse-grain interfacial maps of COO^{-} groups which we used to obtain the functionality of $f_p(\Gamma_{TA})$. $f_p(\Gamma_{TA})$ could be used in the multiscale approach of Kovalchuk et al.[34] to calculate the the mass of calcium-naphthenate precipitates produced per unit process volume.

In Figure 3.12 snapshot from the MD simulations are depicted and a cross-linked network of ARN molecules can be observed and are highlighted in red. The molecules are cross-linked through their carboxylate groups interacting with the calcium atoms which are depicted in yellow. That is one possible configuration of a cross-linked network at the interface and there are more cross-linked molecules in the same simulation, but for clarity only one has been highlighted. Practically, one MD simulation could present only one configuration of the interface density or cross-linked network, therefore it will be very computationally expensive to simulate many different systems in order to have statistically reliable results for the

fractional conversion of the tetra-acid molecules to calcium-naphthenate precipitates. Thus, a coarse-grain representation of the interfacial density based on the MD derived probabilities could be more computationally effective to calculate the fractional conversion $f_p(\Gamma_{TA})$.

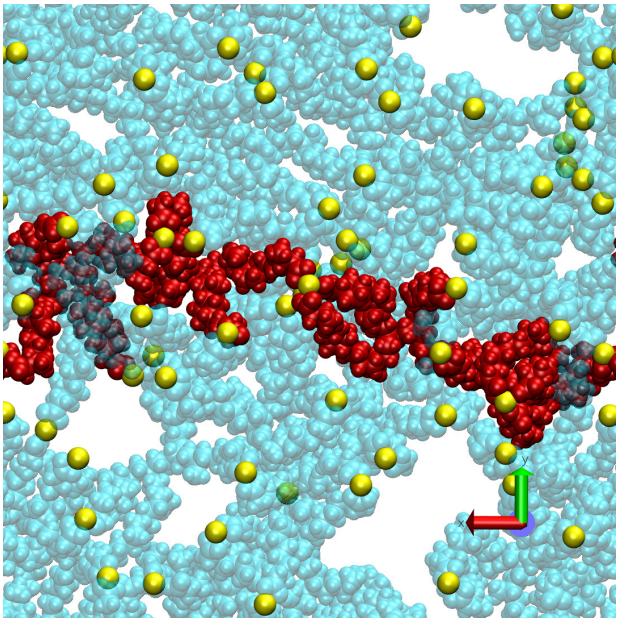

Figure 3.12: Top view of the cross-linked network from the MD simulations. A cross linked-network of ARN molecules is highlighted in red.

We have first carried out MD simulations of ARN and BP10 at an oil-water interface and obtained the structural probability functions described previously by Riccardi et al.[32] In Figure 3.13 the probability distribution functions (PDF) used for generating the coarse-grained interface density maps are shown. The arm vector lengths are generated according to the PDF depicted in Figure 3.13(a). The arm vector lengths are considered to originate from the nearest carbon atom linking the hydrocarbon chains in the case of ARN and from the oxygen atoms linking the benzophenone core in the case of BP10 [18, 32] and to terminate at the carboxylate groups, respectively. The vertical orientation angle is the angle formed by the arm vector and a plane parallel to the oil-water interface and is depicted in Figure 3.13(b). The positive values in Figure 3.13(b) imply that the arm vector points toward the water phase and the negative value to the oil phase, respectively. From Figure 3.13(b) can be seen that the preferable orientation of the molecule arm is toward the water phase, which is due to the fact that the carboxylic acid arms are

deprotonated and are orientated towards the more polar phase. The horizontal orientation angle of the molecular arms is presented in Figure 3.13(c). The horizontal angle is calculated by arbitrarily choosing a single arm vector of the tetra-acid molecule and the distribution of the remaining arms is plotted versus the angle between the selected arm group and the other arm groups in the plane parallel to the oil-water interface. It can be also observed from the horizontal angle distribution that the there is an increase in the probability between -60° to +30°, but is a uniform distribution otherwise. The increased probability would mean that there will be aggregation of more arms to each other most likely because of hydrophilic interactions between the hydrocarbon chains. The intra-molecular COO^- groups distance has been used as a criteria to accept the xy-positions of the COO^- groups and is presented in Figure 3.13(d).

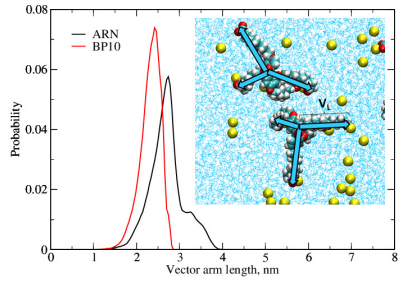

(a) Vector arm length

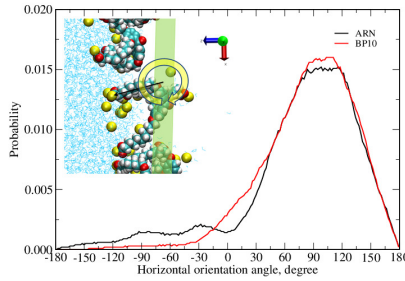

(b) Vertical orientation

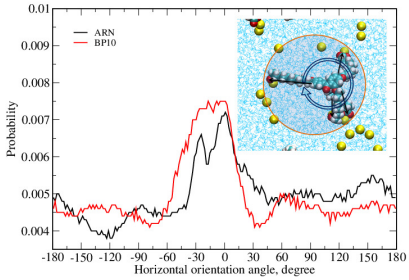

(c) Horizontal orientation

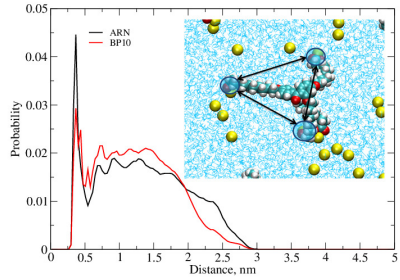

(d) Intra-molecular COO^- - COO^- distances

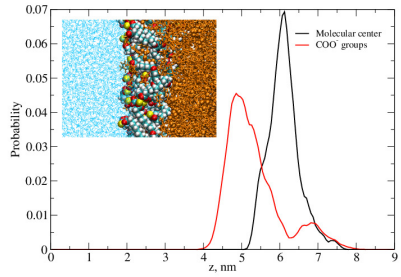

(e) z-position of ARN

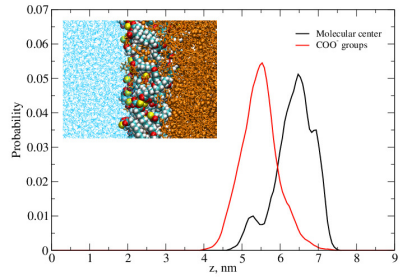

(f) z-position of BP10

Figure 3.13: Probability distribution functions used to generate the carboxylate groups.

To determine how many carboxylate groups are cross-linked we have used the probability of reaction as a function of the distance between two carboxylate groups, which is presented in Figure 3.14. If the distance between the carboxylate groups

are within the distance span of the PDF in Figure 3.14 the respective site is marked as a cross-linked place. In that way we can generate a sufficient number of random static 3D coarse-grain interface maps COO^- groups based on the MD simulated structural probabilities from which the fractional conversion as a function of the interfacial concentration has been calculated.

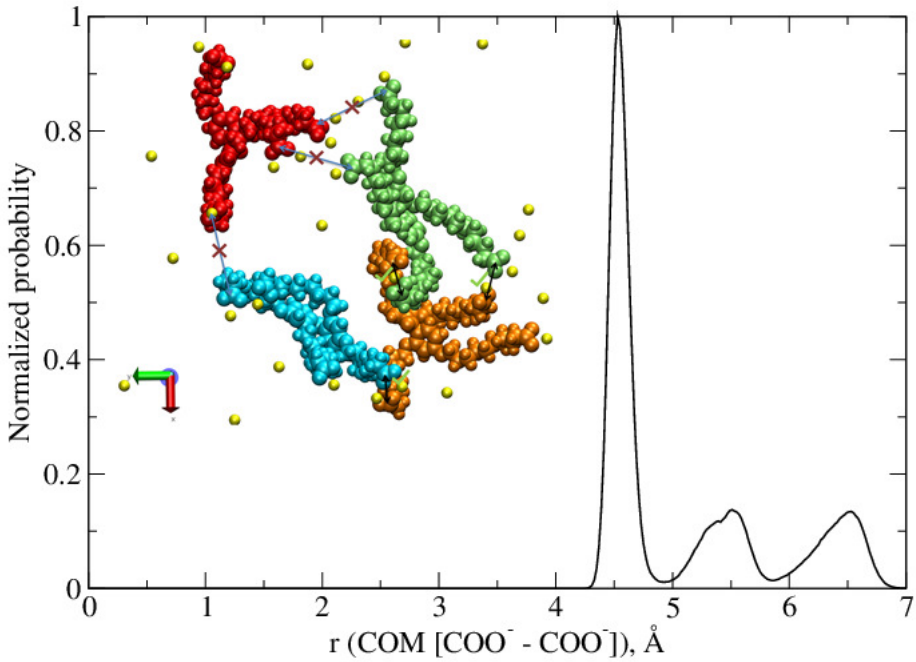

Figure 3.14: Probability of reaction between Ca^{2+} and two COO^- groups as a function of the distance between COO^- - COO^-.

Next, the coarse-grain representation ("interface map") of the interface region and the derived fractional conversion of tetra-acids to calcium-naphthenate precipitates is discussed. In the previous section it has been discussed how the interface maps have been built from MD simulation derived probabilities explicitly accounting for the solvents (oil-water interface region) and the calcium ions. Therefore, the interface maps build in a Monte Carlo like approach implicitly include the solvent and the calcium ions effects.

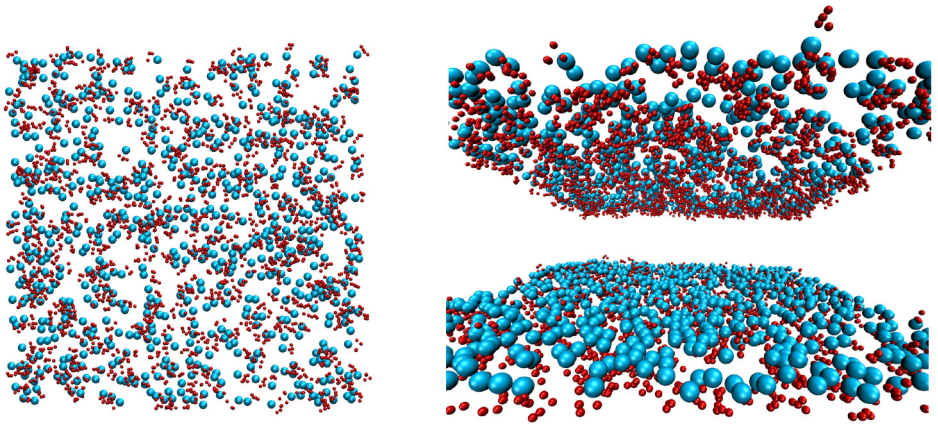

Figure 3.15: Generated interface density map of ARN with Γ_{TA}=0.0687 mol/nm^2. The molecular centers are depicted in blue and the carboxylate groups in red.

In Figure 3.15 an example of an interface map created for the ARN molecule is presented for an interfacial concentration of 0.0687 molecules/nm^2 as an example. The molecule centers are depicted in blue and the carboxylate groups in red. In order to analyse the sensitivity of the behavior with respect to the number of interface maps we have generated 50, 100 and 500 interface maps for every concentration and have calculated the fractional conversion for ARN and BP10 based on their average. The results are presented in Figure 3.16(a) for ARN and Figure 3.16(b) for BP10. First, it can be noted that the results for ARN and BP10 are very similar to each other, since BP10 has been designed to have similar interfacial properties as ARN. A second observation is that averaging over 50 maps gives fluctuation in $f_p(\Gamma_{TA})$, while generating at least 100 maps provides a smoother prediction of $f_p(\Gamma_{TA})$. The fractional conversion appears to increase from 0 to 1 non linearly, but not sigmoidally as assumed by Kovalchuk et al. [34] At 50% surface concentration about 24% of the tetra-acid molecules are converted and the conversion rises to 50% for 70% of surface concentration.

In Figure 3.17 the number of intra- and inter-molecular cross-linked sites as a function of the interfacial concentration for ARN and BP10 and averaged over 500 maps are presented. BP10 overall has more cross-linked sites, both intra- and inter-molecular. The intra-molecular bonding sites are dominating the inter-molecular bonding sites for both TA molecules. The increase of intra-molecular bonding sites is linear with the increase of Γ_{TA}, while the inter-molecular sites are increasing non-linearly.

The MD simulations sampled numerous geometric configurations of the tetra acid

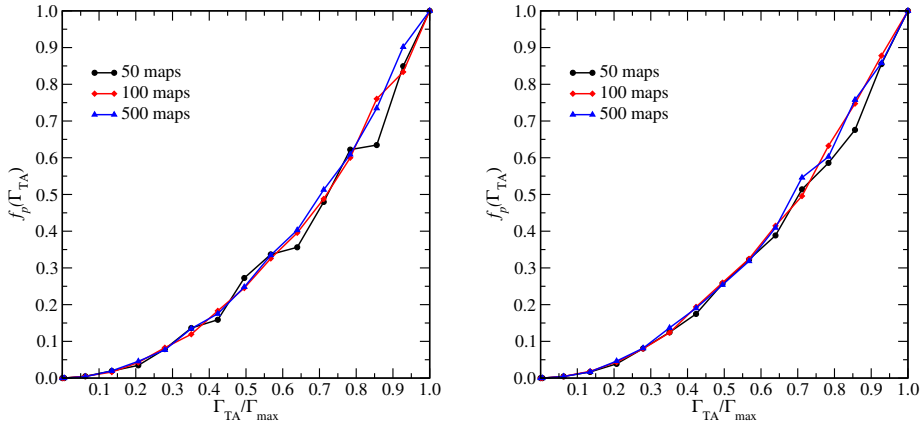

(a) Fractional conversion of ARN (b) Fractional conversion of BP10

Figure 3.16: Fractional conversion ($f_p(\Gamma_{TA})$ of ARN and BP10 to calcium-naphthenate precipitates as a function of the interfacial concentration (Γ_{TA}).

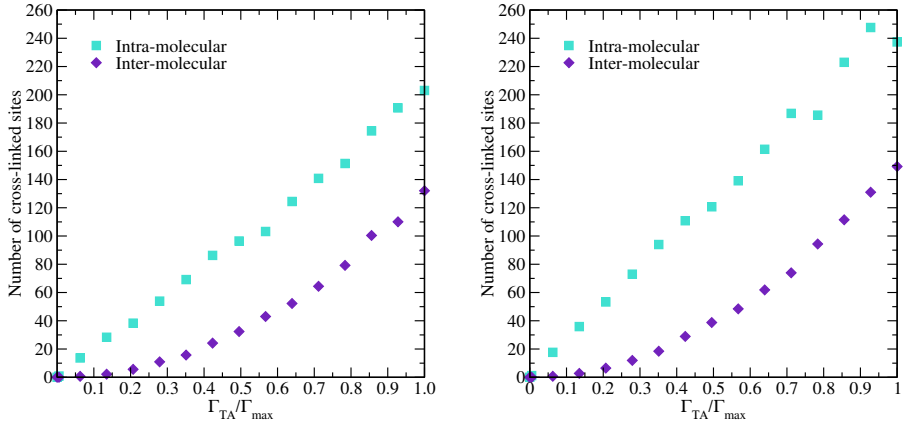

(a) Cross-linked sites of ARN (b) Cross-linked sites of BP10

Figure 3.17: Number of cross-linked intra- and inter-molecular sites of ARN and BP10 as a function of the interfacial concentration (Γ_{TA})

molecules at the oil water interface and indicate that for any carboxylate group, three of the nearest neighbours will most likely be carboxylate groups from the same tetra acid molecule. Figures 3.13(f) and 3.14 clearly indicate that carboxylate groups from the same parent molecule are very likely to be within the mutual displacement range where bonds can form with calcium. The results in Figure 3.17 clearly show that the bonds between carboxylate groups are predominately between carboxylate groups in the same molecule (e.g., not a cross-linked calcium naphthenate precipitate). The linear trend for the intra-molecular bonds in Figure 3.17 should be expected since the relative displacement between carboxylate groups within the same tetra carboxylic acid molecule is not strongly affected by the interfacial concentration of all tetra acids. [32, 33] Increasing the interfacial concentration of tetra acid molecules increases the probability that the set of nearest carboxylate neighbours within the range necessary to form a bond with a given carboxylate will contain an increasing number of carboxylate groups from other tetra acid molecule in addition to the 3 carboxylates attached to its parent molecule. Thus, as one approaches the upper bound of the interfacial concentration domain, the available sites for cross-linking only increase relative to the 3 intramolecular binding sites. Clearly, this would lead to an increased probability to form cross-linked bonds as one approaches the upper bound of the Γ_{TA}/Γ_{max} domain unless there is a bias to form intramolecular bonds. However, Figure 3.17 indicates that intramolecular bonding is not biased to increase from its linear trend near the upper bound of the Γ_{TA}/Γ_{max} domain. Consequently, based on the results presented here, one should not expect a sigmoidal shape for the functional form of $f_p(\Gamma_{TA})$ as assumed by Kovalchuk et al.[34] because a sigmoidal functionality for $f_p(\Gamma_{TA})$ would imply that the probability to cross-link two different parent TA molecules would have to steadily decrease from the inflection point of the sigmoid to the upper bound of the Γ_{TA}/Γ_{max} domain.

Chapter 4

Conclusions and future work

The aim of this work is to theoretically study and advance the basic knowledge of the calcium naphthenate precipitation reaction occurring in the petroleum industry. To wit, molecular modelling on different length and time scales has been conducted in order to investigate the calcium naphthenate reaction.

The interactions between the carboxylate groups from the tetra-carboxylic acids molecules and the divalent metal ions have been identified to be the most important factor influencing the calcium naphthenate precipitation. Therefore, these interactions have been studied in greater detail. In the first paper, the main focus has been put on studying the interactions of up to four carboxylate anions with calcium. The multibody effects in these complexes were assessed by the pair-interaction energy ($E_{pair-inter}$) through DFT and compared with the OPLS-AA force field. A discrepancy between the two methods has been found, although it has been anticipated because of the pair additivity of the interactions in the force field. The most stable complex was formed between three carboxylates and one calcium, which favours the hypothesis of cross-linking discussed already. The strongest pair-interaction was between one carboxylate and one calcium. We have further examined the potential curves to higher separation distances for one and two carboxylates and one calcium or sodium ion. The DFT results were again compared with OPLS-AA and a modification of OPLS-AA by Yan et al. [55] The original force field parameters have shown better agreement with DFT, although a lower interaction energy was computed with DFT. However, the equilibrium distances were shown to be very well represented in the original OPLS-AA, which have been important for the further study of these interactions by MD, especially in determining the probability of reaction presented in Paper 3.

The experimentally observed selectivity of reaction between the TA molecules and divalent metal cations has been studied by BOMD in solvent. The free energy of interaction between one carboxylate and one divalent metal ion has been calculated by thermodynamic integration. However, the observed selectivity was partially explained only by the interaction energy, where the strongest interactions were observed with magnesium followed by calcium, strontium and barium. Therefore, the simulation trajectories were further investigated in order to clarify the selectivity of the reaction. The dynamics of the solvent molecules in the solvation shell along with the self-diffusion of the metal ions appeared to be the most important factors of the preferred selectivity of calcium rather than magnesium. The interaction energy between the magnesium ion and the solvent molecules were the highest, which resulted in fewer exchanges of solvent molecules in the first solvation shell of all the metal ions. Calcium also appeared to have higher self-diffusion and mobility compared to magnesium, especially in the complex with the carboxylate.

In Paper 3, we have calculated the probability of reaction between two carboxylates and with calcium or magnesium as a function of the distance between the carboxylates. Calcium demonstrated a higher probability for reaction compared to magnesium. Therefore, the probability of reaction strengthens and compliments the conclusions drawn from the second paper concerning the selectivity. Moreover, the probability of reaction has been key function for determining the fractional conversion of TA to calcium naphthenate precipitation ($f_p(\Gamma_{TA})$) presented in Paper 4.

The fractional conversion of TA to calcium naphthenate precipitation ($f_p(\Gamma_{TA})$) has been determined by reconstructing the interfacial density of TA molecules in a coarse-grain manner, which we refer to COO^- interface map. MD simulations were performed on the ARN and BP10 molecules at an oil-water interface. Structural probability functions of the orientation of the TA molecules have been obtained from the MD trajectories. A methodology of recreating the interface density by using the MD simulated probabilities has been developed and presented. The fractional conversion increases non linearly as a function of the interfacial concentration of TA and was very similar for both ARN and BP10 molecules. The $f_p(\Gamma_{TA})$ calculated in this work is important constituent function in the multiscale process model of Kovalchuk et al. [34]. Therefore, it should be used to properly characterize the cross-linking mechanism in this multi-scale framework.

The calcium naphthenate precipitation reaction occurring in the petroleum industry is a complex reaction involving many steps and factors. We can conclude in conjunction with the results of Kovalchuk et al. [34] that the cross-linking hypothesis discussed above is the most probable reaction mechanism for the calcium naphthenate reaction. However, this is the idealized reaction mechanism and the reaction can be influenced by many factors due to the complex composition of

crude oil. Some factors can be the presence of mono-acids, asphaltene and resin molecules adsorbed on the oil-water interface. These factors can be included in further studies in order to assess their impact on the formation of calcium naphthenate precipitates. The fractional conversion can also be determined for the other divalent ions by the presented coarse-grain method of creating interface maps. This will further clarify on the process scale the selectivity of the precipitation reaction.

The developed methodology for reconstructing the interfacial density in a coarse-grain manner and assessing the extend of the cross-linked network of surfactant molecules could also be used to study other systems of interest where cross-linking of different molecules is governing the behaviour of the system. The extend of the influence of cross-linking could provide valuable information for the study of such systems. Moreover the methodology is also applicable to bulk systems not only to liquid-liquid interfaces.

Bibliography

[1] J. G. Speight. *The Chemistry and Technology of Petroleum*. Taylor and Francis, fifth edition, 2014.

[2] R. P. Rodgers, C. A. Hughey, C. L. Hendrickson, and A. G. Marshall. Advanced characterization of petroleum crude and products by high field fourier transform ion cyclotron resonance mass spectrometry. *Fuel Chemistry*, 42(2):636–637, 2002.

[3] A. Mendez, R. Meneghini, and J. Lubkowitz. Physical and chemical characterization of petroleum products by gc-ms. *Journal of Chromatographic Science*, 45:683–689, 2007.

[4] F. A. Fernandez-Lima, C. Becker, A. M. McKenna, R. P. Rodgers, A. G. Marshall, and D. H. Russell. Petroleum crude oil characterization by ims-ms and fticr ms. *Analytical Chemistry*, 81(24):9941–9947, 2009.

[5] G. C. Klein, A. Angström, R. P. Rodgers, and A. G. Marshall. Use of saturates/aromatics/resins/asphaltenes (sara) fractionation to determine matrix effects in crude oil analysis by electrospray ionization fourier transform ion cyclotron resonance mass spectrometry. *Energy Fuels*, 20:668–672, 2006.

[6] Y. Cho, J.-G. Na, N.-S. Nho, S. H. Kim, and S. Kim. Application of saturates, aromatics, resins, and asphaltenes crude oil fractionation for detailed chemical characterization of heavy crude oils by fourier transform ion cyclotron resonance mass spectrometry equipped with atmospheric pressure photoionization. *Energy Fuels*, 26:2558–2565, 2012.

[7] A. Gaspar, E. Zellermann, S. Lababidi, J. Reece, and W. Schrader. Characterization of saturates, aromatics, resins, and asphaltenes heavy crude oil frac-

tions by atmospheric pressure laser ionization fourier transform ion cyclotron resonance mass spectrometry. *Energy Fuels*, 26:3481–3487, 2012.

[8] I. Muhammad, N. Tijjani, I.J. Dioha, A. Musa, H. Sale, and A.M. Lawal. Sara separation and determination of concentration levels of some heavy metals in organic fractions of nigerian crude oil. *Chemistry and Materials Research*, 3, 2013.

[9] A. Barrabino. *Phase Inversion, Stability and Deastabilization of Model and Crude Oil Water-in-Oil Emulsions*. PhD thesis, Norwegian University of Science and Technology, 2014.

[10] L. E. Zerpa, J.-L. Salager, C. A. Koh, E. D. Sloan, and A. K. Sum. Surface chemistry and gas hydrates in flow assurance. *Industrial & Engineering Chemistry Research*, 50:188–197, 2011.

[11] S. Gao. Investigation of interactions between gas hydrates and several other flow assurance elements. *Energy & Fuels*, 22:3150–3153, 2008.

[12] M. C. K. de Oliveira, R. M. Carvalho, A. B. Carvalho, F. R. D. Faria B. C. Couto, and R. L. P. Cardoso. Waxy crude oil emulsion gel: Impact on flow assurance. *Energy & Fuels*, 24:2287–2293, 2010.

[13] M. C. K. de Oliveira, A. Teixeira, L. C. Vieira, R. M. de Carvalho, A. B. M. de Carvalho, and B. C. do Couto. Flow assurance study for waxy crude oils. *Energy & Fuels*, 26:2688–2695, 2011.

[14] K. Akbarzadeh, D. Eskin, J. Ratulowski, and S. Taylor. Asphaltene deposition measurement and modeling for flow assurance of tubings and flow lines. *Energy & Fuels*, 26:495–510, 2012.

[15] A. A. Olajire. A review of oilfield scale management technology for oil and gas production. *Journal of Petroleum Science and Engineering*, 135:723–737, 2015.

[16] T.D. Baugh, K. V. Grande, J. E. Vindstad, and N. O. Wolf. The discovery of high molecular weight naphthenic acids (arn acid) responsible for calcium naphthenate deposits. pages 9–15, SPE Seventh International Symposium on Oilfield Scale, Aberdeen, U.K., May 11-12, 2005; SPE 93011; Curran Associates, Inc.: Red Hook, NY, 2006; pp 9-15.

[17] O. Sundman, S. Simon, E. L. Nordgård, and J. Sjöblom. Study of the aqueous chemical interactions between a synthetic tetra-acid and divalent cations as a model for the formation of metal naphthenate deposits. *Energy Fuels*, 24:6054–6060, 2010.

[18] B. F. Lutnaes, Ø. Brandal, J. Sjöblom, and J. Krane. Archaeal c80 isoprenoid tetraacids responsible for naphthenate deposition in crude oil processing. *Org. Biomol. Chem.*, 4:616–620, 2006.

[19] J. S. Clemente and P. M. Fedorak. A review of the occurrence, analyses, toxicity, and biodegradation of naphthenic acids. *Chemosphere*, 60(585-600), 2005.

[20] E. Nordgård and J. Sjöblom. Model compounds for asphaltenes and c 80 isoprenoid tetraacids. part i: Synthesis and interfacial activities. *J. Dispersion Sci. Technol.*, 29:1114–1122, 2008.

[21] E. L. Nordgård, H. Magnusson, and J. Sjöblom A.-M. D. Hanneseth. Model compounds for c 80 isoprenoid tetraacids part ii. interfacial reactions, physicochemical properties and comparison with indigenous tetraacids. *Colloids and Surfaces A: Physicochem. Eng. Aspects*, 340:99–108, 2009.

[22] C. Igwebueze, L. Oduola, O. Smith, P. Vijn, and A. G. Shepherd. Calcium naphthenate solid deposit identification and control in offshore nigerian fields. SPE International Symposium on Oilfield Chemistry, Texas, USA, April 8-10, 2013; SPE 164055.

[23] Ø. Brandal, A.-M. Dahl Hanneseth, and J. Sjöblom. Interactions between synthetic and indigenous naphthenic acids and divalent cations across oil-water interfaces: effects of addition of oil-soluble non-ionic surfactants. *Colloid Polym. Sci.*, 284:124–133, 2005.

[24] L.Ge, S. Simon, B. A. Grimes, E. Nordgård, Z. Xu, and J. Sjöblom. Formation of vesicles and micelles in aqueous systems of tetrameric acids as determined by dynamic light scattering. *J. Dispersion Sci. Technol.*, 32:1582–1591, 2011.

[25] L. Ge, M. Vernon, S. Simon, Y. Maham, J. Sjöblom, and Z. Xu. Interactions of divalent cations with tetrameric acid aggregates in aqueous solutions. *Colloids and Surfaces A*, 396:238–245, 2012.

[26] P. V. Hemmingsen, S. Kim, H. E. Pettersen, R. P. Rodgers, J. Sjöblom, and A. G. Marshall. Structural characterization and interfacial behavior of acidic compounds extracted from a north sea oil. *Energy Fuels*, 20:1980–1987, 2006.

[27] E. L. Nordgård, A.-M. D. Hanneseth, and J. Sjöblom. Inhibition of calcium naphthenate. experimental methods to study the effect of commercially available naphthenate inhibitors. *J. Dispersion Sci. Technol.*, 31:668–675, 2010.

[28] S. Simon, E. Nordgård, P. Bruhei, and J. Sjöblom. Determination of c 80 tetra-acid content in calcium naphthenate deposits. *J. Chromatogr. A*, 1200:136–143, 2008.

[29] S. Simon, C. Reisen, A. Bersås, and J. Sjöblom. Reaction between tetrameric acids and ca^{2+} in oil/water system. *Ind. Eng. Chem. Res.*, 51:5669–5676, 2012.

[30] J. Sjöblom, S. Simon, and Z. Xu. The chemistry of tetrameric acids in petroleum. *Adv. Colloid Interface Sci.*, 205:319–338, 2014.

[31] O. Sundman, E. L. Nordgård, B. A. Grimes, and J. Sjöblom. Potentiometric titrations of five synthetic tetraacids as models for indigenous c 80 tetraacids. *Langmuir*, 26(3):1619–1629, 2010.

[32] E. Riccardi, K. Kovalchuk, A. Y. Mehandzhiyski, and B. A. Grimes. Structure and orientation of tetracarboxylic acids at oil-water interfaces. *J. Dispersion Sci. Technol.*, 35:1018–1030, 2014.

[33] K. Kovalchuk, E. Riccardi, and B. A. Grimes. Multiscale modeling of mass transfer and adsorption in liquid-liquid dispersions. 1. molecular dynamics simulations and interfacial tension prediction for a mixed monolayer of mono- and tetracarboxylic acids. *Ind. Eng. Chem. Res.*, 53:11691–11703, 2014.

[34] K. Kovalchuk, E. Riccardi, and B. A. Grimes. Multiscale modeling of mass transfer and adsorption in liquid-liquid dispersions. 2. application to calcium naphthenate precipitation in oils containing mono- and tetracarboxylic acids. *Ind. Eng. Chem. Res.*, 53:11704–11719, 2014.

[35] P. Hohenberg and W. Kohn. Inhomogeneous electron gas. *Physical Review*, 136(3B):864–871, 1964.

[36] W. Konh and L. J. Sham. Self-consistent equations including exchange and correlation effects. *Physical Review*, 140(4A):1133–1138, 1965.

[37] R.G. Parr and W. Yang. *Density Functional Theory of Atoms and Molecules*. Oxford University Press, 1989.

[38] W. Koch and M. C. Holthausen. *A Chemist's Guide to Density Functional Theory*. Wiley-VCH, 2001.

[39] A. D. Becke. A new mixing of hartree-fock and local density-functional theories. *The Journal of Chemical Physics*, 98:1372–1377, 1993.

[40] A. D. Becke. Density-functional thermochemistry. iii. the role of exact exchange. *The Journal of Chemical Physics*, 98:5648–5652, 1993.

[41] A. R. Leach. *Molecular Modelling*. Pearsons Education Limited, 2001.

[42] W. D. Cornell, P. Cieplak, C. I. Bayly, I. R. Gould, K. M. Merz, D. M. Ferguson, D. C. Spellmeyer, T. Fox, W. Caldwell J, and A. Kollman P. A second generation force field for the simulation of proteins, nucleic acids, and organic molecules. *J. Am. Chem. Soc.*, 117, 1995.

[43] B. R. Brooks, R. E. Bruccoleri, B. D. Olafson, D. J. States, S. Swaminathan, and M. Karplus. Charmm: A program for macromolecular energy, minimization, and dynamics calculations. *Journal of Computational Chemistry*, 4(2):187–217, 1983.

[44] W. L. Jorgensen, D. S. Maxwell, and J. Tirado-Rives. Development and testing of the opls all-atom force field on conformational energetics and properties of organic liquids. *J. Am. Chem. Soc.*, 118:11225–11236, 1996.

[45] J. Hermans, H. J. C. Berendsen, W. F. Van Gunsteren, and J. P. M. Postma. A consistent empirical potential for water-protein interactions. *Biopolymers*, 23(8):1513–1518, 1984.

[46] B. Hess, C. Kutzner, D. van der Spoel, and E. Lindahl. Gromacs 4 algorithms for highly efficient, load-balanced, and scalable molecular simulation. *J. Chem. Theory Comput*, 4:435–447, 2008.

[47] P. Ehrenfest. Bemerkung über die angenäherte gültigkeit der klassischen mechanik innerhalb der quantenmechanik. *Zeitschrift für Physik*, 45:455–457, 1927.

[48] R. Car and M. Parrinello. Unified approach for molecular dynamics and density-functional theory. *Physical Review Letters*, 55(22):2471–2474, 1985.

[49] J. Hutter, M. Iannuzzi, F. Schiffmann, and J. VandeVondele. cp2k: atomistic simulations of condensed matter systems. *Wiley Interdisciplinary Reviews: Computational Molecular Science*, 4(1):15–25, 2013.

[50] D. Marx and J. Hutter. *Ab Initio Molecular Dynamics*. Cambridge University Press, 2009.

[51] D. Frenkel and B. Smit. *Understanding Molecular Simulations*. Academic Press, 2002.

[52] S.r Kumar, D. Bouzida, R. H. Swendsen, P. A. Kollman, and J. M. Rosenberg. The weighted histogram analysis method for free-energy calculations on biomolecules. i. the method. *Journal of Computational Chemistry*, 13(8):1011–1021, 1992.

[53] B. Roux. The calculation of the potential of mean force using computer simulations. *Computer Physics Communications*, 91:275–282, 1995.

[54] I. R. S. Mulliken. Electronic population analysis on lcao-mo molecular wave functions. *J. Chem. Phys.*, 23:1833, 1955.

[55] H. Yan, X. L. Guo, S. L. Yuan, and C. B. Liu. Molecular dynamics study of the effect of calcium ions on the monolayer of sdc and sdsn surfactants at the vapor/liquid interface. *Langmuir*, 27:5762–5771, 2011.

[56] J. P. Foster and F. Weinhold. Natural hybrid orbitals. *J. Am. Chem. Soc.*, 102:7211–7218, 1980.

[57] A. E. Reed, L. A. Curtiss, and F. Weinhold. Intermolecular interactions from a natural bond orbital, donor-acceptor viewpoint. *Chem. Rev.*, 88:899–926, 1988.

[58] Q. Wu and T. van. Voorhis. Direct optimization method to study constrained systems within density functional theory. *Physical Review A: Atomic, Molecular, and Optical Physics*, 72, 2005.

[59] B. Kaduk, T. Kowalczyk, and T. van. Voorhis. Constrained density functional theory. *Chem. Rev.*, 112:321–370, 2012.

[60] P. Atkins and J. de. Paula. *Physical Chemistry*. Oxford Univeristy Press, 8th edition, 2006.

[61] J. Buffle, Z. Zhang, and K. Startchev. Metal flux and dynamic speciation at (bio)interfaces. part i: Critical evaluation and compilation of physicochemical parameters for complexes with simple ligands and fulvic/humic substances. *Env. Sci. & Tech.*, 41:7609–7620, 2007.

Appendix

Paper 1

Density Functional Theory Study on the Interactions of Metal Ions with Long Chain Deprotonated Carboxylic Acids

THE JOURNAL OF PHYSICAL CHEMISTRY A

Article

pubs.acs.org/JPCA

Density Functional Theory Study on the Interactions of Metal Ions with Long Chain Deprotonated Carboxylic Acids

Aleksandar Y. Mehandzhiyski,[†] Enrico Riccardi,[§] Titus S. van Erp,[§] Henrik Koch,[§] Per-Olof Åstrand,[§] Thuat T. Trinh,[§] and Brian A. Grimes*[,†]

[†]Department of Chemical Engineering, Norwegian University of Science and Technology, SemSælandsvei 4, NO-7491 Trondheim, Norway

[§]Department of Chemistry, Norwegian University of Science and Technology, Høgskoleringen 5 Realfagbygget blokk D, 3.etg., NO-7491 Trondheim, Norway

Supporting Information

ABSTRACT: In this work, interactions between carboxylate ions and calcium or sodium ions are investigated via density functional theory (DFT). Despite the ubiquitous presence of these interactions in natural and industrial chemical processes, few DFT studies on these systems exist in the literature. Special focus has been placed on determining the influence of the multibody interactions (with up to 4 carboxylates and one metal ion) on an effective pair-interaction potential, such as those used in molecular mechanics (MM). Specifically, DFT calculations are employed to quantify an effective pair-potential that implicitly includes multibody interactions to construct potential energy curves for carboxylate−metal ion pairs. The DFT calculated potential curves are compared to a widely used molecular mechanics force field (OPLS-AA). The calculations indicate that multibody effects do influence the energetic behavior of these ionic pairs and the extent of this influence is determined by a balance between (a) charge transfer from the carboxylate to the metal ions which stabilizes the complex and (b) repulsion between carboxylates, which destabilizes the complex. Additionally, the potential curves of the complexes with 1 and 2 carboxylates and one counterion have been examined to higher separation distance (20 Å) by the use of relaxed scan optimization and constrained density functional theory (CDFT). The results from the relaxed scan optimization indicate that near the equilibrium distance, the charge transfer between the metal ion and the deprotonated carboxylic acid group is significant and leads to non-negligible differences between the DFT and MM potential curves, especially for calcium. However, at longer separation distances the MM calculated interaction potential functions converge to those calculated with CDFT, effectively indicating the approximate domain of the separation distance coordinate where charge transfer between the ions is occurring.

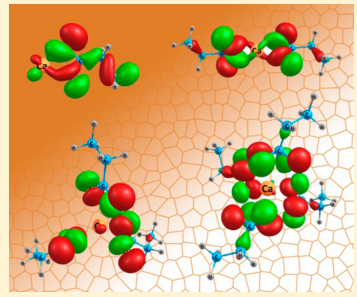

1. INTRODUCTION

The interactions between charged species (ions) are one of the most common in nature,[1−13] among which the interactions between calcium ions and carboxylic acids[1−3,7−10] play an important role in many biological reactions[1,2,5,6] as well as in colloidal[3,4] and interfacial systems.[7−9] The carboxylic acid groups usually dissociate above a certain pH level, which makes them very reactive and allows calcium ions to bind very strongly with them. As an example, in an oil−water biphasic system, the calcium ions dissolved in the water phase could interact with naphthenic acids, originally found in immature crude oil, forming insoluble naphthenate precipitates.[7−9] The current work is in the framework of the study of formation of calcium naphthenate precipitates and, therefore, special focus will be placed on the interactions between carboxylic acid ions with a calcium divalent ion. Quantum chemical calculations can be used to study such reactions. Despite the ubiquitous importance of the calcium−carboxylic acid reactions, few *ab initio* studies exist.[10,11]

In these quantum chemical calculations, the interactions between atoms or molecules can be theoretically studied via the potential energy surface (PES), where the energy of these interactions is a function of interatomic distances. Potential energy surfaces of interactions for different molecules are widely studied by quantum chemistry methods such as Hartree−Fock, post Hartree−Fock and density functional theory (DFT).[14−16] These methods provide a description of the interactions and a quantification of the interaction energies and, therefore, it can provide the potential energy[14−16] and allow the development[17] or improvement[18−20] of force fields for molecular dynamics (MD) simulations.

MD simulations have been successfully employed[3−6,21−23] to study systems in which metal ions are present. To increase the predictive capability of such simulations, accurate force fields are required. Via DFT calculations, local partial charges have

Received: April 30, 2015
Revised: September 1, 2015

DOI: 10.1021/acs.jpca.5b04136
J. Phys. Chem. A XXXX, XXX, XXX−XXX

been recently computed,[21,22] improving existing force fields like OPLS-AA[24] and providing a model enhancement based on fundamental physics that, in principle, can be applicable to different types of systems. Empirically developed improvements to force fields including OPLS-AA, have also been obtained by fitting experimental measured pK's,[25] where nonbonded VdW parameters are adjusted to fit the data. Despite the closer match obtained between experiment and simulation with the latter approach, improved predictions for different types of systems should not be expected because the parameters are tuned to reproduce data for a specific system.

In the past years, intense focus has been placed on improving the predictive capability of force fields used in molecular simulations.[26−33] Mainly, researchers have been working on the introduction and development of polarizable effects[26−31] and multibody interactions[32,33] in the force fields. Despite the large volume of work that has been done,[26−33] there is still much ongoing activity in this field. Including these effects can be computationally expensive and the development of new ways to incorporate such effects is currently still a significant part of MD research. The multibody effects could potentially play an important role in systems where ions of different valences interact, such as the carboxylic acid−calcium system.

In the present work, focus on the interactions of monovalent (sodium) and divalent (calcium) cations with deprotonated carboxylic acid groups have been studied via DFT. More precisely, we investigate the multibody interactions and how these determine the shape of the effective pair-interaction potential. Understanding the influence and importance of multibody effects on effective pair-interaction potentials is of great importance for molecular dynamics simulations. The OPLS-AA[24] force field has been selected to describe the interactions between deprotonated carboxylic acid groups and metal ions, because of its wide applicability to different systems in solution, and therefore, is widely used in MD simulations. The interactions described by OPLS-AA have been compared to DFT-derived potential functions to provide a reference point from which to evaluate the effect of multibody interactions. Furthermore, the present methodology can also be applied to other existing force fields for assessment and optimization of the interactions.

2. MODELS AND METHODS

Density functional theory (DFT) calculations have been performed with Becke's three-parameter hybrid exchange−correlation functional (B3LYP)[34] in the quantum chemical package Gaussian 09[35] and NWChem version 6.1.[36] The B3LYP functional has been shown to produce reliable geometries and energies in many different systems[37−41] including also ionic interactions.[39−41] Triple-ζ basis sets (6-311G) with one diffuse function and one set of d polarization functions for the heavy atoms have been chosen. The presence of ions governs the necessity of adding polarization and diffuse functions.

Carboxylic acid groups have been investigated considering the functional group of deprotonated carboxylic acid. Carboxylic acids can have numerous chain lengths; thus a suitable model must be chosen to mimic many chains in general. Therefore, we initially consider carboxylic acids with chain lengths of 2−6 carbon atoms. Mulliken partial charges[42] have been calculated for them and are presented in Table 1. It can be observed that the prolongation of the carbon−hydrogen tail beyond three carbons minimally affects the charge distribution of the carboxyl group. It should be noted that either the propanoate or butanoate ion could be a possible model molecule for the following calculations because the charge distributions on the oxygens on both ions are nearly identical, as seen from Table 1. That indicates that an explicit comparison of the interaction energy is needed. Thus, calculations of the interaction energies have been carried out for both propanoate and butanoate and presented in the Supporting Information in Figure S1. It can be seen that they give similar results, and therefore, the propanoate ion has been selected as the best compromise between computational efficiency and effects of the chain length on the carboxyl group charge distribution.

Table 1. Mulliken Partial Charges (e^-) of the Carboxylate Group for Different Carboxylate Ions and Schematic Representation of the Propanoate Ion with the Charges Drawn on the Respective Atoms[a]

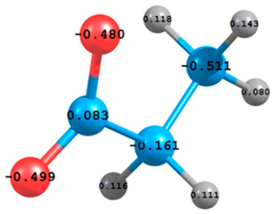

no. of carbon atoms	COO^-	O	O	C
2 (acetate ion)	−0.847	−0.498	−0.498	0.148
3 (propanoate ion)	−0.896	−0.480	−0.499	0.083
4 (butanoate ion)	−0.869	−0.474	−0.498	0.103
5 (pentanoate ion)	−0.872	−0.473	−0.491	0.092
6 (hexanoate ion)	−0.881	−0.472	−0.487	0.077

[a]The blue color depicts carbon atoms, red depicts oxygen, and gray depicts hydrogen.

When the model carboxylate was chosen, ground state geometry optimizations were performed. A metal ion was then added to the system, and the geometry of the whole complex was further optimized. The ground state carboxylate structure has then been replicated the desired number of times and transrotated around the metal ion to a symmetrical structure to maximize the distance between the carboxylate acid groups. With this procedure, all the carboxylates have identical structures and distances from the metal ion positioned at the center of the system, as shown in Figure 1. This implies that for the system with two carboxylates, the acids are in opposite positions with respect to each other and have point group symmetry C_{2h}. For three carboxylates, a triangular distribution (C_{3h}) is obtained, whereas a tetrahedral distribution (T_d) provides the maximum distance between the acid groups for the system with four acid molecules. These geometries allow a minimal interaction between the carboxylates and symmetrical orientation of the acids around the ion, which is desired to make the comparison with the OPLS-AA force field. It should be noted that, in the cases where electroneutrality could not be maintained, the net charge of the system has been considered with respect to the system constituents and their population. The metal ions considered in the present analysis are monovalent sodium and divalent calcium.

2.1. Interaction Potentials. The interaction energies as a function of the separation distance between the metal ion and the carboxylate group have been calculated. The separation

DOI: 10.1021/acs.jpca.5b04136
J. Phys. Chem. A XXXX, XXX, XXX−XXX

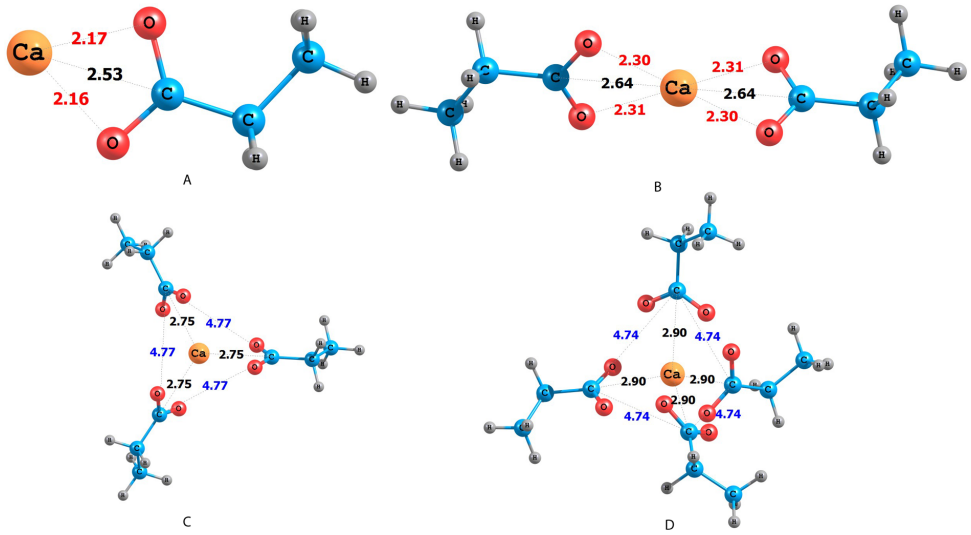

Figure 1. Optimized geometries of the complexes with one (A), two (B), three (C), and four (D) carboxylates and one Ca^{2+}. Distances are given in Å, in black are the distances between Ca^{2+} and C from the (COO^-) group, in red are distances between Ca^{2+} and O from the (COO^-) group, and in blue are distances between the carbon atoms of the carboxylate groups.

distance is defined as the length between the position of the metal ion and the position of the carbon in the carboxylate acid group(s). These distances have been subsequently modified by translating each molecule along its carboxylate acid−metal ion vector. The energy has been then computed at regular intervals (0.2 Å) of separation starting from 2 Å using relaxed scan optimization. In the relaxed scan optimization, the distance between the carbon of the carboxylate acid group and the ion has been kept fixed for every step (different separation distance) whereas for the rest of the complex, a geometry optimization has been applied. Along with the dependence of the energy as the distance increases, the changes in the geometry of the complex with respect to the increasing of the separation distance could also be observed. In principle, the interaction energy can be defined in different ways. In the present study, the total, E_{inter}, and the pair-interaction, $E_{pair\text{-}inter}$, energies have been defined in eqs 1 and 2, respectively.

$$E(r)_{inter} = E(r)_{complex} - E_{ion} - N \times E_{acid} \quad (1)$$

Here, $E(r)_{complex}$ is the total energy of the multibody complex at different carboxylate−ion distances, r, E_{ion} is the energy of the metal ion, E_{acid} is the energy of the carboxylate with net charge −1, and N is the number of propanoates considered in the system. The energy of the complex and the acid have been calculated from their respective optimized geometries.

The pair-interaction energy, $E_{pair\text{-}inter}$, is the interaction energy per pair of cation−carboxylate averaged for the number of acid molecules in the system and is given as follows:

$$E(r)_{pair\text{-}inter} = (E(r)_{complex} - E_{ion} - E_N(r))/N \quad (2)$$

Here, $E_N(r)$ is the energy of the system in the absence of the metal ion (i.e., is the energy of the complex of carboxylates) and N is the number of carboxylate molecules. It should be noted that $E_N(r)$ is taken from a single-point energy calculation on the geometry of the complex of carboxylate(s). $E_N(r)$ depends on the distance between the carboxylate and the metal ion, because the geometry of the carboxylate acid group(s) (valence angle and bond lengths) would be slightly different when the metal ion is closer to or further away from the metal ion. The total interaction energy, eq 1, provides an estimation of the most stable and, respectively, more probable molecular geometry and orientation of the carboxylate acids around the metal ions. The pair-interaction energy, eq 2, on the contrary, evaluates the average relative strength of the ionic interaction between a single carboxylate acid group and the metal ion in the presence of the other carboxylate acid pair interactions. In that way, this is an estimation of the influence of the multibody effects on the ionic interactions in the complex. Because the interactions in the OPLS-AA force field are pairwise additive, the pair-interaction energy calculated by eq 2 allows comparison of the DFT and the molecular mechanics potential and assessment on the role of the multibody interactions. After summing eq 2 over all N-bodies in the system, one is left with the excess energy contribution of the set of carboxylate acid groups that is caused by the presence of the ion, which should facilitate the evaluation of the multibody interaction component to the pair-interaction energy.

The basis set superposition error (BSSE) correction of the interaction energy has been determined by the counterpoise method of Boys and Bernardi.[43]

2.2. Molecular Mechanics. The total interaction energy corresponding to eq 1 and the pair-interaction energy corresponding to eq 2 has also been computed via molecular mechanics (MM) using the GROMACS 4.6 simulation package,[44] where the geometries from the DFT calculations are being used for the MM calculations. Two sets of force field (FF) parameters are being considered in the present study, one set being the original parameters of OPLS-AA[24] as implemented in GROMACS and the other set as given by Yan et al.[21] The parameters presented by Yan et al.[21] are derived for two surfactant molecules: sodium dodecyl

DOI: 10.1021/acs.jpca.5b04136
J. Phys. Chem. A XXXX, XXX, XXX−XXX

carboxylate (SDC) and sodium dodecyl sulfonate (SDSn). These parameters give good correlation to experimentally measured densities and self-diffusion coefficients while providing reasonable structures.[21] These FF parameters can therefore provide a desirable additional basis of comparison alongside the original OPLS-AA force field. The two sets of parameters are presented in Table 2. It can be seen from Table 2 that the difference in the parameters of the carboxylate group is in the magnitude of the partial charges of the constituent atoms, which have been calculated via DFT-B3LYP/6-31+G(d).

Table 2. Molecular Mechanics Parameters and Lennard-Jones and Electrostatic Interactions

	(i) and (ii)		q (e)	
atoms	σ (nm)	ε (kJ/mol)	OPLS-AA (i)	ref 21 (ii)
C (in −CH3)	0.350	0.27614	−0.18	−0.18
C (in −CH2−)	0.350	0.27614	−0.22	−0.12
H	0.250	0.12552	0.06	0.06
C (in $-COO^-$)	0.375	0.43932	0.70	0.91
O (in $-COO^-$)	0.296	0.87864	−0.80	−0.84
Na^+	0.333	0.01160	1.00	1.00
Ca^{2+}	0.241	1.88130	2.00	2.00

3. RESULTS AND DISCUSSION

The interaction energies between the carboxylate and the calcium have been calculated in the presence of one, two, three, and four carboxylates around the calcium ion and the influence of the multibody effects on the potential curves are presented and discussed in section 3.1. In section 3.2, a comparison and assessment of the OPLS-AA potential curves with the DFT-derived potential functions for sodium and calcium have been presented and discussed. Calculations of the potential curves for sodium have been only made for the second part of the paper, because the multibody interactions could be more influential on the behavior of the divalent calcium, because it could potentially coordinate more carboxylate groups.

3.1. Carboxylates Multibody Interaction with Ca^{2+}.

Figure 1 schematically shows the equilibrium structures, of the complexes consisting of one carboxylate and one calcium (A), two carboxylates and one calcium (B), three carboxylates and one calcium (C), and four carboxylates and one calcium (D), where the total interaction energy, $E(r)_{inter}$, and the pair interaction energy, $E(r)_{pair\text{-}inter}$, as a function of distance have been computed according to eqs 1 and 2, respectively. In Figure 2, the total interaction energy, $E(r)_{inter}$, and the pair interaction energy, $E(r)_{pair\text{-}inter}$, are presented for the cases with one, two, three, and four carboxylates. The interaction and the pair-interaction energies have been calculated also for the butanoate ion and are presented in Figure S1 in the Supporting Information as mentioned above. The interaction energy has not been affected by the prolongation of the hydrocarbon chain, meaning that the results presented here could generally be valid for long chain carboxylates as well. This is important because in a subsequent paper the carboxylic acid−metal ion interactions will be further examined, accounting explicitly for the solvent molecules through *ab initio* molecular dynamics (AIMD). Additionally, the basis set superposition error (BSSE) correction has been evaluated for the complex employing the propanoate ion by the counterpoise method[43] and is presented in Figure S2 in the Supporting Information. It can be seen that

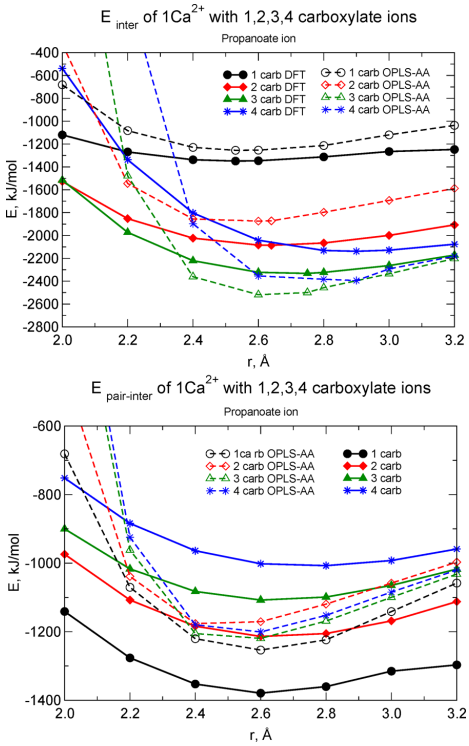

Figure 2. Comparison between the DFT (solid lines) and the MM (dashed lines) total interaction energies, E_{inter}, according to eq 1 (top) and pair-interaction energies, $E_{pair\text{-}inter}$, according to eq 2 (bottom) between complexes with one (black), two (red), three (green), and four (blue) carboxylate groups and Ca^{2+}.

the BSSE changes the equilibrium distance of the potential curves of one and four carboxylates by 0.07 and 0.1 Å, respectively. However, the introduction of BSSE correction does not change the order of appearance of the potential curves and the slight difference in the equilibrium distances should not have a considerable impact on the conclusions drawn from the results. More detailed discussion of the BSSE correction can be found in the Supporting Information.

Both Figures 1 and 2 demonstrate that increasing the number of carboxylate groups increases the equilibrium distance between Ca^{2+} and the carbon in the carboxylate group. The distance varies from 2.5 Å for one carboxylate to 2.9 Å for four carboxylates, as shown in Figure 1. Figure 2 reports how the total interaction energy varies as a function of distance for different numbers of carboxylate acid groups. It appears that the lowest total interaction energy eq 1 for the investigated systems can be reached when three carboxylates are surrounding the metal ion. That has been shown to be valid for both DFT and MM interaction energies, implying that the MM results are qualitatively in agreement with DFT. Although, MM reproduces the same ordering of the potential curves as DFT, it fails to predict the equilibrium distance in the complexes of two and three carboxylates, where they have shifted by 0.04 and 0.15 Å compared to DFT, respectively, toward shorter distances. In DFT, the placement of more

DOI: 10.1021/acs.jpca.5b04136
J. Phys. Chem. A XXXX, XXX, XXX−XXX

negatively charged carboxylates would promote more charge transfer to the positively charged calcium, which decreases the total interaction energy in Figure 2. Then one could expect that by placing more carboxylates, the interaction energy would decrease, because that would imply more charge transfer to the calcium, as shown from the partial charges determined by the natural bond orbital method[45,46] in Table 3. However, the complex with the lowest interaction energy is the one with three carboxylates, not four as one could expect. This observation could be explained by (a) reaching a case where the charge transfer difference is decreasing significantly upon addition of extra carboxylate and (b) the mutual orientation of the carboxylates relative to each other. When more carboxylates are placed around the ion, the mutual distance between them decreases, as seen from Figure 1, which destabilizes the complex (decreases the interaction energy) because they are negatively charged and tend to repel each other. The balance between the effect that stabilizes the complex (charge transfer from the carboxylate group to the metal ion) and the effect destabilizing it (the repulsion between the carboxylates) determines the trends of the potential curves in Figure 2. From Figure 2 it can also be seen that the MM calculated energies, for the equilibrium geometries underestimate the interaction energy compared to DFT for the case with 1 and 2 carboxylates by 92 and 210 kJ/mol, respectively. In contrast, the MM interaction energies for three and four carboxylates are overestimated by 195 and 250 kJ/mol, respectively. This observation clearly highlights the importance of the multibody interactions in the cases where two or more carboxylates interact with the calcium.

Table 3. Partial Atomic Charges Calculated with the Natural Bond Orbital (NBO) Analysis Method

	complex with 1 carboxylate	complex with 2 carboxylates	complex with 3 carboxylates	complex with 4 carboxylates
Ca^{2+}	1.76	1.68	1.56	1.49
COO^- [a]	−0.84	−0.84	−0.80	−0.77
C (from $-COO^-$)[a]	0.82	0.79	0.78	0.76
O (from $-COO^-$)[b]	−0.83	−0.82	−0.79	−0.76

[a]The atomic partial charges are averaged over all carboxylate group(s). [b]Average partial charge from both oxygens and from all carboxylate group(s).

The pair interaction energies (eq 2) calculated with the two methods for different numbers of acid molecules interacting with the metal ion are reported in the bottom plot of Figure 2. The strongest carboxylate−calcium interaction as indicated by the pair-interaction energy is formed when one carboxylate group interacts with the metal ion, as shown by both DFT and MM. However, the pair-interaction energy computed via MM is higher in energy by 125 kJ/mol compared with DFT. The pair-interaction energy for the cases of more than 1 carboxylate acid computed by DFT increases nearly linearly with the addition of more acids to the complex and it is highest with four acids. That could be explained by the fact that as more molecules share the interaction energy with the ion, the energy per acid−ion pair in the complexes of more than one carboxylate acid becomes weaker. Another effect would also be the mutual orientation and repulsion between the carboxylates, as explained in the previous paragraph. In the case of MM, the pair-interaction energies for all the cases are similar, as one would expect. Not only the energy is different, but also the trend does not match the DFT-derived potentials. The strongest pair-interaction is again with 1 carboxylate, but in this case followed by three, then four, and then two. Also the equilibrium distances obtained with MM, in all of the complexes except for one carboxylate, moved to shorter

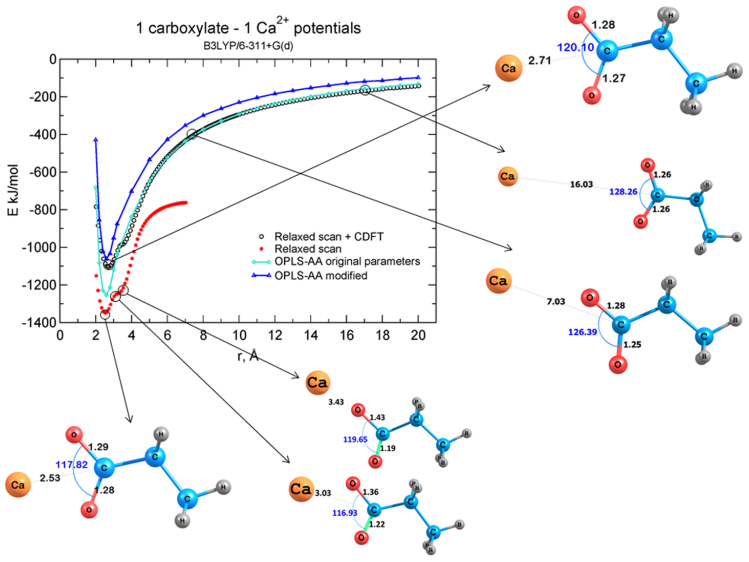

Figure 3. Potential energy curves and molecular structures of one carboxylate−one Ca^{2+}. DFT curves: red dots, relaxed scan; black circles, relaxed scan with CDFT B3LYP/6-311+G(d). MM curves: OPLS-AA original set of parameters, ref 24; OPLS-AA modified, Yan et al.[21]

DOI: 10.1021/acs.jpca.5b04136
J. Phys. Chem. A XXXX, XXX, XXX−XXX

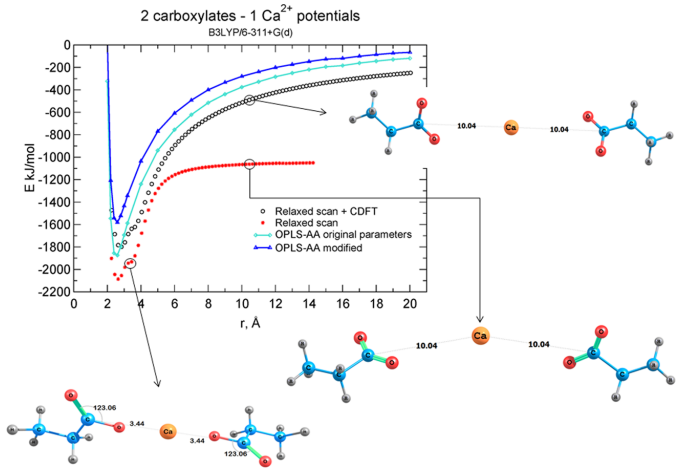

Figure 4. Potential energy curves and molecular structures of two carboxylates—one Ca^{2+}. DFT curves: red dots, relaxed scan; black circles, relaxed scan with CDFT B3LYP/6-311+G(d). MM curves: OPLS-AA original set of parameters, ref 24; OPLS-AA modified, Yan et al.[21]

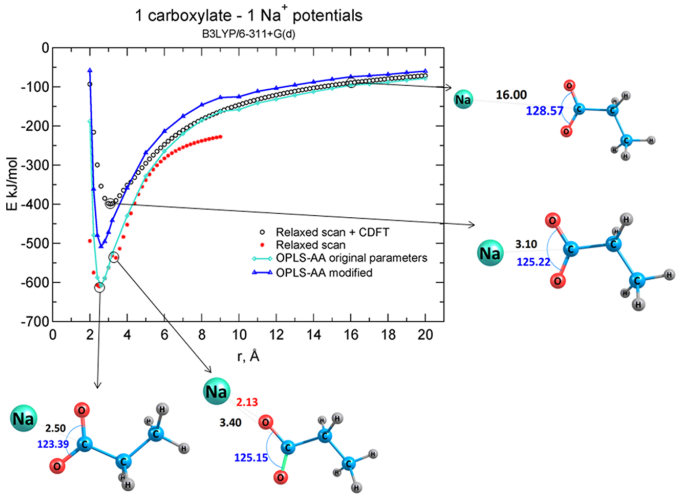

Figure 5. Potential energy curves and molecular structures of one carboxylate—one Na^{+}. DFT curves: red dots, relaxed scan; black circles, relaxed scan with CDFT B3LYP/6-311+G(d). MM curves: OPLS-AA original set of parameters, ref 24; OPLS-AA modified, Yan et al.[21]

distances compared to DFT. These observations also point out the importance of the multibody interactions in the examined complexes, which are not represented in simple pair potentials. In the following section, the case with the lowest pair-interaction energy (one carboxylate) and the electroneutral case (two carboxylates) are examined toward higher separation distances for calcium and sodium. That has been done to examine the tail of the potential functions and how DFT and MM energies compare at high separation distances.

3.2. Potential Curves for Ca^{2+} and Na^{+}. The potential curves for one and two carboxylates with Ca^{2+} and Na^{+} have been calculated for separation distances between 2 and 20 Å and are presented in Figures 3–6 along with the molecular geometries at selected separation distances. The potential curves for one and two carboxylates and one Ca^{2+} are presented in Figures 3 and 4, respectively; the potential curves for one and two carboxylates and one Na^{+} are presented in Figures 5 and 6, respectively. In the plots, the red dot implies that the potential curves are derived with the relaxed scan procedure—optimizing the geometry of the complex for every step while the distances between the ion and the carbon atom in the carboxylate group are kept constant. The results suggest that near the equilibrium distance, the charge transfer favors the stabilization of the complex and, thus, lowers the total interaction energy. On the contary, at a distance of around 6 Å the DFT and the MM potential curves start to diverge and the interaction energy does not converge to 0 in the case of DFT, as seen from Figure 3. It has been found that due to the DFT gas phase calculations, the charge on the calcium ion for separation distances above 6 Å is +1, which leads to different

DOI: 10.1021/acs.jpca.5b04136
J. Phys. Chem. A XXXX, XXX, XXX−XXX

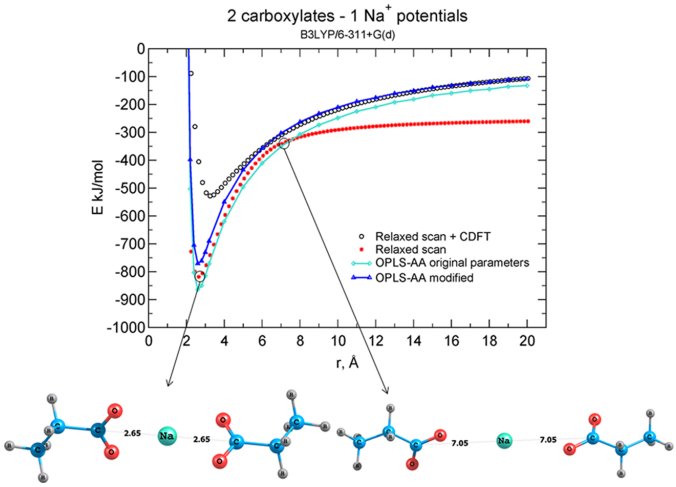

Figure 6. Potential energy curves and molecular structures of two carboxylates−one Na^+. DFT curves: red dots, relaxed scan; black circles, relaxed scan with CDFT B3LYP/6-311+G(d). MM curves: OPLS-AA original set of parameters, ref 24; OPLS-AA modified, Yan et al.[21]

dissociation of the charges than the liquid systems we want to investigate. The carboxylate−calcium complex in water solution dissociates to the following partial charges: −1 located on the carboxylate and +2 on the calcium ion, respectively, and because the OPLS-AA force field is parametrized for liquid simulations, we constrain the charges to mimic dissociation in a liquid phase. To reproduce exactly the dissociation of the charges in the complex at longer distances and to compare the tail of the interaction energy directly with molecular mechanics, constrained density functional theory (CDFT)[47,48] calculations have been carried out. In CDFT, the electron population of the calcium and sodium ions has been constrained so their charge has been kept fixed during the optimization of the complex and, thus, the charge transfer between the ions and the carboxylate group has not been allowed. That could consequently affect the potential curves as can be seen later, in the sense that the potential curves converge to 0 at high separation distances. The calcium and sodium charges have been constrained to +2 and +1, respectively. The black circles (○) in Figures 3−6 represent the CDFT potential functions. By blocking the charge transfer between the carboxylate group and the counterion, the potential curve asymptotically converges to 0. However, at the equilibrium distance, an underestimation of the potential well of about 200 kJ/mol has been recorded with a shift of the equilibrium distance toward higher distances: from 2.53 to 2.71 Å in the complex with one carboxylate and one Ca^{2+}; from 2.64 to 2.78 Å in the case with two carboxylates and one Ca^{2+}; from 2.5 to 3.1 Å for the complex with one carboxylate and one Na^+; from 2.65 to 3.26 Å in the case of two carboxylates and one Na^+.

The MM potential should accurately represent the interactions around the equilibrium distance as well as at higher separations. Around the equilibrium distance, the MM potential should be compared with the relaxed scan curve (red dots), where the charge transfer is allowed, and for longer separation distances, it should match the CDFT curve. In the cases with one carboxylate, the original OPLS-AA potential is shown to be the closest to the obtained DFT potential curves. This potential shows an underestimation of the interactions of about 100 kJ/mol at the equilibrium distances (the minimum in the potential well), whereas using the parameters from ref 21 showed an even greater discrepancy, about 300 kJ/mol. On the contrary, the tail of the potential curve (high separation distance) is well matched by the OPLS-AA FF. For the case of two carboxylates and one calcium, the original parameters of OPLS-AA once again matched the DFT calculated interactions better. However, the difference in the depth of the potential well between DFT and MM is slightly more, about 200 kJ/mol, compared to the case of one carboxylate. The tail of the potential has shifted to lower energies. The parameters of Yan et al.[21] are shown to shift the whole potential to higher interaction energies compared to the original ones.

The potential curve for sodium and one carboxylate, Figure 5, is perfectly matched by the original parameters of OPLS-AA for the whole range between 2 and 20 Å. The MM potential overlaps with the DFT-derived one for short separation distances and with the CDFT for long separation distances. The Yan et al.[21] parameters underestimated the potential depth by approximately 100 kJ/mol. The equilibrium distance of the complex with one carboxylate as depicted in Figure 5 is 2.5 Å, for both DFT and MM. For the case of two carboxylates, the DFT potential falls between the two MM potentials where the OPLS-AA parameters overestimate the interaction energies by 50 kJ/mol and the Yan et al.[21] parameters underestimate the interaction energies by 50 kJ/mol. The equilibrium distance of the complex with two carboxylates is 2.65 Å, for both DFT and MM. For the complexes consisting of one and two carboxylates and one sodium, calculations of the BSSE correction have been performed to confirm that both MM and DFT give the same equilibrium distances and results are presented in Table S1 in the Supporting Information. Table S1 demonstrates that the BSSE correction does not change the equilibrium distances for these cases.

In the cases with calcium at distances around 3.4 Å, the ion coordinates itself to only one of the oxygens, which gives a little plateau and changes the potential curves around that distance. This is observed for both the constrained and unconstrained DFT potential functions. At longer separation distances above

DOI: 10.1021/acs.jpca.5b04136
J. Phys. Chem. A XXXX, XXX, XXX−XXX

10 Å, the coordination of the counterion has been found to be the same as near the equilibrium distance, directly opposite to the carbon atom and at equal distance to the oxygen atoms. The same coordination phenomenon has also been observed in the cases for the sodium ion. However, due to a weaker interaction, the impact on the shape of the potential function is not so significant compared to calcium. In the case of one acid and one Na^+, the change of the coordination of the sodium to only one of the oxygens does not affect the shape of the potential curve as much as compared to calcium. In the case of two acids and one Na^+, the difference in the coordination seems not to affect the shape of the potential curve at all and the observed plateau in the previous cases does not exist.

4. CONCLUSIONS

The interaction energies within an organometallic complex consisting of a metal ion and deprotonated carboxylic acid(s) have been computed via DFT calculations. Such energies have been compared to a molecular mechanics force field to provide a basis of comparison for evaluating the effects of multibody interactions. It has been shown that the multibody effects play important role in the interactions between carboxylates and metal counterions, especially in the case of calcium. The complex consisting of three carboxylates and one calcium has the lowest total interaction energy among the ones studied, whereas the strongest pair-interaction occurs in the complex with one carboxylate. The comparison with MM demonstrates that interaction potentials implicitly considering the multibody effects can quantitatively differ from conventional force fields using simple pair potential functions, especially near the equilibrium distance.

Comparisons of the interaction energy obtained with DFT have been made with the OPLS-AA force field and a modified version of OPLS-AA presented by Yan et al.[21] The potential functions obtained by the two methods (DFT, MM) show an equivalent equilibrium distance for the metal ion−carboxylate group. The interaction energies computed using the original implementation of the OPLS-AA force field was in closer agreement with the DFT-derived potential functions, whereas the potential functions derived using the parameters presented by Yan et al.[21] are less consistent with DFT calculations.

To examine the potential curves with DFT at small and high separation distances, the interaction energy has been computed with and without constraint on the charge of the metal ion. Near the equilibrium distance, the charge transfer between the metal ion and the carboxylate group is high and, respectively, very important in determining the interaction energy. The charge transfer arises from the lack of electron density on the metal ion, the excess of electron density on the carboxylate group, and the difference in the electronegativity between the metal ion and the oxygens. However, going toward high separation distances, the charge transfer should stop and the two constituents should dissociate with integer charge, where Ca has +2 charge. To accomplish that, it was necessary to impose a constraint on the charge of the metal ion. That resulted in the asymptotic convergence of the interaction energy toward zero, whereas the unconstrained potential curve does not converge to zero even at high separation distances because of the different dissociation of the complex. To examine low and high separation distances in the potential curves, it is necessary to calculate the interaction energy near the equilibrium distance allowing charge transfer as well as to examine the tail of the potential. Thus, one has to constrain the charge in the DFT calculations. This means that at some point one should go from the unconstrained to the constrained potential curve. But where is that point? It can be seen from Figures 3−6 that the two curves, unconstrained (red dots) and constrained (black circles), become very close to each other. This most likely is the region where the charge transfer stops and the constraint curve becomes physically more correct for the dissociation described here.

■ ASSOCIATED CONTENT

Supporting Information

The Supporting Information is available free of charge on the ACS Publications website at DOI: 10.1021/acs.jpca.5b04136.

Comparison of the potential energy curves between 1, 2, 3, and 4 propanoate and butanoate ions with 1 calcium (Figure S1), BSSE correction calculated for the propanoate ion(s) complexes (Figure S2 and Table S1), comparison of the distances and angles between the carboxylates from the different complexes (Figure S3), Cartesian coordinates from the equilibrium geometries of the complexes with 1, 2, 3, and 4 propanoates with 1 calcium (PDF)

■ AUTHOR INFORMATION

Corresponding Author

*B. A. Grimes. E-mail: brian.grimes@chemeng.ntnu.no. Tel: +4773590338.

Notes

The authors declare no competing financial interest.

■ ACKNOWLEDGMENTS

The authors acknowledge The Research Council of Norway NFR project no. 209337 and The Faculty of Natural Science and Technology, Norwegian University of Science and Technology (NTNU), for financial support.

■ REFERENCES

(1) Silva, J. J. R. F. D.; Williams, R. J. P. *The Biological Chemistry of the Elements*; Oxford University Press: Oxford, U.K., 2001.

(2) Glusker, J. P.; Katz, A. K.; Bock, C. W. Metal Ions in Biological Systems. *Rigaku J.* **1999**, *16*, 8−16.

(3) Yang, W.; Yang, X. Molecular Dynamics Study of the Influence of Calcium Ions on Foam Stability. *J. Phys. Chem. B* **2010**, *114*, 10066−10074.

(4) Ladanyi, B. M. Computer Simulation Studies of Counterion Effects on the Properties of Surfactant Systems. *Curr. Opin. Colloid Interface Sci.* **2013**, *18*, 15−25.

(5) Auffinger, P.; Bielecki, L.; Westhof, E. Symmetric K1 and Mg21 Ion-binding Sites in the 5 S rRNA Loop E Inferred from Molecular Dynamics Simulations. *J. Mol. Biol.* **2004**, *335*, 555−571.

(6) Serra, M. J.; Baird, J. D.; Dale, T.; Fey, B. L.; Retatagos, K.; Westhof, E. Effects of Magnesium Ions on the Stabilization of RNA Oligomers of Defined Structures. *RNA* **2002**, *8*, 307−323.

(7) Simon, S.; Reisen, C.; Bersås, A.; Sjöblom, J. Reaction Between Tetrameric Acids and Ca^{2+} in Oil/Water System. *Ind. Eng. Chem. Res.* **2012**, *51*, 5669−5676.

(8) Ge, L.; Vernon, M.; Simon, S.; Maham, Y.; Sjöblom, J.; Xu, Z. Interactions of Divalent Cations with Tetrameric Acid Aggregates in Aqueous Solutions. *Colloids Surf., A* **2012**, *396*, 238−245.

(9) Baugh, T. D.; Grande, K. V.; Mediaas, H.; Vindstad, J. E.; Wolf, N. O. The Discovery of High Molecular Weight Naphthenic Acids (ARN Acid) Responsible for Calcium Naphthenate Deposits. *SPE Seventh International Symposium on Oilfield Scale*, Aberdeen, U.K., May 11−12, 2005; SPE: Richardson, TX, 2005; SPE 93011, pp 9−15.

DOI: 10.1021/acs.jpca.5b04136
J. Phys. Chem. A XXXX, XXX, XXX−XXX

(10) Bala, T.; Prasad, B. L. V.; Sastry, M.; Upadhyay, M.; Waghamare, U. Interactions of Different Metal Ions with Carboxylic Acid Groups: a Quantitative Study. *J. Phys. Chem. A* **2007**, *111*, 6183−6190.
(11) Tommaso, D. D.; de Leeuw, N. H. The Onset of Calcium Carbonate Nucleation: A Density Functional Theory Molecular Dynamics and Hybrid Microsolvation/Continuum Study. *J. Phys. Chem. B* **2008**, *112*, 6965−6975.
(12) Riccardi, E.; Wang, J.-C.; Liapis, A. I. Molecular Modeling of Polymeric Adsorbent Media: The Effects of Counter-Ions on Ligand Immobilization and Pore Structure. *J. Sep. Sci.* **2012**, *35*, 3073−3083.
(13) Riccardi, E.; Wang, J.-C.; Liapis, A. I. Modelling the Construction of Polymeric Adsorbent Media: Effects of Counter-Ions. *J. Chem. Phys.* **2014**, *140*, 084901.
(14) Duchovic, R. J.; Hase, W. L.; Schlegel, H. B.; Frisch, M. J.; Raghavachari, K. Ab Initio Potential Energy Curve for CH Bond Dissociation in Methane. *Chem. Phys. Lett.* **1982**, *89*, 120−125.
(15) Varandas, A. J. C. Ab Initio Treatment of Bond-Breaking Reactions: Accurate Course of HO_3 Dissociation and Revisit to Isomerization. *J. Chem. Theory Comput.* **2012**, *8*, 428−441.
(16) Caruso, F.; Rohr, D. R.; Hellgren, M.; Ren, X.; Rinke, P.; Rubio, A.; Scheffler, M. Bond Breaking and Bond Formation: How Electron Correlation is Captured in Many-Body Perturbation Theory and Density-Functional Theory. *Phys. Rev. Lett.* **2013**, *110*, 146403.
(17) Sun, H. COMPASS: An Ab Initio Force-Field Optimized for Condensed-Phase. ApplicationssOverview with Details on Alkane and Benzene Compounds. *J. Phys. Chem. B* **1998**, *102*, 7338−7364.
(18) Butenuth, A.; Moras, G.; Schneider, J.; Koleini, M.; Koppen, S.; Meißner, R.; Wright, L. B.; Walsh, T. R.; Ciacchi, L. C. Ab Initio Derived Force Field Parameters for Molecular Dynamics Simulations of Deprotonated Amorphous-SiO_2/Water Interfaces. *Phys. Status Solidi B* **2012**, *249*, 292−305.
(19) Lindorff-Larsen, K.; Piana, S.; Palmo, K.; Maragakis, P.; Klepeis, J. L.; Dror, R. O.; Shaw, D. E. Improved Side-Chain Torsion Potentials for the Amber ff99SB Protein Force Field. *Proteins: Struct., Funct., Genet.* **2010**, *78*, 1950−1958.
(20) Merzel, F. I.; Cek, M. H.; Janežic, D.; Sanson, A. New Force Field for Calcium Binding Sites in Annexin−Membrane Complexes. *J. Comput. Chem.* **2006**, *27*, 446−452.
(21) Yan, H.; Guo, X. L.; Yuan, S. L.; Liu, C. B. Molecular Dynamics Study of the Effect of Calcium Ions on the Monolayer of SDC and SDSn Surfactants at the Vapor/Liquid Interface. *Langmuir* **2011**, *27*, 5762−5771.
(22) Tsuzuki, S.; Shinoda, W.; Saito, H.; Mikami, M.; Tokuda, H.; Watanabe, M. Molecular Dynamics Simulations of Ionic Liquids: Cation and Anion Dependence of Self-Diffusion Coefficients of Ions. *J. Phys. Chem. B* **2009**, *113*, 10641−10649.
(23) Yan, H.; Yuan, S. L.; Xu, G. Y.; Liu, C. B. Effect of Ca^{2+} and Mg^{2+} Ions on Surfactant Solutions Investigated by Molecular Dynamics Simulation. *Langmuir* **2010**, *26* (13), 10448−10459.
(24) Jorgensen, W. L.; Maxwell, D. S.; Tirado-Rives, J. Development and Testing of the OPLS All-Atom Force Field on Conformational Energetics and Properties of Organic Liquids. *J. Am. Chem. Soc.* **1996**, *118* (45), 11225−11236.
(25) Project, E.; Nachliel, E.; Gutman, M. Parameterization of Ca 12 − Protein Interactions for Molecular Dynamics Simulations. *J. Comput. Chem.* **2008**, *29*, 1163−1169.
(26) Engkvist, O.; Åstrand, P.-O.; Karlström, G. Accurate Intermolecular Potentials Obtained from Molecular Wave Functions: Bridging the Gap between Quantum Chemistry and Molecular Simulations. *Chem. Rev.* **2000**, *100*, 4087−4108.
(27) Halgren, T. A.; Damm, W. Polarizable Force Fields. *Curr. Opin. Struct. Biol.* **2001**, *11*, 236−242.
(28) Soderhjelm, P.; Ryde, U. How Accurate Can a Force Field Become? A Polarizable Multipole Model Combined with Fragment-wise Quantum-Mechanical Calculations. *J. Phys. Chem. A* **2009**, *113*, 617−627.
(29) Gresh, N.; Cisneros, G. A.; Darden, T. A.; Piquemal, J.-P. Anisotropic, Polarizable Molecular Mechanics Studies of Inter- and Intramolecular Interactions and Ligand-Macromolecule Complexes. A Bottom-Up Strategy. *J. Chem. Theory Comput.* **2007**, *3*, 1960−1986.
(30) Warshel, A.; Kato, M.; Pisliakov, A. V. Polarizable Force Fields: History, Test Cases, and Prospects. *J. Chem. Theory Comput.* **2007**, *3*, 2034−2045.
(31) Shi, Y.; Xia, Z.; Zhang, J.; Best, R.; Wu, C.; Ren, J. W. P. Polarizable Atomic Multipole-Based AMOEBA Force Field for Proteins. *J. Chem. Theory Comput.* **2013**, *9*, 4046−4063.
(32) Varma, S.; Rempe, S. B. Multibody Effects in Ion Binding and Selectivity. *Biophys. J.* **2010**, *99*, 3394−3401.
(33) Marcelli, G.; Todd, B. D.; Sadus, R. J. Beyond Traditional Effective Intermolecular Potentials and Pairwise Interactions in Molecular Simulation. *Lecture Notes in Comput. Sci.* **2002**, *2331*, 932−941.
(34) Becke, A. D. Density-functional thermochemistry. III. The Role of Exact Exchange. *J. Chem. Phys.* **1993**, *98*, 5648−5652.
(35) Frisch, M. J.; Trucks, G. W.; Schlegel, H. B.; Scuseria, G. E.; Robb, M. A.; Cheeseman, J. R.; Scalmani, G.; Barone, V.; Mennucci, B.; Petersson, G. A.; et al. *Gaussian 09*; Gaussian, Inc.: Wallingford, CT, 2009.
(36) Valiev, M.; Bylaska, E. J.; Govind, N.; Kowalski, K.; Straatsma, T. P.; van Dam, H. J. J.; Wang, D.; Nieplocha, J.; Apra, E.; Windus, T. L.; et al. NWChem: A Comprehensive and Scalable Open-source Solution for Large Scale Molecular Simulations. *Comput. Phys. Commun.* **2010**, *181*, 1477.
(37) Bryantsev, V. S.; Diallo, M. S.; van Duin, A. C. T.; Goddard, W. A., III. Evaluation of B3LYP, X3LYP, and M06-Class Density Functionals for Predicting the Binding Energies of Neutral, Protonated, and Deprotonated Water Clusters. *J. Chem. Theory Comput.* **2009**, *5*, 1016−1026.
(38) Muzomwe, M.; Boeckx, B.; Maes, G.; Kasende, O. E. Matrix Isolation FT-IR and Theoretical DFT/B3LYP Spectrum of 1-Naphthol. *Spectrochim. Acta, Part A* **2013**, *108*, 14−19.
(39) Miao, R.; Jin, C.; Yang, G.; Hong, J.; Zhao, C.; Zhu, L. Comprehensive Density Functional Theory Study on Serine and Related Ions in Gas Phase: Conformations, Gas Phase Basicities, and Acidities. *J. Phys. Chem. A* **2005**, *109*, 2340−2349.
(40) Sweeney, A. F.; Armentrout, P. B. Guided Ion Beam Studies of the Collision-Induced Dissociation of CuOH + (H_2O) n (n = 1−4): Comprehensive Thermodynamic Data for Copper Ion Hydration. *J. Phys. Chem. A* **2014**, *118*, 10210−10222.
(41) Kolboe, S.; Svelle, S. Does an Ethene/Benzenium Ion Complex Exist? A Discrepancy between B3LYP and MP2 Predictions. *J. Phys. Chem. A* **2008**, *112*, 6399−6400.
(42) Mulliken, I. R. S. Electronic Population Analysis on LCAO−MO Molecular Wave Functions. *J. Chem. Phys.* **1955**, *23*, 1833.
(43) Boys, S. F.; Bernardi, F. Calculation of Small Molecular Interactions by Differences of Separate Total Energies - Some Procedures with Reduced Errors. *Mol. Phys.* **1970**, *19*, 553.
(44) Hess, B.; Kutzner, C.; Spoel, D. van der; Lindahl, E. GROMACS 4: Algorithms for Highly Efficient, Load-Balanced, and Scalable Molecular Simulation. *J. Chem. Theory Comput.* **2008**, *4*, 435−447.
(45) Foster, J. P.; Weinhold, F. Natural Hybrid Orbitals. *J. Am. Chem. Soc.* **1980**, *102*, 7211−7218.
(46) Reed, A. E.; Curtiss, L. A.; Weinhold, F. Intermolecular Interactions from a Natural Bond Orbital, Donor-Acceptor Viewpoint. *Chem. Rev.* **1988**, *88*, 899−926.
(47) Wu, Q.; van Voorhis, T. Direct Optimization Method to Study Constrained Systems Within Density Functional Theory. *Phys. Rev. A: At., Mol., Opt. Phys.* **2005**, *72*, 024502.
(48) Kaduk, B.; Kowalczyk, T.; van Voorhis, T. Constrained Density Functional Theory. *Chem. Rev.* **2012**, *112*, 321−370.

DOI: 10.1021/acs.jpca.5b04136
J. Phys. Chem. A XXXX, XXX, XXX−XXX

Supporting Information

DFT Study on the Interactions of Metal Ions with Long Chain Deprotonated Carboxylic Acids

Aleksandar Y. Mehandzhiyski[†], Enrico Riccardi[§], Titus S. van Erp[§], Henrik Koch[§], Per-Olof Åstrand[§], Thuat T. Trinh[§], Brian A. Grimes[†*]

[†] *Ugelstad Laboratory, Department of Chemical Engineering, Norwegian University of Science and Technology, SemSælandsvei 4, NO-7491 Trondheim, Norway*

[§] *Department of Chemistry, Norwegian University of Science and Technology, Høgskoleringen 5 Realfagbygget blokk D, 3.etg., NO-7491 Trondheim, Norway*

In Figure S1, a comparison between the potential energy curves of the propanoate and butanoate ion with 1 calcium are presented. The propanoate ion is presented in the left set of plots, while the butanoate ion is presented in the right set of plots. The total interaction energy according to Equation 1 and the pair-interaction energy according to Equation 2 are given in the top and bottom plots, respectively. The potential curves of both ions are nearly identical. Therefore, propanoate ion has been used to represent general carboxylate ion.

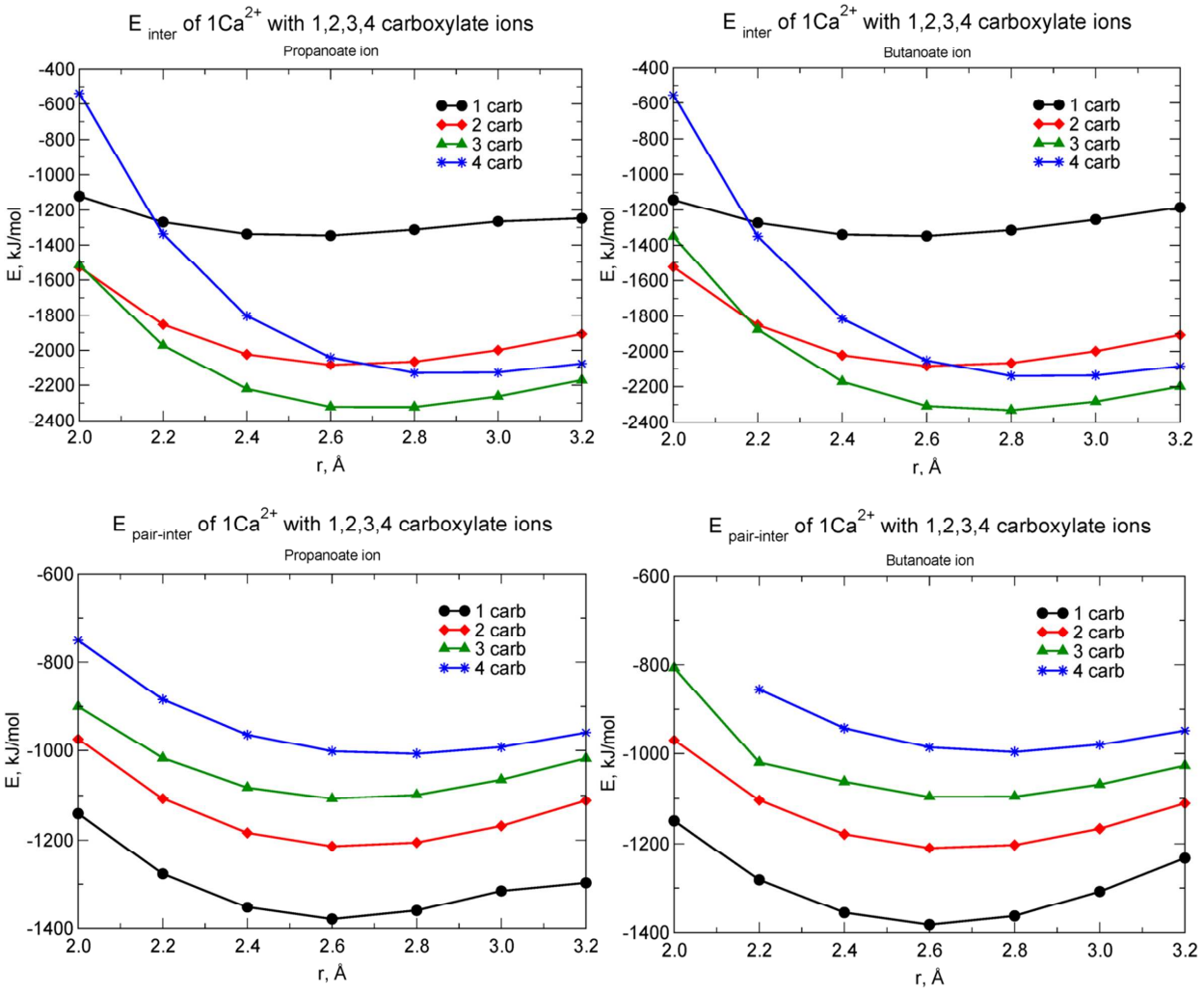

Fig. S1: Comparison between the total interaction energies, E_{inter}, according to Equation 1 and pair-interaction energy, $E_{pair\text{-}inter}$, according to Equation 2 between the propanoate ion(s) and Ca^{2+} (left) and butanoate ion(s) and Ca^{2+} (right).

In Figure S2, the total interaction energy of the propanoate(s) with 1 calcium with and without the BSSE correction is presented. The BSSE correction lowers the interaction energy in all the cases. With the BSSE correction, the equilibrium distance for the complex with 1 carboxylate is changed from 2.53 Å to 2.60 Å (a 0.07 Å difference towards a higher distance) with an energy difference of -3.57 kJ/mol; the equilibrium distances for the complexes of 2 (2.64 Å) and 3 (2.75 Å) carboxylates are the same with and without the correction; the equilibrium distance for the complex with 4 carboxylates has changed from 2.9 Å to 3.0 Å with an energy difference of -3.43 kJ/mol. Although, there is a slight change in the equilibrium distances for two of the examined complexes, the more important fact is that the order of the potential curves have been kept the same. Namely, the complex with 3 carboxylates is the most stable, followed by 4, 2 and 1 carboxylate(s).

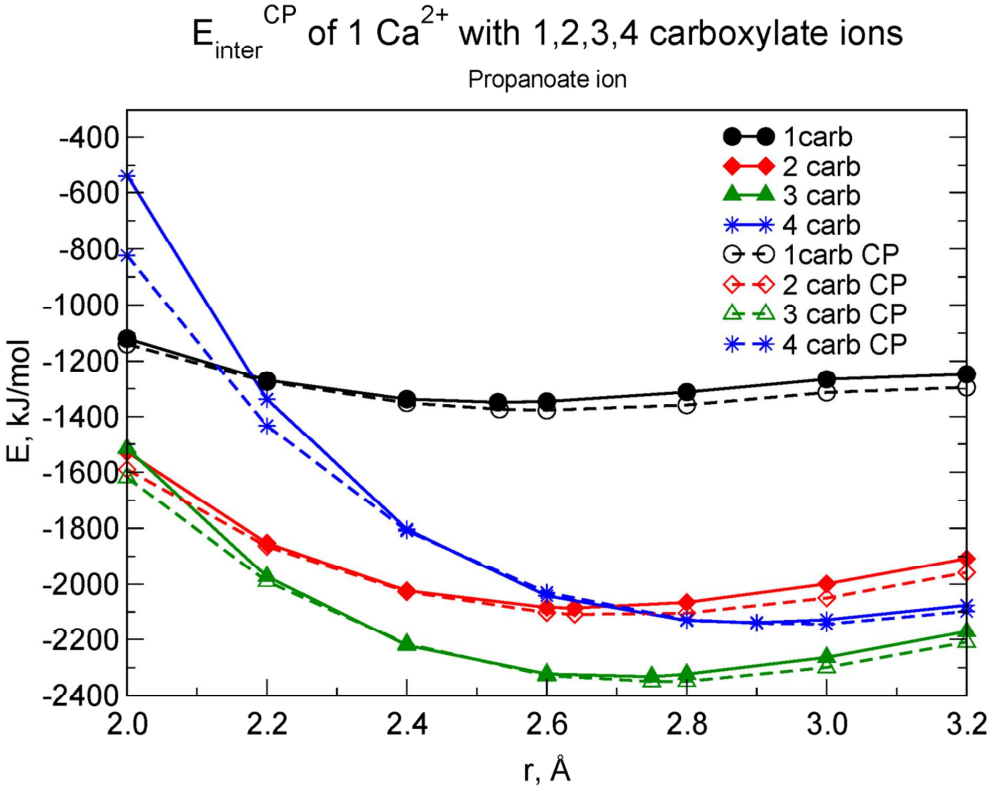

Fig. S2: Total interaction energy according to Equation 1, E_{inter}, (solid lines) and the interaction energy corrected for the basis set superposition error - BSSE (dashed lines) determined by the counterpoise method.

In Table S1 the total interaction energy of 1 and 2 propanoate(s) with 1 sodium with and without the BSSE correction for few points around, and at, the equilibrium distance (2.5 Å for 1 carboxylate and 2.65 Å for 2 carboxylates) is presented. It can be seen from the table that the BSSE correction does not change the equilibrium distance for these complexes.

Table S1: Total interaction energy according to Equation 1, E_{inter}, and the interaction energy corrected for the basis set superposition error, BSSE, determined by the counterpoise method for the complexes consisting of 1 sodium and 1 and 2 propanoate(s), respectively.

1 carboxylate	E_{inter} without BSSE (kJ/mol)	E_{inter} with BSSE (kJ/mol)
2.40 Å	-607.14	-608.02
2.50 Å	-610.49	-613.97
2.60 Å	-607.69	-613.66
2 carboxylates		
2.45 Å	-799.79	-807.57
2.65 Å	-818.60	-828.62
2.85 Å	-805.89	-817.72

In Figure S3, a comparison of the distances and angles between the different carboxylates for the complexes consisting of 2, 3 and 4 carboxylates is presented. It should be noted that when more carboxylates are added to the complex, the distances between the oxygen atoms (depicted in red) and angles (depicted in blue) decrease. This leads to more repulsion between the carboxylate groups and is therefore partially responsible for the multibody effects as explained in the main text.

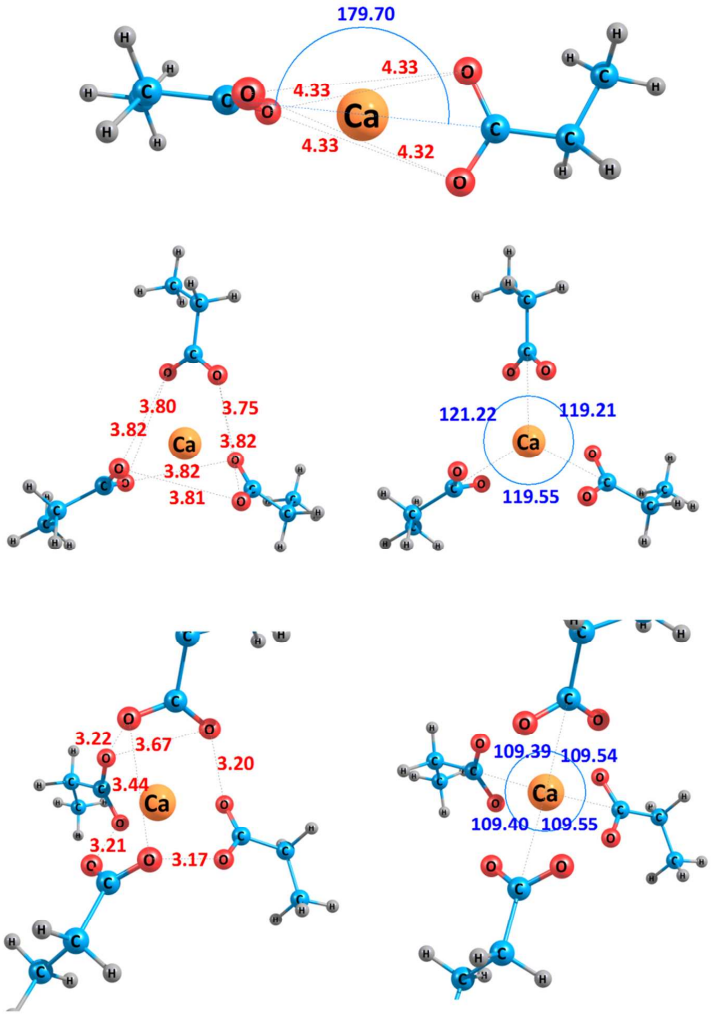

Fig. S3: Distances depicted in red are between the oxygen atoms from the different carboxylate groups for 2 (top), 3 (middle) and 4 (bottom) carboxylates. Angles depicted in blue are between the different carboxylate molecules in the complex.

The Cartesian coordinates of the equilibrium geometries of the complexes consisting of 1, 2, 3 and 4 carboxylates and 1 calcium, respectively, are given below.

1 carboxylate

Ca	0.266949150	-2.066520470	-0.002280660
C	-0.294372790	0.403446530	0.001359690
O	0.926064910	0.005530190	0.001840290
O	-1.219485970	-0.494011080	-0.000072370
C	-0.657457600	1.856716590	0.000735580
C	0.520729640	2.827056980	0.000118530
H	-1.313013370	2.010459980	0.866257630
H	-1.312692200	2.009165630	-0.865258410
H	1.150265220	2.698797150	0.882089260
H	1.150288530	2.697198790	-0.881645610
H	0.151388900	3.853891010	-0.001193130

2 carboxylates

Ca	0.000000000	0.000000000	-0.174766900
C	2.634155350	0.224327770	-0.167762630
O	2.077749800	-0.610427990	0.615847680
O	1.940073900	0.951428920	-0.953623520
C	4.142239460	0.375549900	-0.186741870
C	4.900399850	-0.527298380	0.782593300
H	4.354592050	1.433390160	0.004105020
H	4.461890110	0.207649630	-1.221254750
H	4.603375000	-0.341588540	1.816702200
H	4.711658910	-1.582653490	0.576038790
H	5.977009420	-0.353662080	0.702906160
H	-4.603375000	0.341588540	1.816702200
H	-4.354592050	-1.433390160	0.004105020
C	-4.900399850	0.527298380	0.782593300
H	-5.977009420	0.353662080	0.702906160
C	-4.142239460	-0.375549900	-0.186741870
C	-2.634155350	-0.224327770	-0.167762630
O	-2.077749800	0.610427990	0.615847680
O	-1.940073900	-0.951428920	-0.953623520
H	-4.711658910	1.582653490	0.576038790
H	-4.461890110	-0.207649630	-1.221254750

3 carboxylates

Ca	0.016065190	0.015166880	-0.261858310
C	-1.393894580	-2.349310410	-0.233243120
C	-1.359443810	2.399916000	-0.239401340
C	2.768421450	-0.044932870	-0.239940220
O	-1.529396460	-1.559571950	0.749975260
O	-0.647125570	-2.100913210	-1.230777600
C	-2.171745410	-3.675163010	-0.242752970
C	-2.998443510	-3.948555070	1.010944400
H	-1.446770980	-4.477182190	-0.424295800
H	-2.803158630	-3.671127060	-1.139563630

H	-2.365752400	-3.978204690	1.901544110
H	-3.737749340	-3.160813730	1.174296790
H	-3.526052450	-4.905602800	0.931717400
H	-2.327554670	4.024439440	1.901061860
H	-3.198583930	3.467005930	-0.432570990
C	-1.995492170	4.568933830	1.013503620
H	-2.583836190	5.489415640	0.933921460
C	-2.147558420	3.717440940	-0.243638890
O	-0.608672030	2.121720730	0.744216630
O	-1.487049850	1.625117730	-1.237886320
H	-0.950533520	4.841784520	1.180447970
H	-1.843264980	4.272817410	-1.139801100
O	2.145208010	-0.532137810	0.739812720
O	2.175871520	0.454530600	-1.233891180
C	4.300508580	-0.061950480	-0.248375570
H	4.610549350	-0.618451840	-1.141790000
H	4.637277730	0.962792860	-0.447214810
C	4.950373470	-0.628567910	1.010523650
H	4.664067880	-0.054118050	1.895125190
H	4.636133430	-1.660342630	1.185862790
H	6.042151760	-0.609582350	0.926033350

4 carboxylates

Ca	-0.023405000	-0.000176000	0.012379000
C	-0.023587000	-0.000082000	2.913994000
C	2.710556000	0.000019000	-0.958318000
C	-1.390723000	2.367939000	-0.958336000
C	-1.390657000	-2.367790000	-0.958270000
O	-1.136195000	2.200350000	0.267267000
O	-1.244467000	1.499957000	-1.848585000
O	1.866489000	0.853767000	-1.349737000
O	2.522564000	-0.825569000	-0.035492000
O	-0.653038000	-0.866955000	2.245877000
O	0.782249000	0.830642000	2.435953000
O	-2.163397000	-1.513304000	-0.467273000
O	-0.154059000	-2.201249000	-1.150290000
C	-0.295528000	0.069844000	4.436408000
C	-0.930639000	-1.189177000	5.030396000
H	0.648267000	0.316233000	4.934341000
H	-0.956601000	0.933058000	4.587914000
H	-1.194998000	-1.050016000	6.088120000
H	-1.828690000	-1.454447000	4.469046000
H	-0.248141000	-2.042118000	4.959645000
C	4.060773000	-0.031675000	-1.713077000
C	5.192030000	-0.731512000	-0.957799000
H	3.868617000	-0.543161000	-2.665261000
H	4.327017000	0.999476000	-1.968454000
H	6.101440000	-0.810225000	-1.569757000
H	5.443470000	-0.187736000	-0.041757000
H	4.876934000	-1.732651000	-0.656078000
C	-1.889908000	3.762951000	-1.406590000
C	-2.381482000	4.663803000	-0.272155000

H	-1.047515000	4.235315000	-1.928086000
H	-2.668182000	3.610613000	-2.162224000
H	-2.636704000	5.669465000	-0.635066000
H	-3.268680000	4.239327000	0.207995000
H	-1.614171000	4.747347000	0.500157000
C	-2.014095000	-3.718167000	-1.387094000
C	-1.006981000	-4.842629000	-1.632689000
H	-2.745342000	-3.999199000	-0.621649000
H	-2.591181000	-3.517453000	-2.299627000
H	-1.501699000	-5.757741000	-1.988056000
H	-0.262712000	-4.532724000	-2.369583000
H	-0.460982000	-5.082675000	-0.715741000

Paper 2

Ab Initio Molecular Dynamics Study on the Interactions between Carboxylate Ions and Metal Ions in Water

THE JOURNAL OF PHYSICAL CHEMISTRY B

Article

pubs.acs.org/JPCB

Ab Initio Molecular Dynamics Study on the Interactions between Carboxylate Ions and Metal Ions in Water

Aleksandar Y. Mehandzhiyski,[†] Enrico Riccardi,[‡] Titus S. van Erp,[‡] Thuat T. Trinh,[‡] and Brian A. Grimes*[,†]

[†]Ugelstad Laboratory, Department of Chemical Engineering, Norwegian University of Science and Technology, SemSælandsvei 4, NO-7491 Trondheim, Norway

[‡]Department of Chemistry, Norwegian University of Science and Technology, Høgskoleringen 5 Realfagbygget blokk D, 3.etg., NO-7491 Trondheim, Norway

Supporting Information

ABSTRACT: The interaction between a carboxylate anion (deprotonated propanoic acid) and the divalent Mg^{2+}, Ca^{2+}, Sr^{2+}, Ba^{2+} metal ions is studied via ab initio molecular dynamics. The main focus of the study is the selectivity of the carboxylate−metal ion interaction in aqueous solution. The interaction is modeled by explicitly accounting for the solvent molecules on a DFT level. The hydration energies of the metal ions along with their diffusion and mobility coefficients are determined and a trend correlated with their ionic radius is found. Subsequently, a series of 16 constrained molecular dynamics simulations for every ion is performed, and the interaction free energy is obtained from thermodynamic integration of the forces between the metal ion and the carboxylate ion. The results indicate that the magnesium ion interacts most strongly with the carboxylate, followed by calcium, strontium, and barium. Because the interaction free energy is not enough to explain the selectivity of the reaction observed experimentally, more detailed analysis is performed on the simulation trajectories to understand the steric changes in the reaction complex during dissociation. The solvent dynamics appear to play an important role during the dissociation of the complex and also in the observed selectivity behavior of the divalent ions.

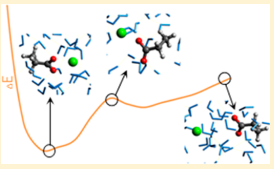

1. INTRODUCTION

Most chemical and biological reactions proceed in solution and, particularly, in aqueous solution. The dissociation of ions in aqueous solution is an important step in a myriad of chemical and biochemical processes. Of course, most ionic compounds tend to dissociate to their respective cations and anions in aqueous solution due to the polarity of water. The dissociation of sodium chloride has been extensively studied,[1−4] and it has been shown that although it is a simple ionic compound, its dissociation is rather complicated.[1] For ion dissociation to occur, several different steps are required to facilitate the increase in the distance between the two ions. The solvent effects accompanying the reaction, such as the rearrangement of the solvent molecules in the solvation shells during the reaction, should be taken into account as well because the solvent has an energetic and dynamic contribution to the ionic dissociation.

Sodium chloride is a typical ionic compound and interesting case study of ionic dissociation processes in solution; however, another important ionic dissociation/association processes is the interaction between carboxylic acids and divalent cations at a phase boundary because carboxylic acids are abundant in biochemistry[5] and chemical engineering processes.[6]

During the production of crude oil, certain types of carboxylic acids, particularly tetra naphthenic carboxylic acids,[6] can dissociate above a certain pH level and become negatively charged carboxylate ions. Additionally, typical offshore petroleum production involves contacting crude oil with huge amounts of seawater, which brings the carboxylate ions into contact with a diversity of dissolved ions.[5] When brought into contact via interfacial mass transport,[7,8] the carboxylic acids and positively charged ions[9] can react to form insoluble products.[10] The proposed mechanism suggests that carboxylic acid groups from different molecules can react with the divalent ions and form a cross-linked network at the oil−water interface. Also, it has been experimentally shown through potentiometric titration and elemental analysis of the formed precipitates that the reaction between the metal ions and the carboxylic acids is very selective[9,11] and not all of the ions bind equally. The affinity of binding is as follows: $Ca^{2+} > Ba^{2+} \approx Sr^{2+} > Mg^{2+}$. This affinity has been explained[9] by the number of water molecules coordinated to the cation and its size. That affinity was associated with the shielding density from the solvation molecules. This suggestion was speculative due to the fact that experimental conformation of this explanation was beyond the scope of their study. Consequently, the principal motivation for the present work is to obtain a rigorous mechanistic description of this ion selectivity based on first principle calculations.

Molecular dynamics has been successful to study microscopic changes occurring during the dissociation of ions.[1−4] Dellago and Ballard[1] have recently studied the dissociation of NaCl using molecular dynamics simulations and explained the

Received: June 12, 2015
Revised: August 3, 2015
Published: August 3, 2015

DOI: 10.1021/acs.jpcb.5b05616
J. Phys. Chem. B 2015, 119, 10710−10719

sensitivity of the process to solvent rearrangement. In that work[1] the reaction coordinate has been defined as the distance separating the two ions but was shown to be a poor reaction coordinate that could not adequately describe the process. Besides the detailed picture of the NaCl dissociation, the microscopic mechanism is still not completely known. Because of the usage of semiempirical force fields, classical molecular dynamics has limitations to describe chemical reactions. In that sense, ab initio molecular dynamics (AIMD) is more robust and is able to capture and describe the reaction mechanism[12−15] of different chemical and enzymatic reactions as well as quantitatively assess the electronic delocalization and electron transfer during reactions. AIMD uses the principles of quantum mechanics to calculate the forces between the atoms on the fly. Therefore, it does not need semiempirical potentials to determine the forces. The role of the solvent can be taken into account explicitly, which can provide more details of the microscopic reaction in solution; however, density functional theory (DFT) calculations result in higher computational costs. This confines feasible case studies to smaller systems and time scales as compared with classical MD.

The main focus of the present paper is to study the interaction between a carboxylate ion and different metal ions in the aqueous phase, explicitly accounting for the solvent molecules. By studying the microscopic mechanism using AIMD, we study the role of the solvent on the selectivity behavior of different metal ions toward their reaction with carboxylate ions. To accomplish that we have used AIMD and, in particular, Born−Oppenheimer molecular dynamics (BOMD) simulations to calculate the forces between a carboxylate ion and different metal cations. By knowing the constrained forces acting between the ions, the free-energy surface can be obtained by simple integration of the time-averaged forces. As Ballard and Dellago[1] and Geissler et al.[2] have previously shown, the solvent and solute degrees of freedom must be included into the reaction coordinate because the distance between the two reaction centers is not enough to fully understand the reaction mechanism. Therefore, to have a more complete understanding of the metal ion−COO^- interaction, we have investigated the simulation trajectories by (a) calculating the water binding energies, (b) self-diffusivity and mobility of ions, (c) radial distribution functions (RDFs), and (d) water coordination numbers and exchanges of water molecules in the first solvation shell of the ions during the simulations.

2. MODELS AND METHODS

Born−Oppenheimer molecular dynamics (BOMD) simulations have been performed with the Quickstep[16] algorithm implemented in the simulation package CP2K.[17] The program implements the hybrid Gaussian and plane-wave (GPW) method[18] for calculating the DFT electronic ground structure at every time step. The BLYP functional[19] with a double-ζ valence polarized (DZVP) basis set has been used for all the atomic species along with Goedecker−Teter−Hutter (GTH) pseudopotentials.[20] The electronic density cutoff was set to 400 Ry. A DFT-D2 type dispersion correction[21] has been used, except in the case with barium, where parameters are not available; however, for several of the simulated systems, we calculated the dispersion energy to be <0.04% of the total energy of the system, and the lack of dispersion correction for barium should not significantly affect the end results. The time step for integrating the equation of motion was set to 0.5 fs. The temperature was maintained at 300 K through a velocity rescaling thermostat - CSVR[22] with time constant of 100 fs. Periodic boundary conditions were applied to all three spatial directions.

To systematically study the reaction, first the water binding energies of the metal ions are going to be assessed. The metal ions chosen for this study are the divalent metal ions from the second group of the periodic table, Mg, Ca, Sr, Ba. After studying the water binding energies of the metal ions, their behavior in bulk aqueous solution will be studied in both the presence and absence of a carboxylate ion. Finally, a constrained BOMD simulation will be performed to study the interaction energies and solvent/solute dynamics as a function of the separation distance between the carboxylate group and the respective metal ions.

The procedure described by Ramaniah et al.[23] and Pavlov et al.[24] is employed to calculate the water binding energies of the metal ions. The successive binding energy[24] corresponds to the energy required to successively add water molecules to the metal-water cluster and is given by

$$\Delta E = E\{M(H_2O)_{n-1}^{2+}\} + E(H_2O) - E\{M(H_2O)_n^{2+}\} \quad (1)$$

The first term on the right is the energy of the metal ion−water complex with $(n - 1)$ water molecules, the second is the energy of an isolated water molecule, and the third term is the energy of the metal ion−water complex with n water molecules. The charge of the metal ions (Mg, Ca, Sr, Ba) has been set to $q = +2$.

After studying the water binding energy, a cubic simulation box with dimensions of 14 Å consisting of the selected metal ion and 86 water molecules has been created and equilibrated for 10 ps. The overall charge of the system was set to $q = +2$. The density of the constructed simulation box is close to the density of liquid water at the simulated temperature. After the initial equilibration, a production run of 12 ps has been performed and the RDF of the metal ions with the oxygen atoms from the water molecules was calculated. Deprotonated propanoic acid (propanoate ion) has been chosen to represent a general carboxylate ion because of its simple structure and a good compromise between number of atoms and computational cost, as shown in a previous study.[25] After the initial pre-equilibration, the metal ion and the carboxylate ion were combined together in the same simulation box, where the geometries of the complexes were constructed according to our previous study[25] and water molecules were added in the simulation box. For this simulation box, equilibration for 10 ps was followed by a production run of 12 ps.

Finally, 12 ps NVT simulations were performed by fixing the distance between the metal ion and the carbon from the carboxylate group for different separation distances varying from 2 (r_1) to 6 Å (r_2). For every simulation, the average constrained force has been calculated from the last 10 ps. Then, the free-energy profile has been obtained by thermodynamic integration according to eq 2

$$A = -\int_{r_1}^{r_2} \langle \bar{F}(r) \rangle dr \quad (2)$$

where A is the Helmholtz free energy, $\bar{F}$ is the constrained time-averaged force from the simulations, and r is the separation distance. Fourteen constrained MD simulations were performed for 14 distances, between r_1 and r_2 implying a total simulation time of 140 ps.

DOI: 10.1021/acs.jpcb.5b05616
J. Phys. Chem. B 2015, 119, 10710−10719

3. RESULTS AND DISCUSSION

In Section 3.1, the water binding energies of the different metal ions are presented. In Section 3.2, the unconstrained simulations are presented from which the RDFs as well as the self-diffusion and mobility coefficients of the metal ions are calculated. In Sections 3.3 and 3.4, the results from the constrained MD simulations are presented; these include the free-energy curves and a more detailed analysis of the simulation trajectories where the interaction energies and the dynamic behavior of the solute and the solvent are expected to be observed.

3.1. Water Binding Energies. The successive water binding energies for the first hydration shell of the metal ions have been calculated according to eq 1 and are presented in Figure 1. The optimized geometries of the metal ion−water complexes with the lowest energy and full first hydration shell are presented in Figure 2. The magnesium ion in Figure 1 is depicted in the color black, calcium in orange, strontium in red, and barium in turquoise. The same coloring scheme for the different ions is kept throughout all Figures.

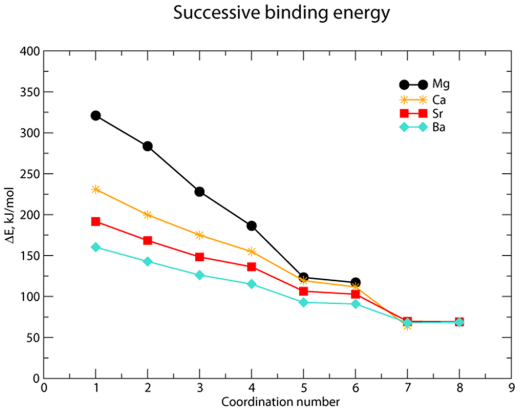

Figure 1. Successive water binding energy, ΔE, according to eq 1 as a function of the coordination number.

From Figure 1, it can be seen that the magnesium ion has the highest successive binding energies with water among the studied ions, followed by calcium, strontium, and barium. The highest change in the successive binding energy by adding more water molecules to the first solvation shell is for the magnesium ion, which can be seen from the most negative magnitude of the average slopes of the curves in Figure 1. The average slope represents the average change in energy for adding or removing water molecules. For the calcium ion the magnitude of the average slope is 41% lower compared with magnesium, while the slope is 57% lower for strontium and 67% lower for barium compared with magnesium, respectively. The first water molecule successive binding energies differ among the different ions. The values for Mg^{2+}, Ca^{2+}, Sr^{2+}, and Ba^{2+} are 320.9, 230.9, 191.6, and 160.2 kJ/mol, respectively. The successive binding energies of the fifth, sixth, and, especially, the seventh and eight water molecules binding energies are almost the same. It appears that the binding energies follow the group trend and the smaller ions from the second group in the periodic table have higher binding energies. Therefore, the smaller second group ions appear to form stronger complexes with the water molecules. The geometries depicted in Figure 2 show that the Me^{2+}−H_2O distance is increasing from 2.1 to 2.9 Å from Mg^{2+} to Ba^{2+} in the same way that the ionic radius increases from 0.65 to 1.35 from Mg^{2+} to Ba^{2+},[5] respectively. The geometry of the magnesium ion−water complex is regular octahedral, while the other ions have irregular coordination geometry.[5] The slopes of the curves in Figure 1 combined with the water binding energies imply that the magnesium ion attracts the water molecules more strongly. The binding energies presented are in a very good agreement with previous theoretical[23,24] and experimental results.[26]

3.2. Unconstrained Molecular Dynamics Simulations. In the present section, the results from the unconstrained MD simulations of the metal ions in the water phase and the metal ion−carboxylate group complex in the water phase are presented. A snapshot of the simulation box with propanoate and calcium is presented in Figure 3. Figure 4a,b presents the metal ion−water RDFs without and with the presence of the carboxylate ion, respectively. The RDF is denoted as $g(r)$ and constructed based on the separation distance between the metal ion and the oxygen atom of the water molecule. The magnesium ion has the most compact solvation shell, which can be seen from the distance at which the first solvation shell peak appears. At the shortest distance, 2.10 Å, is Mg^{2+}, followed by Ca^{2+} (2.45 Å), Sr^{2+} (2.65 Å), and Ba^{2+} (2.85 Å). The peak magnitude is highest for Mg^{2+} and lowers in the order Ca^{2+} > Sr^{2+} > Ba^{2+}. Beside the magnitude, the first peak is also narrower for the small ions, and it becomes wider for the larger ions. The coordination number of water molecules increases with increasing ionic radius; the coordination number is 6 for Mg^{2+} (ionic radius of 0.65 Å) in the case without carboxylate and 4 with carboxylate and up to 8 and 7 without and with carboxylate, respectively, for Ba^{2+} which has an ionic radius of 1.35 Å. These observations imply that the smaller ions have stronger interactions with the water molecules, as seen also from the magnitude in Figure 1, and also that the structure of the first solvation shell around the small ions is more compact compared with the larger ones. A more broad second coordination shell is observed for Mg^{2+} at 4.25 Å, Ca^{2+} and Sr^{2+} around 4.6 Å, and Ba^{2+} between 4.75 and 5 Å, meaning the second coordination shell is less ordered and more diffuse. From Figure 4a,b can also be seen that when the metal ion is in a complex with carboxylate, its water coordination number is lower. It is also apparent from Figure 4b that the first solvation shell for Ca^{2+} became more compact and the peak has moved to shorter distance in the presence of the carboxylate, which means that its hydrodynamic radius[27] has decreased. All of the above results concerning the RDFs and coordination numbers are in very good agreement with previous simulation and experimental results.[28−31]

We have also calculated the self-diffusion and mobility coefficients of the metal ions in the presence and absence of carboxylate. The self-diffusion coefficients are obtained from the mean-square displacement and the Einstein relation

$$D = \lim_{t\to\infty} \frac{1}{6Nt} \left\langle \sum_{i=1}^{N} [r_i(t) - r_i(t_0)]^2 \right\rangle \quad (3)$$

where N is the number of molecules, t is time, $r_i(t)$ are the spatial coordinates at time t, and $r_i(t_0)$ are the coordinates at time t_0. The mobilities[32] of the ions have been calculated from the self-diffusion coefficients by

DOI: 10.1021/acs.jpcb.5b05616
J. Phys. Chem. B 2015, 119, 10710−10719

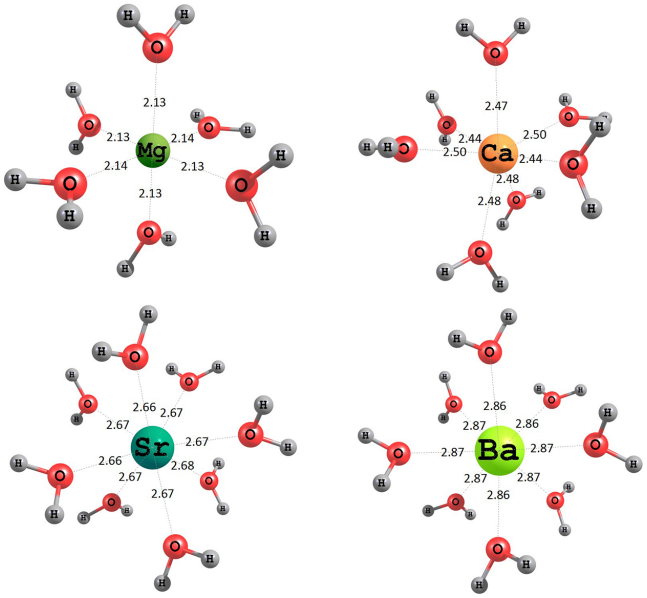

Figure 2. Optimized molecular geometries of the metal ion−water clusters; the distances are given in Ångstrom.

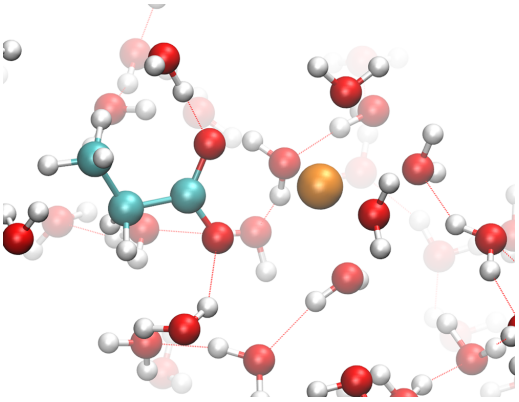

Figure 3. Snapshot of the simulation box containing propanoic acid, calcium and water molecules. The oxygen atoms are depicted in red, calcium in orange, carbon in cyan, and hydrogens in white.

$$u = Dq/k_bT \quad (4)$$

where k_b is the Boltzmann constant, T is the temperature of the system, and q is the charge of the ion. The self-diffusion and mobility coefficients, D and u, respectively, of the ions are presented in Table 1. The values of D and u for the ions decrease with the ionic radius from Ba^{2+} to Mg^{2+}, as seen from Table 1. The same trend for the self-diffusion coefficients of the divalent ions in water at 298.15K has been reported by Buffle et al.[33] The results presented here for the self-diffusion coefficients follow the same trend as the experimental data[33] and are qualitatively in agreement with the literature.[33] To improve the accuracy of the diffusion and mobility coefficients, more extensive simulations with presence of more ions should be done, which is beyond the scope of the current study. When the metal ions are in the complex with the carboxylate, the self-diffusion and the mobility coefficients decrease, except in the cases of Ca^{2+}, where they have increased. The increase in the self-diffusion and the mobility coefficients can be associated with the decrease in the hydrodynamic radius observed in Figure 4b in the presence of carboxylate because the hydrodynamic radius is inversely proportional to the diffusion coefficient.[27]

To have an even more detailed description of the solvent dynamics, we have studied the exchanges of water molecules in the first solvation shell of the metal ions. The exchange processes of solvation molecules within the solvation shells of ions[34−37] and biomolecules[38] have been extensively studied by classical[36−38] as well as ab initio MD.[34,35] Different methods have been presented and discussed regarding how to evaluate the exchanges and dynamics of the solvent molecules from molecular simulations; however, in all of them a time parameter t^* is being used,[34−38] which accounts for exchange processes by the minimum time a solvation molecule spends in or out its original solvation shell. The choice of t^* is arbitrary, and different suggestions for choosing this parameter have been made, where t^* is varied between 0 and 2 ps.[35] In MD studies of biomolecules,[38] t^* has been set to 0 ps and in that way counting every event irrespective of its duration. By using a small value for t^*, an associative processes cannot be described, only dissociative, starting from the maximum coordination number,[35] and it cannot account for any correlated movements. In our study, t^* has been set to 2.5 fs. That could provide qualitative description of the random movements of water molecules in and out of the solvation shell of the metal ions, which irrespective of their duration, could be a characteristic basis of comparison between the different metal ions. For a quantitative description, the rate of exchanges of solvent molecule in the solvation shell, a rare event technique like

DOI: 10.1021/acs.jpcb.5b05616
J. Phys. Chem. B 2015, 119, 10710−10719

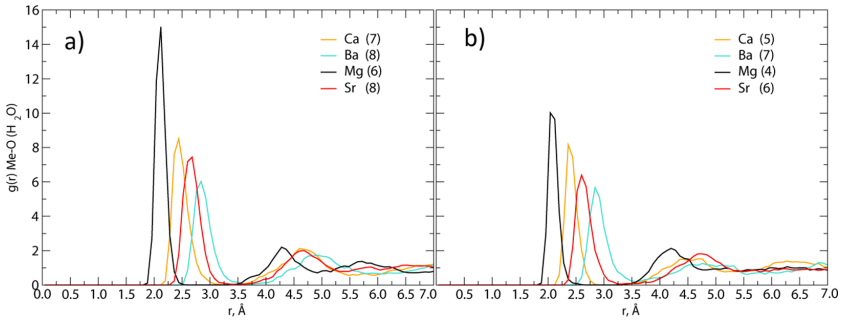

Figure 4. Radial distribution functions between a given metal ion and the oxygen from the water molecules (a) without carboxylate and (b) in the presence of carboxylate. In the legend, the coordination number of the respective ions is given in parentheses.

Table 1. Calculated Self-Diffusion Coefficients, *D*, Mobility, u, and Number of Exchanges of the Water Coordination Shell for the Metal Ions within and without Carboxylate during the Simulation Time of 12 ps and t^* = 2.5 fs

	ion without COO^-				ion with COO^-			
	Ba^{2+}	Ca^{2+}	Mg^{2+}	Sr^{2+}	Ba^{2+}	Ca^{2+}	Mg^{2+}	Sr^{2+}
D (10^{-10} m^2/s)	6.59 ± 2.43	2.16 ± 0.74	0.68 ± 0.06	2.84 ± 0.91	4.52 ± 1.64	5.17 ± 1.98	0.0003 ± 0.00009	1.73 ± 0.72
u (10^{-8} $m^2/(V\ s)$)	5.10 ± 1.88	1.69 ± 0.57	0.53 ± 0.05	2.19 ± 0.71	3.49 ± 1.27	3.99 ± 1.53	0.0002 ± 0.00007	1.34 ± 0.56
change in coordination	11	2	0	8	31	0	0	16

transition interface sampling,[39] could be used. In Table 1, the numbers of water molecules entering or leaving the first hydration shell of the metal ions are presented. As a criterion, to determine the spatial boundaries of the first hydration shell, we employed the RDFs from Figure 4b, precisely, where the $g(r)$ is closest to zero after the maximum of the first solvation shell peak. It can be noticed from Table 1 that Sr^{2+} and Ba^{2+} have more changes in their coordination numbers compared with Ca^{2+} and Mg^{2+}. The calcium ion has only two exchanges when the ion is by itself and no exchanges in the complex with carboxylate. The magnesium ion in both cases has no change in the water coordination number over the simulated time. That is consistent with the results for the successive binding energies presented in Figure 1, where the smaller ions (Ca^{2+}, Mg^{2+}) have higher binding energies and the water molecules are strongly bound to them. That implies that the interchange of water molecules in the first solvation shell is easier and happens relatively more frequently for the larger ions.

3.3. Constrained Molecular Dynamics Simulations and Potential Curves. In the following sections, the results from the constrained BOMD simulations are presented. In these simulations, the distance between the metal ion and the carbon atom from the carboxylate group was kept constant, between 2 and 6 Å at intervals of 0.25 Å, and the force between them was calculated. Integrating the resulting force over the separation distance, the interaction free energy between the ion and the carboxylate group was calculated according to eq 2, and the results of these calculations are presented in Figure 5. In Figure 5, the interaction free energy with the magnesium ion is represented by the right ordinate axis, while the interaction free energy with the rest of the ions is given by the left ordinate axis. The interaction free energy with magnesium is highest, −78 kJ/mol, followed by calcium −19.5 kJ/mol, strontium −17.8 kJ/mol, and barium −16.9 kJ/mol. The interaction free energy is decreasing as the ionic radius of the divalent ions increases. The location of the minimum of the potential well is increasing with increasing ionic radius, and it is located as follows: Mg^{2+} (2.5 Å), Ca^{2+} (3 Å), and Sr^{2+} (3.25 Å), while Ba^{2+} is located at ∼3.5 Å. A free-energy barrier for the metal ion−carboxylate association reaction has also been observed in Figure 5 and Table 2. The highest free-energy barrier is for Ba^{2+} − 9.3 kJ/mol, followed by Sr^{2+} − 4.3 kJ/mol and Ca^{2+} − 2.4 kJ/mol, and in the case of Mg^{2+} there was no observable free-energy barrier. The location of the free-energy barrier for Ca^{2+} is at 4 Å and for Ba^{2+} and Sr^{2+} around 4.5 Å. The magnitude of the free-energy barrier seems to increase with increasing radius for the divalent ions, which follows the trend of increasing radius in the second group of the periodic table.

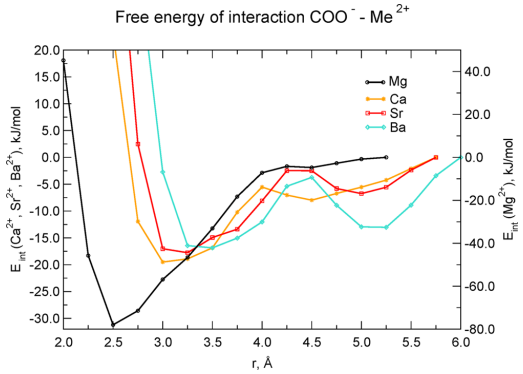

Figure 5. Helmholtz free-energy, E_{int}, curves of the metal ion−carboxylate ion complex in solvent. The distance in the abscissa is given in Ångstroms and represents the distance between the metal ion and the carbon atom from the COO^- group. Along the right ordinate axis, the interaction free energy with the magnesium ion is given, and along the left ordinate axis the interaction free energy with the other ions is given.

The current study is also in the framework of the calcium-naphthenate precipitation problem occurring in the petroleum

DOI: 10.1021/acs.jpcb.5b05616
J. Phys. Chem. B 2015, 119, 10710−10719

Table 2. Calculated Helmholtz Free Energy and Free-Energy Barriers for the Carboxylate−Metal Ion Interaction

ion	free energy (kJ/mol)	free-energy barrier (kJ/mol)
Mg^{2+}	−77.99	0.56
Ca^{2+}	−19.50	2.43
Sr^{2+}	−17.76	4.26
Ba^{2+}	−16.86	9.30

industry and, therefore, the selectivity of the reaction is also studied based on this application.[9−11] The above observations of the potential curves could partially explain the selectivity of the reaction for calcium−naphthenate precipitation.[9−11] Because the free-energy barrier is higher for Sr^{2+} and Ba^{2+}, the possibility of reaction with carboxylate ions is much lower compared with Ca^{2+} and Mg^{2+}; therefore, the formation of precipitates with Sr^{2+} and Ba^{2+} should not be very likely as the experiments suggest.[9,11] As seen from the potential curves, the magnesium interaction free energy is 4 times greater than the calcium interaction free energy, and, moreover, there is no free-energy barrier, which suggests that the carboxylate preferably would undergo a reaction with magnesium rather than with calcium; however, that contradicts the experimental results of Sundman et al.[11] As it was shown for the case of NaCl,[1] the distance between the two reacting centers is an insufficient descriptor, and the mechanism could not be fully explained only by considering the distance between the two ions. To be able to explain the experimental results for the selectivity of the reaction, we have further analyzed the simulation trajectories by calculating the RDFs, water coordination numbers, and exchanges of water molecules in the first solvation of the metal ions for different separation distances and presented the results in the next section. It is important to note that Sundman et al.[11] also studied the interactions between tetracarboxylate anions and sodium; therefore, we added the free energy of interaction between COO^-−Na^+ as Supporting Information.

3.4. Radial Distribution Functions, Charge Radial Distribution Functions, and Water Dynamics of the Constrained Molecular Dynamics Simulations. The RDF between a given metal ion and oxygen atoms from the water molecules have been calculated for different constrained separation distances. The RDFs are presented in Figure 6, where every subplot from a to d represents different separation distances between the metal ion and the carbon from the carboxylate group, starting from 2.5 Å and ending at 4 Å, respectively, at some particular points of interest like in the vicinity of the minimum on the potential well or energy barrier. The water coordination numbers are indicated with the bracketed numbers in the legend.

The RDFs and coordination numbers in subplot Figure 6a show that when the metal ion is coordinated with the carboxylate group there are on average two water molecules less in the first coordination shell of the ions, as seen also from the comparison between Figure 4a,b. The positions of the peaks are the same as they were in the bulk water phase without the presence of the carboxylate, which was described in Section

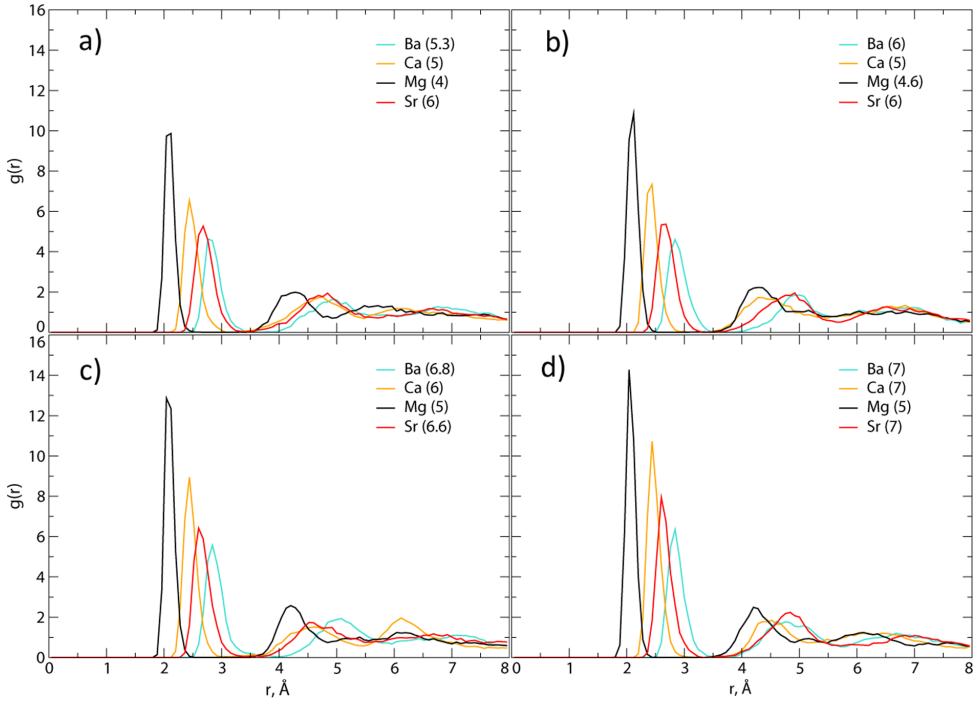

Figure 6. Radial distribution functions between the metal ions and the water oxygen in the presence of carboxylate at different separation distances (a) 2.5, (b) 3, (c) 3.5, and (d) 4 Å between the carbon of the COO^- group and the metal ion. In brackets, the coordination numbers of the metal ions are presented.

DOI: 10.1021/acs.jpcb.5b05616
J. Phys. Chem. B 2015, 119, 10710−10719

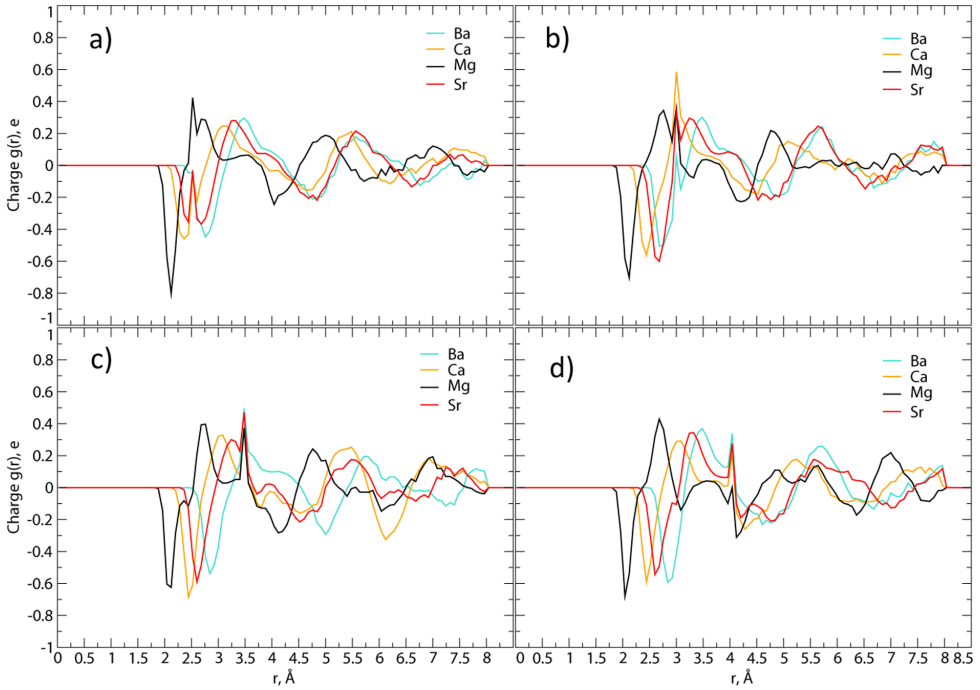

Figure 7. Charge radial distribution functions around the metal ions at different separation distances (a) 2.5, (b) 3, (c) 3.5, and (d) 4 Å between the carbon of the COO^- group and the metal ion.

3.2. The first solvation shell peak represents Mg^{2+} at 2.10 Å, which is followed by Ca^{2+} (2.45 Å), Sr^{2+} (2.65 Å), and Ba^{2+} at (2.85 Å). The magnitude of the peaks is lower compared with Figure 3; however, the trend regarding the most pronounced peaks for the smaller ions and lower peak magnitude for the bigger ions remains the same throughout all of the separation distances. With increasing separation distances to 3 Å, 3.5 Å, Figure 6b,c respectively, an average of one water molecule has entered from the bulk into the first solvation shell for all of the ions. In Figure 6d, an increase in the peak magnitude by approximately two units along with a narrower peak of the Ca^{2+} has been observed. As seen from Figure 5, a separation distance of ∼4 to 4.5 Å corresponds to maximum in the potential curves (transition state) for calcium. With increasing separation distance between the ion and the carboxylate group, as depicted in Figure 6a,d, the dissociation proceeds with insertion and rearrangements of water molecules into the first coordination shell of the metal ions, which has been consistent with previous findings of ionic dissociation.[1,2]

We have calculated and presented in Figure 7 the charge radial distribution function (CRDF), which is given by

$$\mathrm{CRDF} = \frac{1}{N_{st}} \int_0^{\infty} 2\pi r^2 e^- \, dr \tag{5}$$

where e^- is the Mulliken charges obtained from the simulations and N_{st} is the number of simulations steps. The Figure 7a,d represents the same separation distances as in Figure 6. The CRDF represents the charge distribution around a central atom in the same way as an RDF represents the local spatial arrangement around a chosen center, with the difference that the charge in a spherical volume element (r+dr) has been summed, instead of the number of pairs. First, it should be noticed that CRDFs have a direct relation to the structure and ordering in the liquid phase, as the RDFs show in Figure 6. The first negative valued peak in all of the subfigures is for Mg^{2+} at a distance 2.10 Å, followed by Ca^{2+} (2.45 Å), Sr^{2+} (2.65 Å), and Ba^{2+} at (2.85 Å), and correspond to the peak in Figure 6 for the $g(r)$. These are the same values for the first solvation shell in Figure 6, meaning that the negative charge is coming from the oxygen atoms in the water molecules. Shortly after, in about 0.8 to 0.9 Å, a positive peak appears, resulting from the hydrogen atoms from the water molecules. The following peaks can also be associated with the solvation structure extending to the second solvation shell and so on. In all the subfigures, there are sharp positive peaks that belong to the carbon atom from the carboxylate because the distance has been kept constant between them through the simulation. In almost of all the subfigures, the Mg^{2+} has the most negative charge (around −0.7 to $-0.8e^-$) in the first solvation shell, again indicating the strongest interaction with the water, as was shown in Figures 1 and 6. In Figure 7c,d, the magnesium's peak has risen to $-0.6e^-$ and has become more or less equal to the Ca^{2+}, Sr^{2+}, and Ba^{2+} peaks.

It might be concluded from the CRDF figures that Mg^{2+} has been surrounded by the most negatively charged environment than all of the other divalent ions, despite the fact that Mg^{2+} has the lowest coordination number. Because the magnesium interactions with the water are strongest among the divalent ions studied, a more negative charge accumulates around Mg^{2+} relative to the other cations, which may lead to more repulsion

DOI: 10.1021/acs.jpcb.5b05616
J. Phys. Chem. B 2015, 119, 10710−10719

with the negatively charged carboxylate groups. In that way, the electrostatic interactions may affect the behavior of the complex and may, for example, reduce the probability for the magnesium ion to associate with a second carboxylate ion because it is screened with the most negative charge by the surrounding water molecules.

In Table 3, the number of exchanges of water molecules[34−38] in the first solvation shell has been reported for separation

Table 3. Number of Exchanges of Water Molecules in the First Coordination Shell of the Different Metal Ion for Simulation Time of 12 ps and t^* = 2.5 fs[a]

r (Å)	Ba^{2+}	Ca^{2+}	Mg^{2+}	Sr^{2+}
2.00		0	0	
2.25		0	0	
2.50	8	0	0	8
2.75	25	0	0	0
3.00	3	8	1	0
3.25	18	1	2	8
3.50	21	10	0	10
3.75	4	1	0	15
4.00	1	0	0	2
4.25	0	4	0	34
4.50	12	0	0	25
4.75	35	1	0	13
5.00	30	8	0	6
5.25	18	12	0	2
5.50	37	18	0	21

[a]Constrained separation distance between the metal ion and the carbon from the COO^- group is given in the first column. Every distance in the first column represents a different 12 ps simulations, respectively.

distances from 2 to 6 Å. For the divalent ions, most exchanges are found for the bigger ions, Ba^{2+} and Sr^{2+}, compared with the small ones (Mg^{2+} and Ca^{2+}). The magnesium does not exchange water molecules (for the present simulation time), except for at separation distances of 3 and 3.25 Å, where only 1 and 2 exchanges have been observed, respectively. The calcium ion has exchanged water molecules significantly more often compared with magnesium. The strontium and barium ions exchange water molecules in their first solvation shell more frequently, which can also be correlated with the successive hydration energy plot in Figure 1, although it has been derived for 0 K and the molecular dynamics simulations are performed at 300 K. Because the successive water binding energy between Mg^{2+} and water is strongest and decreases in the order of Ca^{2+} > Sr^{2+} > Ba^{2+}, it is expected to see an increase in water exchanges going in the opposite direction Ba^{2+} > Sr^{2+} > Ca^{2+} > Mg^{2+}, which can be observed in Table 3. In ref 5, it is reported that Mg^{2+} exchanges water molecules at 10^{-6} s, while Ca^{2+} exchanges water at 10^{-9} s, respectively. That is also in good agreement with the presented simulations and it is not surprising that we did not observe any exchanges for the magnesium because the simulation time is on the order of 10^{-11} to 10^{-12} s.

The reluctance of Mg^{2+} to exchange water molecules could suggest that there is a lower probability that the metal ion will be associated with a second carboxylate group. The magnesium needs to lose some of the water molecules coordinated around it to be able to coordinate an additional carboxylate group. As we also can see from Figure 1, the change in the coordination to a lower number of water molecules is not energetically favorable compared with the other divalent ions because of the steepest average slope of the curve. Moreover, the ionic radius of the magnesium is the smallest of all of the divalent ions studied here, and sterically it cannot sustain the possibility to coordinate many functional groups with bigger van der Waals radius. The mobility coefficient of the magnesium is also lower in magnitude compared with the calcium, as was pointed out in Section 3.2, especially in the presence of COO^-. All of the above observations suggest that the calcium ion could have more binding potential than the magnesium. That could explain the experimentally observed selectivity toward a reaction of the tetracarboxylic acids anions with calcium and the formation of naphthenate precipitates[9,11] preferably with calcium and not with the other divalent ions.

In Figure 8, the results presented in the previous sections are schematically summarized in an attempt to explain the specific

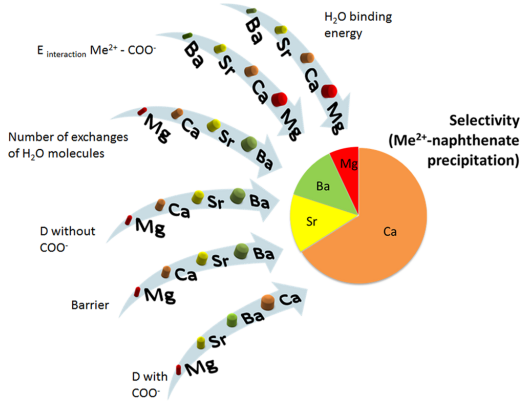

Figure 8. Schematic summary of the results from all of the previous sections. The scaling does not represent the true values.

ion selectivity. It should be noted that the scaling in the Figure does not represent the true values, and it is made just for clarity of illustration. The reported selectivity of the reaction between divalent metal ions with carboxylic groups[11] shown in Figure 8 can be interpreted by considering that an increasing arrow indicates an increased value of the property that it describes. First, the factors determining the selectivity can be roughly divided into two groups: (i) the first group contains properties that promote the interaction between the metal ions and the COO^- group(s), such as the interaction free energy between the metal ion and the COO^- group along with the self-diffusion coefficient, and (ii) the second group contains the properties that weaken the interaction between the metal ion and the COO^- group, such as the interaction energy of the metal ion with the solvent molecules, the number of exchanges of solvent molecules, and the free energy barrier for the Me^{2+}−COO^- reaction. The preference of binding Ca^{2+} instead of Sr^{2+} and Ba^{2+} could be explained by the fact that Ca^{2+} has a higher interaction free-energy and lower free-energy barrier for a reaction with COO^-. On the contrary, taking into account only those two properties suggests that Mg^{2+} would have higher binding probability when compared with Ca^{2+}. Thus, a more detailed examination of the ion−solvent interactions must be considered to understand the experimental and simulation

DOI: 10.1021/acs.jpcb.5b05616
J. Phys. Chem. B 2015, 119, 10710−10719

results for Ca^{2+} and Mg^{2+}. First, the successive binding energy of water molecules to the ion was examined, showing that Mg^{2+} has a much higher binding energy with water than Ca^{2+}. This potentially could affect the ion−water dynamics. That is exactly what has been shown from the number of exchanges for both ions because Mg^{2+} has higher interaction energy with the water molecules and it has a lower amount of exchanges of water into its first solvation shell. This observation could become important when a second COO^- group is in close proximity to the ion because with more exchanges of solvent molecules there is a higher probability for this second COO^- group to bind with the ion. Finally, the self-diffusion coefficient of Ca^{2+} is higher than that of Mg^{2+}, which in solution indicates that Ca^{2+} is a more mobile ion compared with Mg^{2+}. This means that when the two metal ions (Ca^{2+}, Mg^{2+}) are present in a solution, most likely Ca^{2+} will be able to diffuse faster to any available COO^- groups, especially for tetracarboxylic acids adsorbed at an oil−water interface where transport dynamics[7,8] should affect the selectivity; however, it should be pointed out that some of the estimated features, such as the interaction free energy and the free-energy barrier or the water binding energies and number of exchanges of water molecules, are strongly interrelated, so a conclusion about one of them naturally applies to the others.

4. CONCLUSIONS

The interactions between deprotonated carboxylic acid and different metal ions in the aqueous phase have been calculated through thermodynamic integration and ab initio molecular dynamics. The main focus has been on the selectivity of divalent alkaline earth metal ions toward a reaction with deprotonated carboxylic acids, which is an important phenomenon in industrial processes[9−11] and in general.[5]

It has been shown that the Mg^{2+} has the strongest interaction free energy among the divalent ions, and the Ca^{2+}, Sr^{2+}, and Ba^{2+} have almost the same interaction free energy. Ba^{2+} and Sr^{2+} have a higher free-energy barrier toward the association with the carboxylate compared with Ca^{2+}, while Mg^{2+} has a negligible activation energy toward the association reaction. Thus, the selectivity was not able to be fully explained only by the interaction free-energy profiles between the metal ions and the COO^- group. This result is consistent with conclusion from other studies[1] as well. Therefore, the molecular dynamics trajectories were further examined. A probable explanation was found in the ion−solvent interactions and dynamics of the solvent molecules. First, a lower mobility of the Mg^{2+} ion has been observed in comparison with the Ca^{2+} in aqueous solution. The RDFs, the CRDFs, and the successive binding energies of the water molecules and the metal ions suggested stronger interactions between water and magnesium compared with calcium. The stronger interactions between the solvent molecules and the magnesium resulted in fewer exchanges of solvent molecules during the dissociation of the ion−carboxylate complex and, consequently, a lower probability of interaction with more carboxylate groups. When all of the above observations are taken into account, interaction free energy between the COO^- group and the metal ion, free-energy barrier, solvent−solute interaction, and solvent and ion dynamics suggest that the probability of reaction and association between Ca^{2+} and carboxylate groups is higher than a reaction with the other divalent ions.

■ ASSOCIATED CONTENT

Supporting Information

The Supporting Information is available free of charge on the ACS Publications website at DOI: 10.1021/acs.jpcb.5b05616.

Free energy curve between the propanoate ion and sodium ion in water. (PDF)

■ AUTHOR INFORMATION

Corresponding Author

*E-mail: brian.grimes@chemeng.ntnu.no.

Notes

The authors declare no competing financial interest.

■ ACKNOWLEDGMENTS

We acknowledge The Research Council of Norway NFR project no. 209337 and The Faculty of Natural Science and Technology, Norwegian University of Science and Technology (NTNU) for financial support.

■ REFERENCES

(1) Ballard, A. J.; Dellago, C. Toward the Mechanism of Ionic Dissociation in Water. *J. Phys. Chem. B* **2012**, *116*, 13490−13497.
(2) Geissler, P. L.; Dellago, C.; Chandler, D. Kinetic Pathways of Ion Pair Dissociation in Water. *J. Phys. Chem. B* **1999**, *103*, 3706−3710.
(3) Rey, R.; Guardia, E. Dynamical Aspects of the Na^+-Cl^- Ion Pair Association in Water. *J. Phys. Chem.* **1992**, *96*, 4712−4718.
(4) Karim, O. A.; McCammon, J. A. Dynamics of a Sodium Chloride Ion Pair in Water. *J. Am. Chem. Soc.* **1986**, *108*, 1762−1766.
(5) Silva, J. J. R. F. D.; Williams, R. J. P. *The Biological Chemistry of the Elements: The Inorganic Chemistry of Life*; Oxford University Press: New York, 2001.
(6) Baugh, T. D.; Grande, K. V.; Mediaas, H.; Vindstad, J. E.; Wolf, N. O. The Discovery of High Molecular Weight Naphthenic Acids (ARN Acid) Responsible for Calcium Naphthenate Deposits. SPE Seventh International Symposium on Oilfield Scale, Aberdeen, U.K., May 11−12, 2005; SPE 93011; Curran Associates, Inc.: Red Hook, NY, 2006; pp 9−15.
(7) Kovalchuk, K.; Riccardi, E.; Grimes, B. A. Multiscale Modeling of Mass Transfer and Asorption in Liquid-liquid Dispersions. 1. Molecular Dynamics Simulations and Interfacial Tension Prediction for a Mixed Monolayer of Mono- and Tetracarboxylic Acids. *Ind. Eng. Chem. Res.* **2014**, *53*, 11691−11703.
(8) Kovalchuk, K.; Riccardi, E.; Grimes, B. A. Multiscale Modeling of Mass Transfer and Asorption in Liquid-liquid Dispersions. 2. Application to Calcium Naphthenate Precipitation in Oils Containing Mono- and Tetracarboxylic Acids. *Ind. Eng. Chem. Res.* **2014**, *53*, 11704−11719.
(9) Sjöblom, J.; Simon, S.; Xu, Z. The Chemistry of Tetrameric Aids in Petroleum. *Adv. Colloid Interface Sci.* **2014**, *205*, 319−338.
(10) Lutnaes, B. F.; Brandal, Ø.; Sjöblom, J.; Krane, J. Archaeal C_{80} Isoprenoid Tetraacids Responsible for Naphthenate Depositionin Crude Oil Processing. *Org. Biomol. Chem.* **2006**, *4*, 616−620.
(11) Sundman, O.; Simon, S.; Nordgard, E. L.; Sjöblom, J. Study of the Aqueous Chemical Interactions between a Synthetic Tetra-acid and Divalent Cations as a Model for the Formation of Metal Naphthenate Deposits. *Energy Fuels* **2010**, *24*, 6054−6060.
(12) Trinh, T. T.; Jansen, A. P. J.; van Santen, R. A.; VandeVondele, J.; Meijer, E. J. Effect of Counter Ions on the Silica Oligomerization Reaction. *ChemPhysChem* **2009**, *10*, 1775−1782.
(13) Pavlova, A.; Trinh, T. T.; van Santen, R. A.; Meijer, E. J. Clarifying the Role of Sodium in the Silica Oligomerization Reaction. *Phys. Chem. Chem. Phys.* **2013**, *15*, 1123−1129.
(14) Zhou, Y.; Wang, S.; Zhang, Y. Catalytic Reaction Mechanism of Acetylcholinesterase Determined by Born-Oppenheimer Ab Initio QM/MM Molecular Dynamics Simulations. *J. Phys. Chem. B* **2010**, *114*, 8817−8825.

DOI: 10.1021/acs.jpcb.5b05616
J. Phys. Chem. B 2015, 119, 10710−10719

(15) Motta, A.; Fragalà, I. L.; Marks, T. J. Insight into Group 4 Metallocenium-Mediated Olefin Polymerization Reaction Coordinates Using a Metadynamics Approach. *J. Chem. Theory Comput.* **2013**, *9*, 3491−3497.
(16) VandeVondele, J.; Krack, M.; Mohamed, F.; Parrinello, M.; Chassaing, T.; Hutter, J. QUICKSTEP: Fast and Accurate Density Functional Calculations Using a Mixed Gaussian and Plane Waves Approach. *Comput. Phys. Commun.* **2005**, *167*, 103−128.
(17) Hutter, J.; Iannuzzi, J.; Schiffmann, M.; VandeVondele, F. CP2K: Atomistic Simulations of Condensed Matter Systems. *WIREs. Comput. Mol. Sci.* **2014**, *4*, 15−25.
(18) Lippert, G.; Hutter, J.; Parrinello, M. A Hybrid Gaussian and Plane Wave Density Functional Scheme. *Mol. Phys.* **1997**, *92*, 477−487.
(19) Becke, A. D. Density-Functional Exchange-Energy Approximation with Correct Asymptotic Behavior. *Phys. Rev. A: At., Mol., Opt. Phys.* **1988**, *38*, 3098−3100.
(20) Krack, M. Pseudopotentials for H to Kr Optimized for Gradient-corrected Exchange-Correlation Functionals. *Theor. Chem. Acc.* **2005**, *114*, 145−152.
(21) Grimme, S. Semiempirical GGA-type Density Functional Constructed with a Long-range Dispersion Correction. *J. Comput. Chem.* **2006**, *27*, 1787−1799.
(22) Bussi, G.; Donadio, D.; Parrinello, M. Canonical Sampling through Velocity Rescaling. *J. Chem. Phys.* **2007**, *126*, 014101.
(23) Ramaniah, L. M.; Bernasconi, M.; Parrinello, M. Density Functional Study of Hydration of Sodium in Water Clusters. *J. Chem. Phys.* **1998**, *109*, 6839−6843.
(24) Pavlov, M.; Siegbahn, P. E. M.; Sandstrom, M. Hydration of Beryllium, Magnesium, Calcium, and Zinc Ions Using Density Functional Theory. *J. Phys. Chem. A* **1998**, *102*, 219−228.
(25) Mehandzhiyski, A. Y.; Riccardi, E.; van Erp, T. S.; Koch, H.; Åstrand, P.-O.; Trinh, T. T.; Grimes, B. A. DFT Study on the Interactions of Metal Ions with Long Chain Carboxylic Acids. *J. Phys. Chem. A* **2015**, submitted.
(26) Hertel, I. V.; Hüglin, C.; Nitsch, C.; Schulz, C. P. Photoionization of $Na(NH_3)_n$ and $Na(H_2O)_n$ Clusters: A Step Towards the Liquid Phase? *Phys. Rev. Lett.* **1991**, *67*, 1767−1770.
(27) Atkins, P.; Paula, J. de. *Physical Chemistry*, 8th ed.; Oxford Univeristy Press: Oxford, U.K., 2006.
(28) Larentzos, J. P.; Criscenti, L. J. A Molecular Dynamics Study of Alkaline Earth Metal-Chloride Complexation in Aqueous Solution. *J. Phys. Chem. B* **2008**, *112*, 14243−14250.
(29) Jiao, D.; King, C.; Grossfield, A.; Darden, T. A.; Ren, P. Simulation of Ca^{2+} and Mg^{2+} Solvation Using Polarizable Atomic Multipole Potential. *J. Phys. Chem. B* **2006**, *110*, 18553−18559.
(30) Piquemal, J.-P.; Perera, L.; Cisneros, G. A. Towards Accurate Solvation Dynamics of Divalent Cations in Water Using the Polarizable Amoeba Force Field: From Energetics to Structure. *J. Chem. Phys.* **2006**, *125*, 054511.
(31) Ohtaki, H.; Radnai, T. Structure and Dynamics of Hydrated Ions. *Chem. Rev.* **1993**, *93*, 1157−1204.
(32) Hiemenz, P. C.; Rajagopalan, R. *Principles of Colloid and Surface Chemistry*; Marcel Dekker: New York, 1997.
(33) Buffle, J.; Zhang, Z.; Startchev, K. Metal Flux and Dynamic Speciation at (Bio)interfaces. Part I: Critical Evaluation and Compilation of Physicochemical Parameters for Complexes with Simple Ligands and Fulvic/Humic Substances. *Environ. Sci. Technol.* **2007**, *41*, 7609−7620.
(34) Cauët, E.; Bogatko, S.; Weare, J. H.; Fulton, J. L.; Schenter, G. K.; Bylaska, E. J. Structure and Dynamics of the Hydration Shells of the Zn^{2+} Ion from *Ab Initio* Molecular Dynamics and Combined *Ab Initio* and Classical Molecular Dynamics Simulations. *J. Chem. Phys.* **2010**, *132*, 194502.
(35) Hofer, T. S.; Tran, H. T.; Schwenk, C. F.; Rode, B. M. Characterization of Dynamics and Reactivities of Solvated Ions by *Ab Initio* Simulations. *J. Comput. Chem.* **2004**, *25*, 211−217.
(36) Tiwari, S. P.; Rai, N.; Maginn, E. J. Dynamics of Actinyl Ions in Water: a Molecular Dynamics Simulation Study. *Phys. Chem. Chem. Phys.* **2014**, *16*, 8060−8069.
(37) Chorny, I.; Benjamin, I. Hydration Shell Exchange Dynamics during Ion Transfer Across the Liquid/Liquid Interface. *J. Phys. Chem. B* **2005**, *109*, 16455−16462.
(38) Garcıa, A. E.; Stiller, L. J. Computation of the Mean Residence Time of Water in the Hydration Shells of Biomolecules. *J. Comput. Chem.* **1993**, *14*, 1396−1406.
(39) van Erp, T. S.; Moroni, D.; Bolhuis, P. G. A Novel Path Sampling Method for the Calculation of Rate Constants. *J. Chem. Phys.* **2003**, *118*, 7762−7774.

DOI: 10.1021/acs.jpcb.5b05616
J. Phys. Chem. B 2015, 119, 10710−10719

Supporting Information

Ab Initio Molecular Dynamics Study on the Interactions between Carboxylate Ions and Metal Ions in Water

Aleksandar Y. Mehandzhiyski[+], Enrico Riccardi[++], Titus S. van Erp[++], Thuat T. Trinh[++], Brian A. Grimes[+]*

+ Ugelstad Laboratory, Department of Chemical Engineering, Norwegian University of Science and Technology, SemSælandsvei 4, NO-7491 Trondheim, Norway

++ Department of Chemistry, Norwegian University of Science and Technology, Høgskoleringen 5 Realfagbygget blokk D, 3.etg., NO-7491 Trondheim, Norway

The main focus in the experimental studies of the calcium-naphthenate precipitation problem has always been the interaction between divalent metal ions in the second group elements with carboxylic anions, because of their ability to coordinate carboxylate groups from different tetracarboxylicacids to form precipitates of cross-linked tetracarboxylate ions. However, the monovalent Na^+ ion has also been studied, although it does not produce any precipitates and it differs from the divalent ions in its charge and properties in general. Because Na^+ was studied along with the divalent ions in the experimental work, we have also calculated the free energy of interaction between sodium and the propanoate ion as a function of the distance between the metal ion and the carbon atom the carboxylate group in water and the result is presented in Figure S1. It can be seen from Figure S1, that the free energy of interaction is -2.98 kJ/mol at the minimum of the potential well at 3.5 Å, which compared to the divalent ions is a significantly weaker interaction. The free energy barrier for association is 7.78 kJ/mol, which is also relatively high compared to the divalent ions. Because of the relatively weak interaction and high energy barrier, the carboxylate groups are more likely to interact with the divalent ions rather than sodium, as Sundman et al.[1] have shown.

(1) Sundman, O.; Simon, S.; Nordgard, E. L.; Sjöblom, J. Study of the Aqueous Chemical Interactions between a Synthetic Tetra-acid and Divalent Cations as a Model for the Formation of Metal Naphthenate Deposits. Energy Fuels **2010**, *24*, 6054–6060.

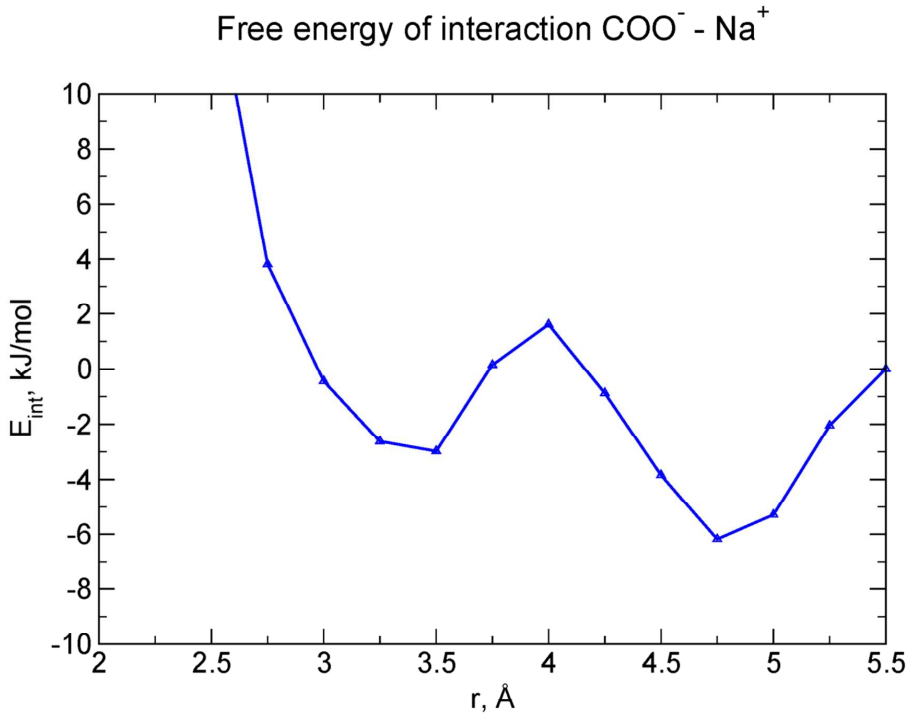

Figure S1: Helmholtz free energy, E_{int}, curves of the sodium – carboxylate ion complex in water. The distance in the abscissa is given in Ångstrom and represents the distance between the metal ion and the carbon atom from the COO^- group.

Paper 3

Calculation of the probability for ionic association and dissociation reactions by molecular dynamics and umbrella sampling

Calculation of the probability for ionic association and dissociation reactions by molecular dynamics and umbrella sampling

Aleksandar Y. Mehandzhiyski, Brian A. Grimes*

Department of Chemical Engineering, Norwegian University of Science and Technology, Trondheim, Norway

* Department of Chemical Engineering, Norwegian University of Science and Technology, SemSælandsvei 4, NO-7491 Trondheim, Norway
brian.a.grimes@chemeng.ntnu.no; tel.: +4773590338

Calculation of the probability for ionic association and dissociation reactions by molecular dynamics and umbrella sampling

Investigating chemical reactions by computational techniques and finding new ways to study these reactions is an important necessity in the fields of chemistry, chemical engineering and biology. In this study, we have presented a new procedure for studying the interactions between divalent metal ions and carboxylates by using umbrella sampling. In some cases, it is more convenient to use variable coordinate reaction probabilities instead of potential energy or free energy curves, which in general are more widely used and available in the literature. Particularly, for practical purposes in building multi-scale models it could be more convenient to use the probability of reaction as a function of the separation distance between two carboxylate moieties when they are simultaneously associated to a metal ion. In the present work, we have modelled the interactions between two carboxylates (propanoate ions) and divalent metal ions (calcium or magnesium) in order to obtain the probability of reaction as a function of the separation distance between the two carboxylates. By calculating the probability, it also became apparent that in the system containing calcium, the carboxylates have higher probability of reaction compared to the system containing magnesium. Furthermore the presented probability could be used also for other multi-scale modelling purposes where these interactions are of main importance. The proposed procedure could also have application in other systems of interest.

Keywords: probability of reaction; umbrella sampling; divalent ions; carboxylates; ionic dissociation

Introduction

Dissociation and association of ions in a polar solvent, such as water, is an important reaction within the field of chemistry [1-3], chemical engineering [4,5] and biology [6,7]. The interactions between divalent metal ions and functional groups of organic molecules is an example of such a reaction. For example, relevant interactions are the

carboxylate moieties – metal ion reactions. Specifically, carboxylic acid groups dissociate above a certain pH level becoming negatively charged carboxylate ions, which makes them very reactive towards positively charged metal ions, which are widely distributed in different systems of practical importance. The dissociation and association of carboxylic acids and divalent metal ions are rather simple ionic reactions in which there is no formation of covalent bonds. Thus, classical molecular dynamics (MD) simulations have been widely used to study such reactions [2,7,8].

Understanding the microscopic mechanism of the reactions on a molecular level is important and usually not a trivial task [1,2]. There are several techniques for studying chemical reactions and obtaining the energy of interaction on a molecular level such as umbrella sampling [9-12] and thermodynamic integration [11-13]. In combination with MD, these powerful techniques could provide essential information for understanding the dynamics and the role of the solvent during the dissociation reactions of interacting ions.

Despite the abundance of calcium-carboxylates interactions in nature and engineering processes as well as their wide experimental study [3,14-17], they are not many theoretical studies in the literature [1,18,19]. Most of the experimental studies focus on clarifying the mechanistic structures, complexation and interactions of calcium-carboxylate reactions in various systems. Studying these reactions employing a combination of theoretical and experimental approaches [14,16,17] or only theoretical studies in the scope of experiments[1,19], however strengthens the fundamental understanding of these systems.

In this present study, we have focused on the interactions between two deprotonated carboxylic acids (propanoate ions) and one divalent metal ion (magnesium or calcium). This reaction is of particular interest in chemical and biochemical

engineering and more specifically, in the field of petroleum chemistry and engineering. To wit, the reaction of tetra-carboxylic acids with divalent ions leads to the formation of calcium-naphthenate precipitates [4,5], which can be a serious economic and environmental problem in petroleum production. In order for these precipitates to form, two carboxylic acid groups from different tetra-acid molecules must coordinate to one metal ion and form a cross-linked network leading to the formation of high molecular weight polymeric salts [4,5]. The calcium-naphthenate precipitates are not known to be part of any coordination or chelation complexes. To be able to more accurately model this process the probability of reaction between the carboxylic groups with the metal ions as a function of the distance between the two carboxylic acids is needed. In this study, we have used MD simulations together with umbrella sampling to obtain the functionality of the probability for reaction and for a more detailed physical understanding of the dissociation process for these complexes in explicit solvent.

Models and Methods

Simulation protocol

The MD simulations were carried out in the canonical statistical ensemble at 300 K using a velocity rescaling thermostat with stochastic term of Bussi-Parrinello with a time constant of 100 fs [20]. The time step for integrating the equations of motion was set to 1 fs. The carboxylate molecules as well the metal ions are modelled with an all atom representation using the Optimised Potential for Liquid Simulations (OPLS-AA) force field [21]. The water molecules are modelled by the TIP4P/2005 water model [22]. The non-bonded interactions were modelled by the Lennard-Jones and Coulomb potentials and the atomic partial charges were used as described in the OPLS-AA force field with no modifications. The geometrical average combination rule has been used

for the non-bonded interactions according to the OPLS-AA force field specification. The electrostatic interactions have been modelled by the Particle-Mesh Ewald summations with cutoff distance of 1.2 nm. The simulations were performed with the GROMACS 5.0.4 simulation package [23].

A cubic simulation box with dimensions of 5x5x5 nm was constructed, where periodic boundary conditions (PBC) were applied to all three spatial directions. The size of the box is large enough to sustain dissociation of the carboxylates from the metal ion. The initial configuration of the carboxylate-metal ion complex was constructed according to previous density functional theory (DFT) study on these complexes [19] and water molecules were added to fill the simulation box. In that study [19] we have shown that the equilibrium distances for the complexes consisting of 1 metal ion and 2 carboxylates are equivalent for DFT and OPLS-AA force field. That has been important finding, because for studying the probability for reaction one needs an accurate description of the carboxylate – metal ion interactions by the force field.

Umbrella sampling

The initial configuration for the umbrella sampling has been shown in Figure 1. The carboxylic acid chosen for this study is propanoic acid in its deprotonated form (carboxylate) with an overall charge of q=-1. The metal ions considered are magnesium and calcium with a partial charge of q=+2. The overall charge of the system is neutral. In the initial configuration of the complex, the carboxylates are in opposite position with respect to each other with point group symmetry C_{2h}. The complex is centred in the geometrical centre of the simulation box and the coordinates of the metal ion have been frozen. Umbrella potentials have been imposed at the centre of mass (COM) of the two carboxylate groups by employing a harmonic potential with a force constant of 2000 kJ/mol. We have performed 14 simulations per ion where every simulation has been 1.2

ns long from which the last 1.0 ns has been used for the production run. After the first 0.2 ns the total energy and the temperature of the systems oscillate around an average value indicating that sufficient equilibration time. The umbrella windows have been separated by 0.25 Å starting from 2 Å as depicted in Figure 1. In that way we have initial separation distances between the carboxylates of 4.0, 4.5, 5.0, 5.5, 6.0, 6.5, 7.0, 7.5, 8.0, 8.5, 9.0, 10.0, 12.0 and 14.0 Å. By imposing the umbrella potentials on the COM of the carboxylate groups and starting from opposite positions of the two carboxylates, we have assumed that the distance between the carboxylates would be double the distance between one carboxylate and the metal ion. By using the above assumption as well as the frozen position of the metal ion, we have assured that the two carboxylates are sampling equally the distances around the metal ion. In that way, we are avoiding the probability of only one of the carboxylates to interact preferentially with the metal ion, since the main objective is to find the probability for reaction as a function of the distance between the carboxylates, providing the requirement that the metal ion is interacting with both carboxylates at the same time.

Weighted Histogram Analysis Method (WHAM)

In order to obtain the unbiased probability from umbrella sampling, we have used the Weighted Histogram Analysis Method (WHAM) [24,25]. The set of equations needed to solve in order to unbias the probability distributions are:

$$P(\xi)^{un} = \frac{\sum_{i=1}^{N_w} n_i p(\xi)_i^b}{\sum_{j=1}^{N_w} n_j e^{-[\omega_j(\xi)-F_j]/k_bT}} \quad (1)$$

$$e^{-F_i/k_bT} = \int d\xi e^{-\omega_i(\xi)/k_bT} P(\xi)^{un} \quad (2)$$

Here, k_b is the Boltzmann constant, T the temperature, n_j is the total number of data points in the biased probability histogram $p(\xi)_i^b$. N_w is the simulation windows, $P(\xi)^{un}$ is

the unbiased probability and F_i are the free energy constants. $P(\xi)^{un}$ and F_i are unknown, therefore the two equations must be solved simultaneously.

The unbiased probability distribution in Equation 1 is the actual probability of reaction as a function of the reaction coordinate ξ, which respectively is the distance between the carboxylate groups. The highest probability in the distribution function would correspond to the most probable distance where the carboxylate are located and are bound to the divalent metal ion.

Results and discussion

The systems studied here are composed of one metal ion (Ca^{2+} or Mg^{2+}) and two deprotonated carboxylic acids. In order to obtain the domain or the upper limiting distance where the carboxylates are dissociated from the metal ion, we have calculated the radial distribution functions (RDF) between the metal ion and the oxygen atoms from the water molecules. By knowing the water coordination numbers of the first solvation shell of the ions we can determine when the carboxylates are dissociated. From a previous study [1] we have obtained the coordination numbers of calcium and magnesium in bulk water as being 7 and 6, respectively. When the carboxylates are associated with the metal ion, the water coordination numbers of the metal ions will be reduced due to the presence of the acids and for any value above these the complexes can be considered dissociated. The carboxylates will displace some of the water molecules in the first solvation shell when associated with metal ions. The results for the systems with Ca^{2+} and Mg^{2+} are shown in Figures 2 and 3, respectively. From Figure 2 we can determine where the carboxylates are associated with Ca^{2+} which is in the region between 4 and 9 Å. It should be noted here that the results given below are from the simulation windows where 4 and 9 Å etc. are being the initial separation distance between the carboxylates and not the actual distance during the simulation,

since by the applied umbrella potential, which is harmonic, the distance can oscillate around the initial distance. In that region the water molecules coordinated to the metal ion are 4 or 5, which is below the number of water molecules in the first solvation shell in bulk water [1]. At 10 Å, the water coordination has risen to 8. Various experimental and simulation studies [26-29] had shown that the coordination number of calcium vary between 7 and 8, which is in a good agreement with our previous [1] and current study and therefore the complex can be considered dissociated. In Figure 3, for magnesium, the carboxylates are associated with the metal ion in the region between 4 and 9 Å as seen from the lower coordination of water molecules in the first solvation shell. Moving from 7 Å to 9 Å, there is a slight increase in the coordination from 2 to 4, before the complex completely dissociates at 10 Å where the metal ion has its first coordination shell filled with 6 water molecules. In Figure 4, snapshots representing typical configurations of the systems with Ca^{2+} and Mg^{2+} are given for different separation distances, where the coordination of the water molecules around the metal ions is highlighted with white dotted lines. Figure 4a) shows a snapshot taken from the system with calcium for an initial separation distance of 4 Å in which the two carboxylates are associated with the metal ion and there are 4 water molecules coordinated to it. In Figure 4b) a snapshot for the same separation distance for magnesium shows a typical configuration of the two carboxylates and two water molecules coordinated to the metal ion. In Figures 4 c) and d) snapshots from the simulation window with initial separation distance of 10 Å are shown for calcium and magnesium, respectively. They illustrate typical bulk water coordination structure around the metal ion and it can also be seen that the carboxylates are separated by a layer of water molecules from the metal ion and the complex could be considered as dissociated. The obtained radial distribution

functions and coordination numbers of the divalent ions can be compared to X-ray and neutron scattering experiments [30-33].

The angle (θ) probability distributions of carbon – Me^{2+} – carbon atoms from the carboxylate groups are depicted in Figures 5 and 6 for Ca^{2+} and Mg^{2+}, respectively. Every distribution has been obtained from the respective simulation with the increase of the separation distance between the carboxylates. In the case of calcium, Figure 5, the carboxylates are preferably situated at opposite positions with respect to each other, with the highest probability centred around 140 and 170 degrees for the cases between 4 and 8 Å. An exception is the case of 6 Å, where the angle θ is centred around 95°. It can be also observed that there is a minima at 120°. With the increase of the distance between the carboxylates (9 - 10 Å) the distributions are becoming broader and more flat, meaning that the carboxylates are less restricted, more mobile and move randomly in the bulk water phase. That is also another indication that the complex is dissociated at these distances. For the case of magnesium in Figure 6, it can be observed that the distributions are more compact and at lower separation distances between 4 and 8 Å, the distributions are centred between 120° and 140°. At a distance 10 Å the distribution flattens, indicating again that the complex is most likely dissociated. Comparing the complexes of Ca^{2+} with Mg^{2+}, the latter one has a more rigid structure, as demonstrated by the more compact and pronounced probabilities.

The probability of reaction as a function of the separation distance between the centre of masses of the carboxylate group is depicted in Figure 7, where the error bars indicate the standard deviation of the probability obtained from three independent simulations. The RDFs and the angle distributions suggest that the complex is completely dissociated in the simulation where the initial separation distance has been set to 10 Å. Therefore, that simulation along with the others with higher initial

separation distances have been omitted for further analysis. First it should be noted that the probability of reaction has been rescaled such that the highest peak takes the value of 1, because of its convenience for further use in multi-scale modelling approaches. In both cases for Ca^{2+} and Mg^{2+}, the probability of reaction has three distinct peaks with highest probability located at 4.53 Å and 3.65 Å, respectively. The probability of reaction for Ca^{2+} spans the region between 4.3 Å to almost 7 Å, while the probability of reaction for Mg^{2+} is located between 3.5 and 6.1 Å. However, the probability for calcium never quite goes to zero between the peaks, whereas the probability function for magnesium clearly goes to zero between the peaks in the regions between 3.8 – 4.2 Å and 5.0 – 5.7 Å. It can also be observed that the peaks for Mg^{2+} are narrower compared to Ca^{2+}, which has a wider probability distribution in all regions. According to a previous study [1] magnesium has much higher interaction free energy and more tightly coordinated 1st solvation shell compared to calcium which could also be a reason for the narrower distribution. That would mean the carboxylates would be more strongly attracted to the magnesium and most likely within shorter distances. However, from Figure 7 it can be seen that for calcium, the carboxylates have higher probability of binding to it, because of the non-zero values between the peaks and the broader span of the probability. Additionally from Figure 7, it can be inferred that the complexes are dissociated when the distance between the COM of the carboxylate groups is larger than 6.9 Å and 6.1 Å for calcium and magnesium, respectively.

Conclusions

The interactions between two deprotonated carboxylic acids and one divalent metal ion have been studied by molecular dynamics simulations and umbrella sampling. Emphasis has been put on obtaining the probability of reaction (association) of the two carboxylates to the metal ion as a function of the separation distance between them

given the condition that the metal ion is associated with both of them at the same time. This approach has been used for the first time to study the probability of reaction as a function of the separation distance between particular functional groups of interest with molecular dynamics simulations. The concept of reaction probabilities based on functional group separation could be used in multi-scale modelling approaches for different chemical processes. In particular, the obtained probabilities here could be used in a multi-scale modelling framework to address the problem of calcium-naphthenate precipitation in the petroleum industry.

In the system with calcium, the two carboxylates have higher probability of reaction compared with the system with magnesium. That could be seen from the non-zero probability distribution function and the fact that with calcium the range of the function is more spread. The two carboxylates are dissociated when the distance between them is larger than 6.9 Å for calcium and 6.1 Å for magnesium. The angle distribution probabilities also showed a more rigid structure for the complex with magnesium, which also suggests that the complex with calcium has a higher probability of reaction.

Preferred binding and reaction of carboxylates with calcium compared to magnesium has been also experimentally [4] observed in the study of the calcium-naphthenate precipitation. The results presented here also suggest a higher probability to bind calcium relative to magnesium which is in agreement with the observed [4] selectivity of the divalent metal ions – carboxylates reaction. That particular selectivity of divalent ions [4] has been also studied and explained by *ab initio* MD [1] where only one carboxylate is interacting with the metal ion and showed although magnesium has higher interaction free energy, calcium would preferably bind to the carboxylate. To wit, the present study complements the findings presented previously [1] with the

addition of one carboxylate molecule and further demonstrates how the experimentally observed preferred selectivity of calcium can also be interpreted based on the probability of reaction.

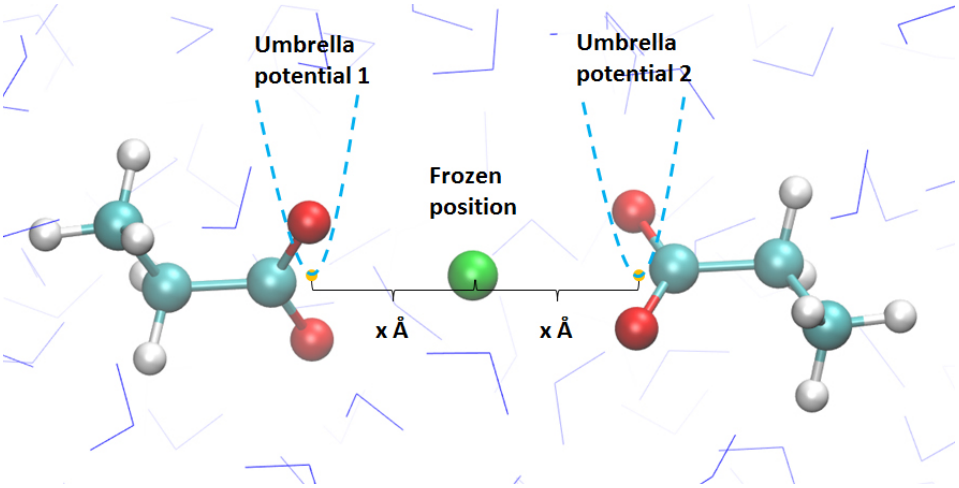

Figure 1. Initial configuration of the system. The initial distance between the two carboxylate groups has been set to 2x Å and umbrella potentials have been applied to the centre of mass of both carboxylate groups. The carbon atoms are depicted in cyan, oxygen in red, hydrogen in white, the metal ion in green and the water molecules are depicted as blue sticks.

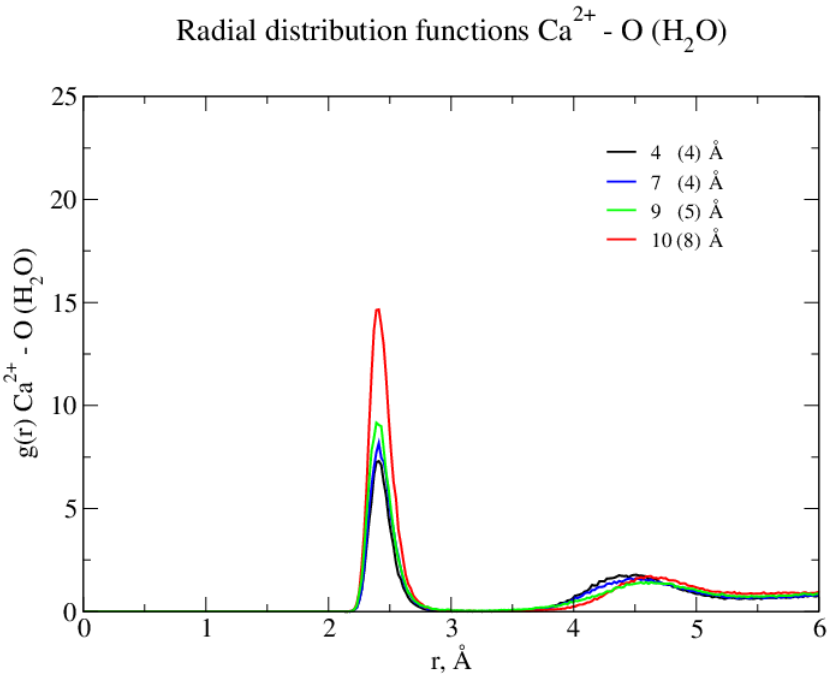

Figure 2. Radial distribution functions between calcium and the oxygen atom of the water molecules obtained from different simulation windows where the initial separation distance between the carboxylate groups is being set to 4 Å (black), 7 Å (red), 9 Å (blue) and 10 Å (green). The water coordination numbers for each curve are given by the number in parenthesis in the legend.

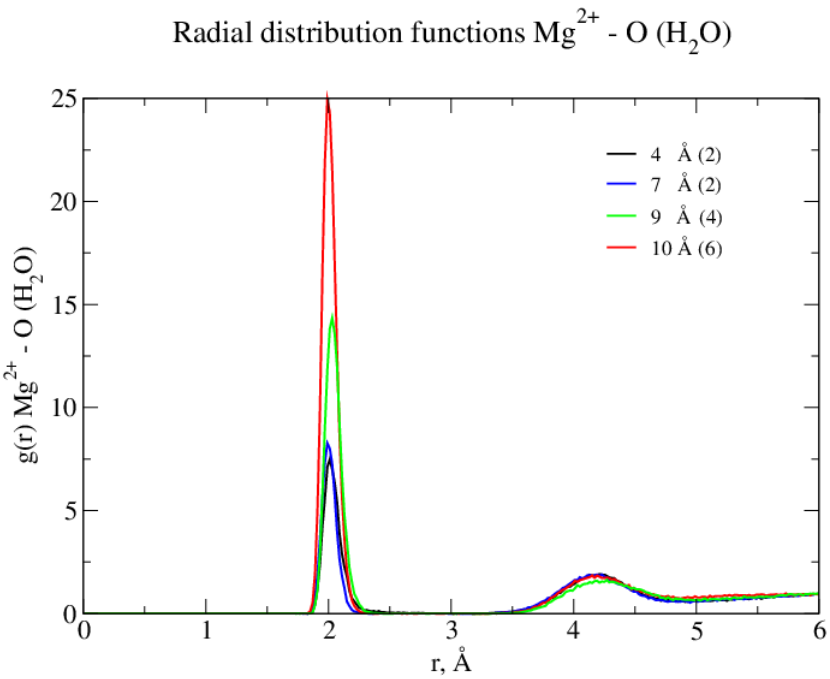

Figure 3. Radial distribution functions between magnesium and the oxygen atom of the water molecules obtained from different simulation windows where the initial separation distance between the carboxylate groups is being set to 4 Å (black), 7 Å (red), 9 Å (blue) and 10 Å (green). The water coordination numbers for each curve are given by the number in parenthesis in the legend.

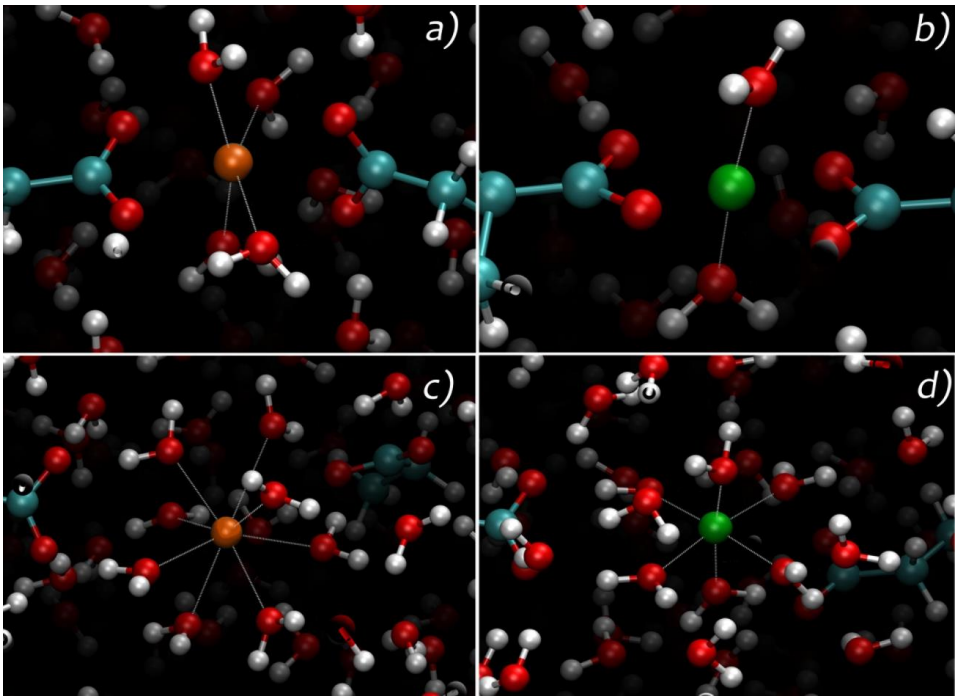

Figure 4. Snapshots from the simulations a) Ca^{2+} at 4 Å initial separation distance, b) Mg^{2+} at 4 Å initial separation distance, c) Ca^{2+} at 10 Å initial separation distance and d) Mg^{2+} at 10 Å initial separation distance.

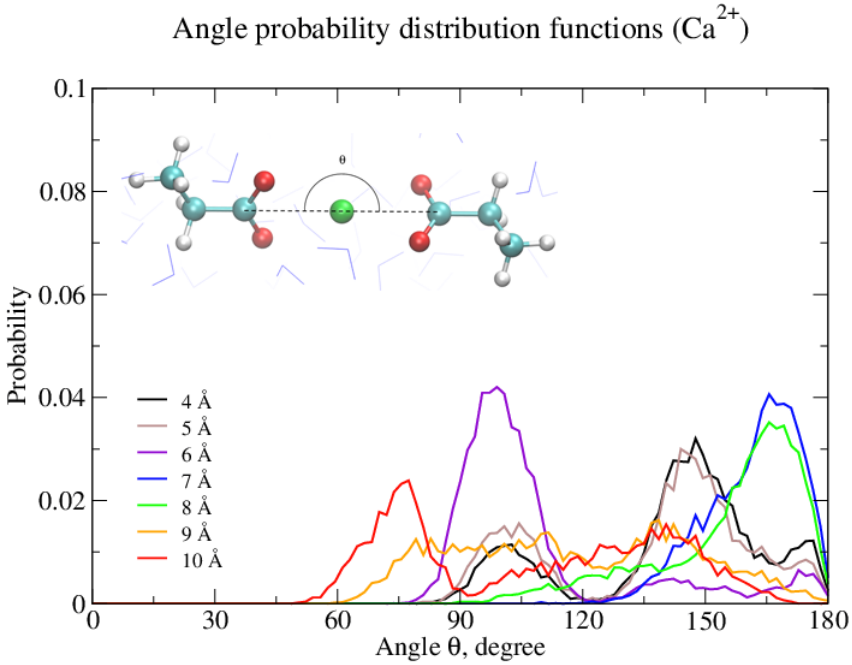

Figure 5. Angle probability distribution functions of the $C(COO^-) – Ca^{2+} – C(COO^-)$ complex from the simulation windows where the initial separation distance between the COM of the carboxylate ions has been set between 4 and 10 Å.

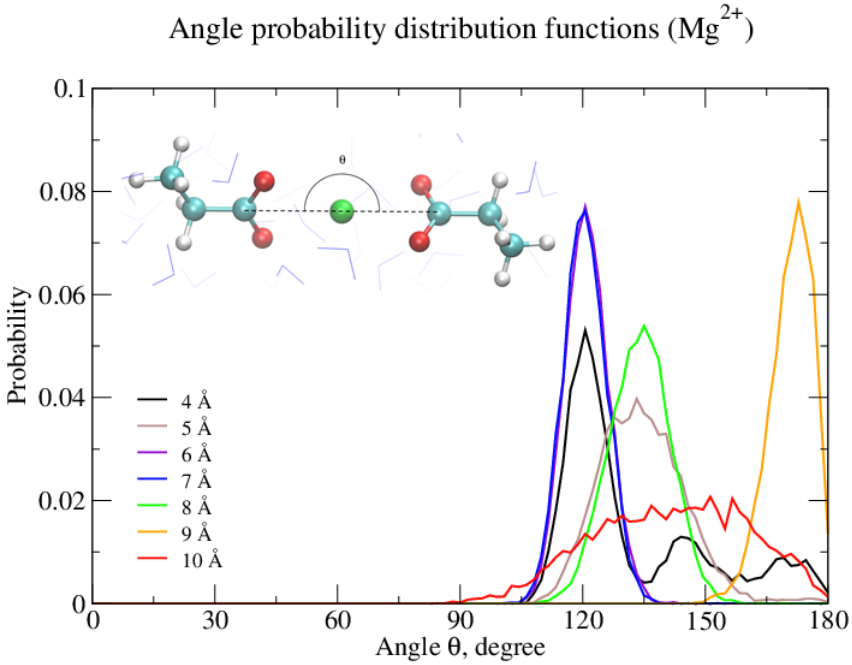

Figure 6. Angle probability distribution functions of the $C(COO^-) – Mg^{2+} – C(COO^-)$ complex from the simulation windows where the initial separation distance between the COM of the carboxylate ions has been set between 4 and 10 Å.

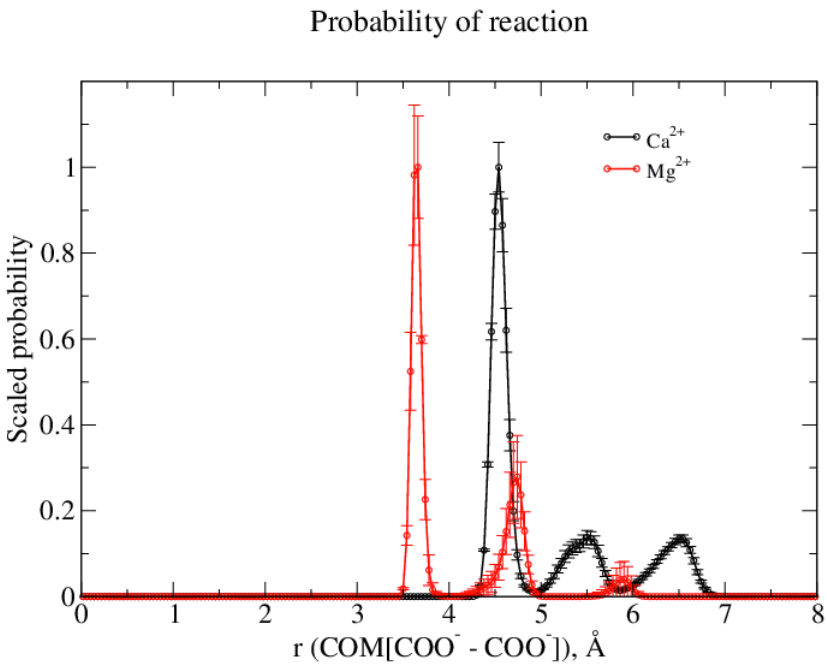

Figure 7. Probability of reaction as a function of the separation between the centres of masses of the carboxylate groups.

References

[1] A. Y. Mehandzhiyski, E. Riccardi, T. S. van Erp, T. T. Trinh and B. A. Grimes, J. Phys. Chem. B., **119**, 10710-10719 (2015)

[2] A. J. Ballard and C. Dellago, J. Phys. Chem. B., **116**, 13490−13497 (2012)

[3] R. F. P. Pereira, A. J. M. Valente, M. Fernandes and H. D. Burrows, Phys. Chem. Chem. Phys., **14**, 7517–7527 (2012)

[4] O. Sundman, S. Simon, E. L. Nordgard and J. Sjöblom, Energy Fuels, **24**, 6054–6060 (2010)

[5] J. Sjöblom, S. Simon and Z. Xu, Adv. Col. Inter. Sci., **205**, 319–338 (2014)

[6] J. J. R. F. D. Silva and R. J. P. Williams, *The Biological Chemistry of the Elements,* (Oxford University Press, New York, 2001)

[7] H. B. Mayes, J. Tian, M. W. Nolte, B. H. Shanks, G. T. Beckham, S. Gnanakaran and L. J. Broadbelt, J. Phys. Chem. B., **118**, 1990-2000 (2014)

[8] M. Kohagen, E. Pluharova, P. E. Mason and P. Jungwirth, J. Phys. Chem. Lett., **6**, 1563-1567 (2015)

[9] G.M. Torrie and J.P.Valleau, Chem. Phys. Lett., **28**, 578–581 (1974)

[10] G.M. Torrie and J.P.Valleau, J Comput Phys, **23**,187–199 (1977)

[11] D. Frenkel and B. Smit, *Understanding Molecular Simulation: From Algorithms to Applications,* 2nd edition (Academic Press, 2001)

[12] D. A. Kofke and P. T. Cummings, Mol. Phys., **92**, 973-996 (1997)

[13] E. A. Carter, G. Ciccotti, J. T. Hynes, R. Kapral, Chem. Phys. Lett., **156**,472–477 (1989)

[14] K. M. N. Burgess, Y. Xu, M. C. Leclerc and D. L. Bryce, Inorg. Chem., **53**, 552-561, (2014)

[15] H. Ju, X. Feng, Y. Ye, L. Zhang, H. Pan, C. T. Campbell and J. Zhu, J. Phys. Chem. C, **116**, 20465−20471 (2012)

[16] V. Martin-Diaconescu, M. Gennari, B. Gerey, E. Tsui, J. Kanady, R. Tran, J. Pécaut, D. Maganas, V. Krewald, E. Gouré , C. Duboc, J. Yano, T. Agapie, M. Collomb and S. DeBeer, Inorg. Chem., **54**, 1283−1292 (2015)

[17] B. Gerey, M. Gennari, E. Gouré, J. Pécaut, A. Blackman, D. A. Pantazis, F. Neese, F. Molton, J. Fortage, C. Duboc and M. Collomb, Dalton Trans., **44**, 12757-12770 (2015)

[18] T. Bala, B.L.V. Prasad, M. Sastry, M. Upadhyay, U. Waghamare. J. Phys. Chem. A, **111**, 6183-6190 (2007)

[19] A. Y. Mehandzhiyski, E. Riccardi, T. S. van Erp, H. Koch, P-O. Åstrand, T. T. Trinh and B. A. Grimes, J. Phys. Chem. A, **119**, 10195–10203 (2015)

[20] G. Bussi, D. Donadio, and M. Parrinello, J. Chem. Phys. **126**, 014101 (2007)

[21] W. L. Jorgensen, D. S. Maxwell and J. Tirado-Rives. J. Am. Chem. Soc., **118**, 11225-11236 (1996)

[22] J.L.F. Abascal and C. Vega, J. Chem. Phys., **123**, 234505–234517 (2005)

[23] B. Hess, C. Kutzner, D. van der Spoel, and E. Lindahl, J. Chem. Theory Comput. **4**, 435-447 (2008)

[24] S. Kumar, D. Bouzida, R.H. Swendsen, E. A. Kollman and J.M. Rosenberg. J. Comp. Chem. **13,** 1011-1021 (1992)

[25] B. Roux, Comp. Phys. Comm. **91**, 275-282 (1995)

[26] J. P Larentzos and L. J. Criscenti, J. Phys. Chem. B, **112**, 14243−14250, (2008)

[27] D. Jiao, C. King, A. Grossfield, T. A. Darden, P. J. Ren, Phys. Chem. B, **110**, 18553−18559 (2006)

[28] J.-P. Piquemal, L. Perera, G. A. Cisneros, J. Chem. Phys., **125**, 054511 (2006)

[29] H. Ohtaki, T. Radnai, Chem. Rev., **93**, 1157−1204 (1993)

[30] R. J. McQueeney, Phys. Rev. B, **57**, 10560-10568 (1998)

[31] T. Megyes, I. Bako, S. Balint, T. Grosz, T. J. Radnai, Mol. Liq., **129**, 63-74 (2006)

[32] T. Megyes, T. Grosz, T. J. Radnai, I. Bako, G. Palinkas, J. Phys. Chem. A, **108**, 7261-7271 (2004)

[33] Y. S. Badyal, A. C. Barnes, G. J. Cuello, J. M. Simonson, J. Phys. Chem. A, **108**, 11819-11827 (2004)

Paper 4

Coarse-Grain Interface Surfactant Density Maps for the Calculation of the Fractional Conversion of Tetra-Carboxylic Acids to Calcium-Naphthenate Precipitates

Coarse-Grain Interface Surfactant Density Maps for the Calculation of the Fractional Conversion of Tetra-Carboxylic Acids to Calcium-Naphthenate Precipitates

Aleksandar Y. Mehandzhiyski and Brian A. Grimes*

Department of Chemical Engineering, Norwegian Univeristy of Science and Technology, 7491, Trondheim, Norway

E-mail: brian.a.grimes@ntnu.no

Abstract

Modelling molecular interactions on different length scales is often necessary and presents a significant challenge in chemical engineering. In the present study, we apply molecular dynamics (MD) simulations on different tetrameric carboxylic acid (TA) molecules absorbed at a water-oil interface, which tend to form cross-linked network in the presence of calcium. From the MD simulations we obtain various spatial probabilities describing molecular geometries of TAs in the interfacial region. The MD obtained probability distribution functions are then used to recreate a coarse-grained representation (interface map) of the interfacial density of the TA molecules. The interface maps are created by randomly placing molecules in an interfacial region and calculating the coordinates of the carboxylate groups according to the MD probability functions. By

*To whom correspondence should be addressed

creating a large amount of interface maps we can obtain a better statistical representation of how the molecules are spatially arranged at the interface at different interfacial concentrations. The orientation and distance between the carboxylate groups from different TA molecules is important for the study of the formation of calcium-naphthenate precipitates occurring in petroleum industry. After an interface map has been build we have assessed how many molecules are cross-linked for a given interfacial concentration based on MD calculated carboxylate-calcium binding probabilities. Subsequently, we can obtain the fractional conversion ($f_p(\Gamma_{TA})$) of tetrameric acids to cross-linked calcium-naphthenate precipitates. The fractional conversion function can then be used in multi-scale approaches for further elucidating the phenomena of calcium-naphthenate precipitation.

Introduction

During the production and processing of crude oil, some undesirable reactions such as calcium-naphthenate precipitation[1,2] can occur in upstream separation and transport operations. The calcium-naphthenate precipitation phenomena is associated with a newly found class of high molecular weight naphthenic acids[2] and have been first observed in the Heidrun oil field on the Norwegian continental shelf, but have been subsequently found in other offshore fields in the North Sea, West Africa, Brazil and China.[3] These precipitates are adhesive and could plug and damage various process equipment, leading to costly shut-down, cleaning, and restart processes.

As mentioned above the main constituent of these calcium-naphthenate precipitates is a new class of naphthenic tetra-carboxylic acids[3–5] and given the generic name "ARN acids". These naphthenic acids possess four carboxylic acid groups attached to a mono- or bi- cyclopentane moiety and are linked together through long hydrocarbon chains, see Figure 1.[3] The aliphatic chemical structure of the tetra-carboxylic acids indicates that they are highly interfacially active compounds. However, the indigenous tetra-carboxylic acids are difficult

to purify to the extent that they can be used for quantitative laboratory experiments. Thus, a synthetic analogue of the indigenous compounds has been developed[6,7] to mimic the interfacial behaviour of the naturally occurring acids and has been named BP10.

The tetra-acids (TA) are preferably located at the oil-water interface, because of their high interfacial affinity. Because of that, the proposed reaction mechanism[6] of the calcium-naphthenate precipitation formation is that carboxylic acid groups from different molecules adsorbed at the oil-water interface interact with calcium[8,9] and could form a cross-linked network at the interface when calcium interacts with carboxylic groups from two separate TAs, which results in a high molecular weight polymeric salt. Thus, the mutual distance between the carboxylate groups of individual TA's absorbed on the interface is a critical factor that determines the extent of cross-linking. Molecular dynamics (MD) simulations[10] of tetra-carboxylic acids at the oil-water interface have demonstrated that carboxylate groups (COO^-) from different molecules could be cross-linked due to the presence of divalent metal ions dissolved in the water phase. The extent of cross-linking is dependent on the interfacial concentration of TAs - Γ_{TA}. Consequently, a multi-scale framework[11,12] employing MD simulations and continuum modelling has been developed for liquid-liquid dispersions to predict Γ_{TA} on the process scale, which could provide quantitative results for the mass of calcium-naphthenate precipitates produced per unit process volume. An important constituent function in this multi-scale approach is the fractional conversion ($f_p(\Gamma_{TA})$) of tetra-carboxylic acids to calcium-naphthenate precipitates as a function of the interfacial concentration of tetra-acids. Since the functionality of the fractional conversion is not known, Kovalchuk et al.[12] assumed $f_p(\Gamma_{TA})$ to have a sigmoidal shape.

The fractional conversion of tetra-acids to calcium-naphthenate precipitates has been challenging to obtain experimentally. Thus, molecular simulations are a promising alternative to experiments to derive the fractional conversion as a function Γ_{TA}. In the present paper, we introduce a novel methodology to calculate the fractional conversion of tetra-acids to calcium-naphthenate precipitates based on MD. Our approach includes MD simulations

of the tetra-acids at the oil-water interface from which we obtain different probability distributions describing the molecular geometry of the TAs and relative displacement of the active moieties (COO^-). The probability distributions used to describe the molecular structuring at the oil-water interface are the absolute position of the surfactant layers, orientation angles of the hydrocarbon chains relative to the interface and to each other, effective length of the chains, distance between the carboxylate groups which have been presented by Riccardi et al.[10] and probability for binding two carboxylate groups to one calcium ion as a function of the separation distance between them which have been determined by Mehandzhiyski et al.[13] The probability distributions then are used to create a 3-dimensional (3D) coarse-grain representation of the tetra-acid density at the oil-water interface in a Monte Carlo based approach. Finally, the fractional conversion of tetra-carboxylic acids to calcium-naphthenate precipitates has been assessed by determining how much of the carboxylate groups from different molecules are cross-linked based on the mutual displacement of carboxylate groups and their probability to bind with calcium at the given displacement[13]. The tetra-carboxylic acid molecules considered here are the indigenous molecule ARN and its synthetic analogue BP10.

Models and Methods: Molecular Dynamics Simulations

Molecular dynamics simulations have been carried out for the two molecules of interest ARN and BP10 at a water-oil interface. The molecular and 3D structures of ARN and BP10 are depicted in Figure 1. The molecules are modelled using the Optimised Potential for Liquid Simulations in all atom representation (OPLS-AA).[14] The polar phase in the simulations is comprised of water and the non-polar phase (for convenience referred as oil) is modelled by 9:1 volume ratio of p-Xylene and chloroform to mimic experimental solubility of BP10. We have used the TIP4P/2005[15] force field to model the water and the p-Xylene and chloroform are modelled in all-atom representation by the OPLS-AA force field.[14] The initial configuration of the system is shown in Figure 2. The water phase, depicted in blue, is placed in the middle of the simulation box. On both sides are placed 32 surfactant molecules (ARN or BP10) for each interface. Next to the surfactant molecules a layer of the oil phase is positioned, which is depicted in orange in Figure 2. Periodic boundary conditions (PBC) are applied to all three spatial directions. In that way, two oil-water interfaces are created in the z-direction, which in the simulations is the direction normal to the interface. The interfacial area (xy plane) is kept constant during the simulations. The MD simulations are carried out with the GROMACS 5.0.4 simulation package[16] in the isothermal-isobaric (NPT) ensemble. The pressure during the initial equilibration run has been controlled by the Berendsen barostat[17] with a time constant of 1.0 ps at 1 bar and compressibility of 4.5×10^{-10} bar^{-1} and the Parrinello-Rahman[18] pressure coupling has been used during the production run. The temperature during the simulations was maintained at 300 K and it was controlled by the velocity rescaling thermostat[19] with a time constant of 100 fs. The electrostatic interactions have been modelled via Particle-Mesh Ewald summations.[20] The Newton's equations of motion were integrated with a time step of 1 fs.

Before building the interfacial system, the water and oil phases have been first equilibrated in independent simulations. The water phase was comprised of 16702 water molecules and the oil phase is a mixture of 2250 p-Xylene and 382 chloroform molecules, which represents a

9:1 volume ratio. That particular configuration for the oil phase was chosen, because of the solubility limit of BP10. As mentioned before, 32 surfactant molecules (ARN or BP10) are placed at each interface. The surfactant molecules are in their deprotonated state, meaning that their charge is $q = -4$. Two calcium ions per surfactant molecule, or 128 in total, have been added at random positions in the water phase in order to balance the overall charge in the system. During the initial 10 ps equilibration of the systems, a temperature of 400 K and a pressure coupling of 10 000 bar was applied in the z-direction in order to close the initial gap between the water and oil phases and to position the surfactants at the interfaces. Afterwards, the systems were kept for 1 ns at 300 K and 1 bar pressure. The final equilibration was carried out at 300 K and 1 bar for 5 ns, which then was followed by a production run of 10 ns at the same conditions. The dimensions of the simulation box are $8.0 \times 8.0 \times 17.5$ nm.

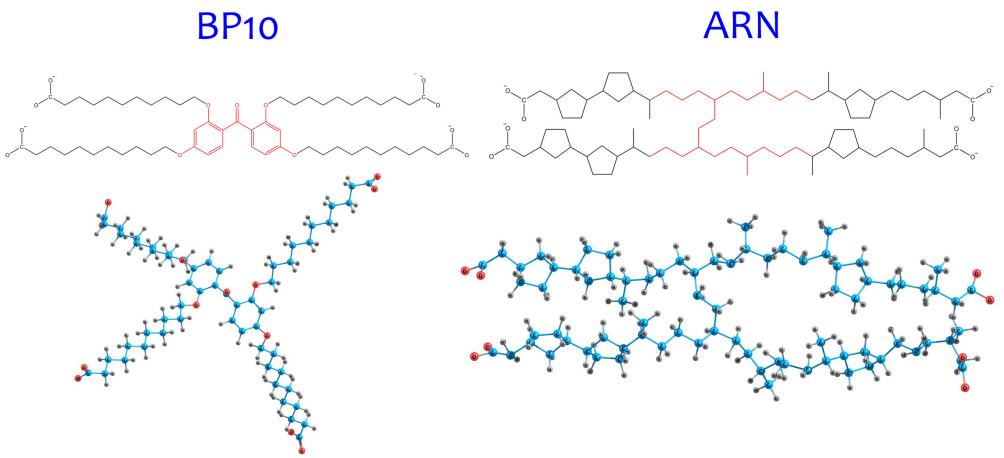

Figure 1: Structural formulas (top) and 3D molecular geometries (bottom) of BP10 and ARN.

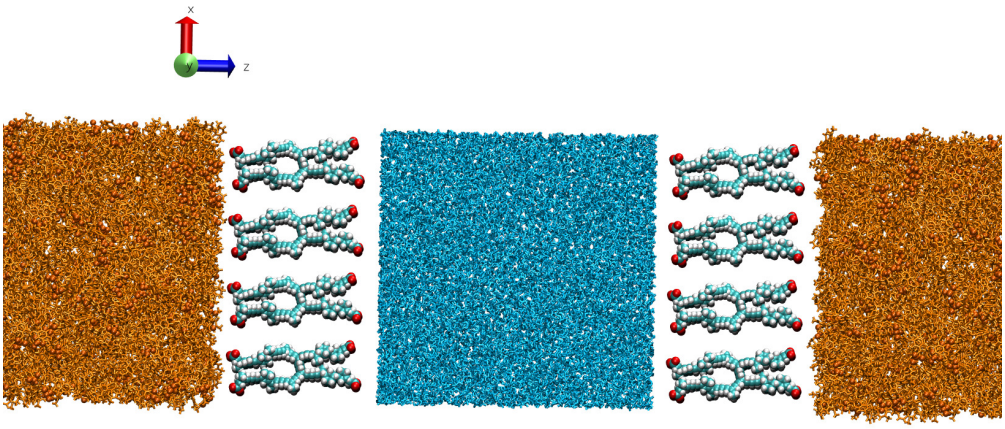

Figure 2: Initial configuration of the MD simulation box.

Results: Molecular Dynamics Simulations of ARN and BP10 at the Oil-water Interface

In the following section, the results from the MD simulations of ARN and BP10 at the oil-water interface are presented. In Figure 3 the probability distribution functions (PDF) used for generating the coarse-grained interface density maps are shown. The arm vector lengths are generated according to the PDF depicted in Figure 3(a). The arm vector length are considered to originate from the nearest carbon atom linking the hydrocarbon chains in the case of ARN and from the oxygen atoms linking the benzophenone core in the case of BP10[3,10] and to terminate at the carboxylate groups, respectively. The vertical orientation angle is the angle formed by the arm vector and a plane parallel to the oil-water interface and is depicted in Figure 3(b). The positive values in Figure 3(b) imply that the arm vector points toward the water phase and the negative value - to the oil phase, respectively. From

Figure 3(b) can be seen that the preferable orientation of the molecule arm is toward the water phase, which is due to the fact that the carboxylic acid arms are deprotonated and are orientated towards the more polar phase. The horizontal orientation angle of the molecular arms is presented in Figure 3(c). The horizontal angle is calculated by arbitrarily choosing a single arm vector of the tetra-acid molecule and the distribution of the remaining arms is plotted versus the angle between the selected arm group and the other arm groups in the plane parallel to the oil-water interface. It can be also observed from the horizontal angle distribution that the there is an increase in the probability between -60° to $+30^\circ$ and is a uniform distribution otherwise. The increased probability would mean that there will be aggregation of more arms to each other most likely because of hydrophobic interactions between the hydrocarbon chains. The intra-molecular COO^- groups distance has been used as a criteria to accept the xy-positions of the COO^- groups and is presented in Figure 3(d). Figures 3(e) and 3(f) depict the z-position of the molecular centers and the COO^- groups at the oil-water interface for ARN and BP10, respectively. In the onset with blue (left) is depicted the water phase and in brown (right) the oil phase. The same convention also corresponds to the probability distributions. The COO^- groups are orientated towards the water phase and the molecular centers to the oil phase.

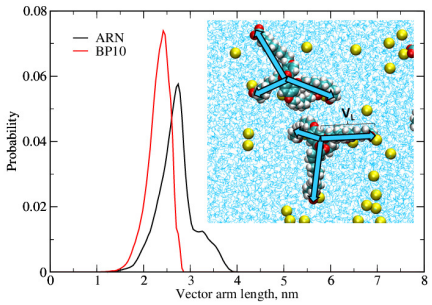

(a) Vector arm length

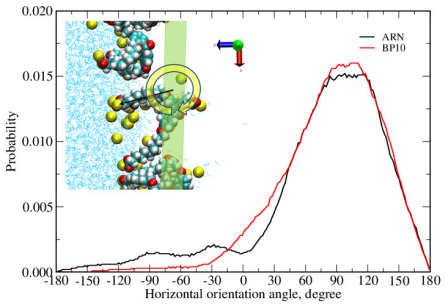

(b) Vertical arm orientation

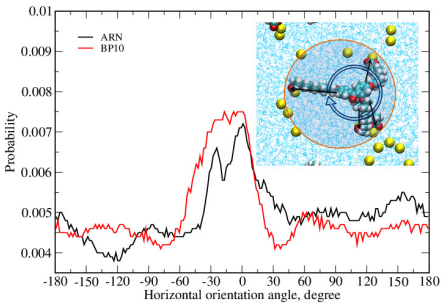

(c) Horizontal arm orientation

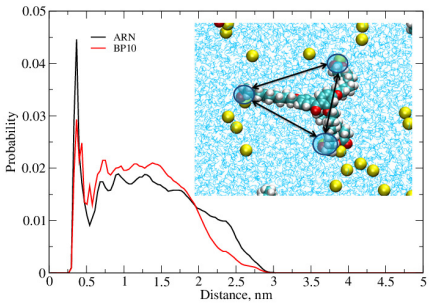

(d) Intra-molecular COO^- - COO^- distances

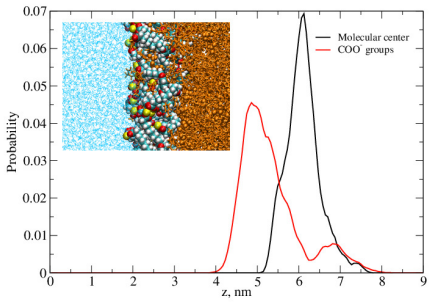

(e) z-position of ARN

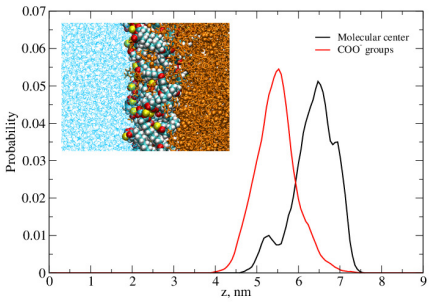

(f) z-position of BP10

Figure 3: Probability distribution functions of a) vector arm length b) vertical arm orientation c) horizontal arm orientation d) intra-molecular COO^- - COO^- distances e) z-position of ARN molecular centers and COO^- groups f) z-position of BP10 molecular centers and COO^- groups used to generate the random interface maps.

To determine how many carboxylate groups are cross-linked we have used the probability of reaction[13] as a function of the distance between two carboxylate groups, which is presented in Figure 4. If the distance between the carboxylate groups are within the distance span of the PDF in Figure 4 the respective site is marked as a cross-linked place. In that way we can generate a sufficient number of random static 3D coarse-grain interface maps based on the MD simulated structural probabilities from which the fractional conversion as a function of the interfacial concentration has been calculated.

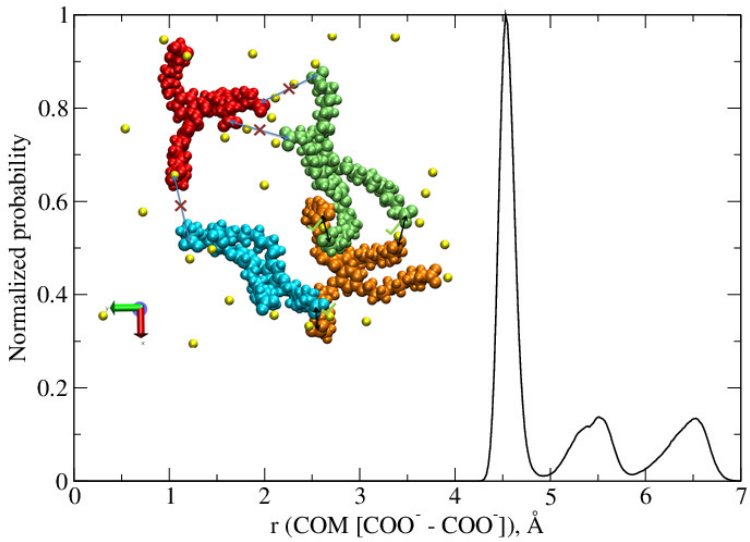

Figure 4: Probability of reaction between Ca^{2+} and two COO^- groups as a function of the distance between COO^- - COO^-.

In Figure 5 snapshots from the MD simulations are depicted and a cross-linked network of ARN molecules can be observed and are highlighted in red. The molecules are cross-linked through their carboxylate groups interacting with the calcium atoms which are depicted in yellow. That is one possible configuration of a cross-linked network at the interface and there are more cross-linked molecules in the same simulation, but for clarity only one has

been highlighted. Practically, one MD simulation could present only one configuration of the interface density or cross-linked network, therefore it will be very computationally expensive to simulate many different systems in order to have statistically reliable results for the fractional conversion of the tetra-acid molecules to calcium-naphthenate precipitates. Thus, a coarse-grain representation of the interfacial density based on the MD derived probabilities could be more computationally effective to calculate the fractional conversion and is presented in the next sections.

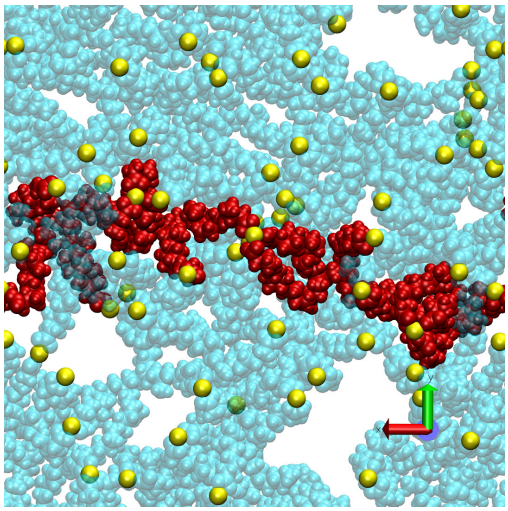

Figure 5: Top view of the cross-linked network from the MD simulations. A cross linked-network of ARN molecules is highlighted in red.

Models and Methods: Algorithms for Generating the Coarse-Grain Interface Density Maps

In order to generate a coarse-grained representation of the density of the TA molecules at the oil-water interface we have used various probability distributions[10] obtained from the MD simulations described previously and presented in Figures 3 and 4. Using these distribution functions we can recreate the interfacial distribution of a large number of ARN and BP10 at the interface in a Monte Carlo approach. By generating a substantial amount of random interface maps for fixed Γ_{TA}, the fractional conversion of the tetra-carboxylic acid to calcium-naphthenate precipitates could be calculated as a function of the interfacial concentration. The main algorithm for generating the random density maps is shown in Figure 6. First, the input parameters have been passed to the main program. The necessary input parameters are the interface map dimensions (A) and the interfacial concentration of the tetra-carboxylic acids - Γ_{TA}. The condition on A is that it should be large to accommodate a large number of TA molecules. Based on the values of Γ_{TA} and A, the number of TA molecules ,N_{TA}, in simulation is given by:

$$N_{TA} = \Gamma_{TA} A \tag{1}$$

where Γ_{TA} is given in molecules/nm^2.

For the specified interfacial concentration, lateral dimensions (x and y) of the N_{TA} molecule centers have been randomly placed on a plane representing the interface region and the probability distributions from Figure 3 have been used to generate the positions of the COO^- groups based on arm lengths, orientation angles and vertical displacement from arbitrary "dividing" surface as done by Ricardi et al. [10] Once, the intermolecular distances between the COO^- groups have been determined, the fractional conversion of tetra-carboxylic acids to calcium-naphthenate precipitation can be obtained from the binding probability in Figure 4. More detailed algorithms for generating the coordinates of molecular centers and

COO^- groups are presented in Figures 7 and 8, respectively.

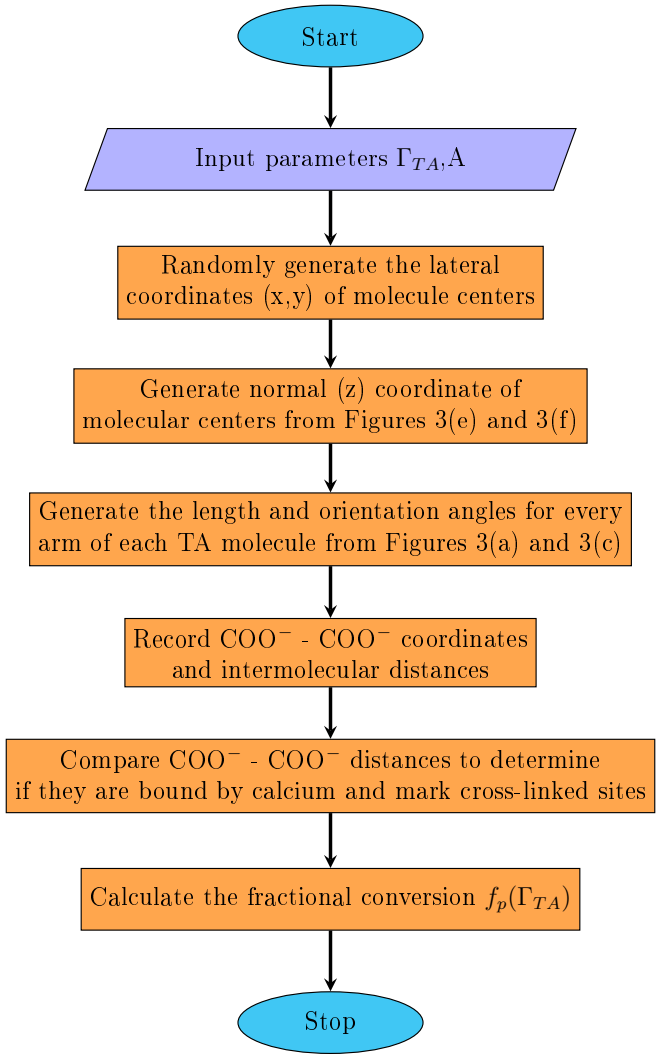

Figure 6: Main algorithm for generating the interface maps based on the probability distributions obtained from MD simulations.

In Figure 7, the algorithm for randomly generating the molecular centers is presented. The molecular centers of BP10 and ARN are highlighted in red in Figure 1. The center of BP10 is composed of a benzophenone core and the center of ARN is comprised of the

central hydrocarbon moiety connecting the four carboxylate groups. The molecular centers are placed randomly on a plane with dimensions of 100 $\times$ 100 nm using PBC. We have set the interfacial concentrations of the TAs in the range of 0.0007 - 0.1387 molecules/nm^2. Kovalchuk et al.[11] have calculated the minimum interfacial area per molecule to be 7.21 nm^2 for BP10, which for Γ_{TA} gives a maximum value Γ_{max}=0.1387 molecules/nm^2. Γ_{max} for ARN is not available, therefore we have used the same value as for BP10, although it might slightly differ. After the first random assignment of molecule centers, we check to see if the required value of Γ_{TA} is reached. Specifically, when a new molecule center is placed, the program checks if there is overlap with the previously placed TA molecule. If the distance between the new molecule and any previously placed TA is smaller than a certain threshold the new molecule is rejected. The molecular center distance threshold has been set to 1.4 nm and 1.0 nm for ARN and BP10, respectively. These values represent roughly the molecule center diameter depicted in Figure 1. The random assignment of molecule centers continues until the desired value of Γ_{TA} is reached.

If the threshold is satisfied the molecule center coordinates are saved and the program generates the z position of the respective molecule center according to a cumulative distribution function (CDF). The CDF is constructed based on the probability distribution function (PDF) for the molecular center obtained from the MD simulations, Figures 3(e) and 3(f). To assign the z-coordinate, a random number generator (RNG) has been used to generate a random number between 0 and 1. Since both the CDF and the random number are between 0 and 1, the random number will correspond to a value for the z-coordinate from the CDF. Then the assigned z-coordinate is compared to the PDF obtained from the MD simulation and is checked to determine if it falls within the boundaries of the PDF. If the condition is not satisfied, a new z-coordinate is generated, until the new z-coordinate is accepted according to the criteria discussed above.

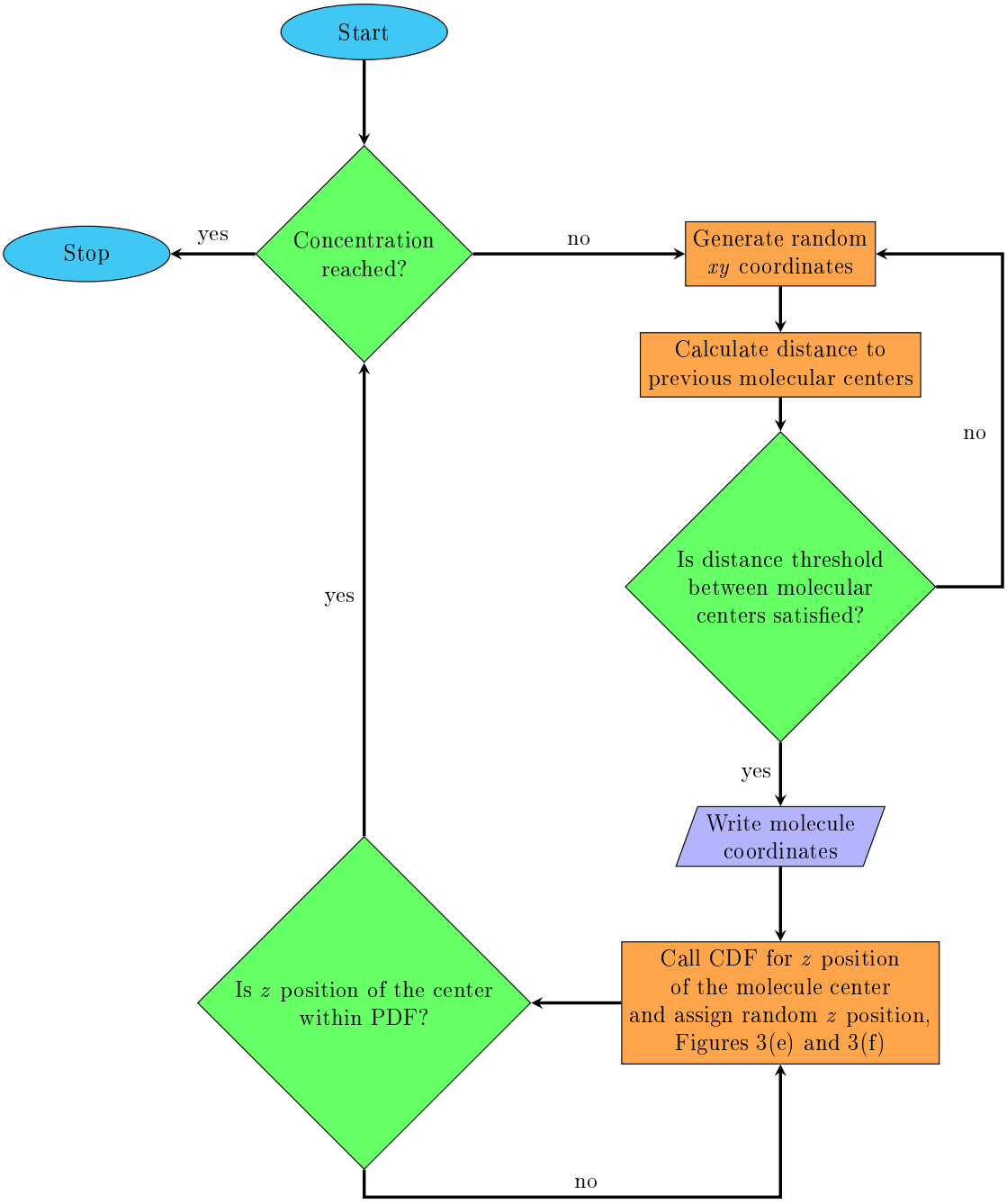

Figure 7: Algorithm for generating the coordinates of the molecule centers.

Once all the coordinates of the molecular centers are determined, four arm groups must be assigned to each molecular center. The algorithm for generating the length and orientation angles of the four long hydrocarbon chains on each TA molecule, referred as "arms", is depicted in Figure 8. For each molecule center we generate four arms where in the first step of the algorithm, four lengths are generated in accordance with the PDF in Figure 3(a) of the arm vector lengths. After that, the vertical orientation angle of each of the 4 the molecule arms relative to the interface has been generated using the PDF in Figure 3(b). Then the z-position of each COO^- group for the respective arm is calculated by:

$$Z^{n,m}_{COO^-} = Z^n_{cn} + V^{n,m}_L \sin\Theta^{n,m} \tag{2}$$

$Z^{n,m}_{COO^-}$ is the z-position of the COO^- group of the mth arm of the nth TA molecule, Z^n_{cn} is the z-position of the molecular center, $V^{n,m}_L$ is the arm vector length, $\Theta^{n,m}$ is the vertical orientation angle of the arm, n and m are the indexes for molecule center and COO^- group, respectively. Afterwards, the generated z-position is checked to determine if it is within the PDF obtain from the MD simulation shown in Figures 3(e) and 3(f) for ARN and BP10, respectively. Once all vertical orientation angles are determined a horizontal orientation angle of the molecular arm is generated according to Figure 3(c). Then the arm xy-position is calculated by:

$$X^{n,m}_{COO^-} = X^n_{cn} + V^{n,m}_L \cos\gamma^{n,m} \tag{3}$$

$$Y^{n,m}_{COO^-} = Y^n_{cn} + V^{n,m}_L \sin\gamma^{n,m} \tag{4}$$

$X^{n,m}_{COO^-}$ and $Y^{n,m}_{COO^-}$ are the respective xy-positions of the COO^- group, X^n_{cn} and Y^n_{cn} are the respective xy-position of the molecule center and $\gamma^{n,m}$ is the horizontal orientation angle of the arms. In the next step, the distances between the intra-molecular carboxylate groups as well as the distance of the carboxylate group with the molecular centers are checked, if

they overlap or fall into the acceptable region of the PDF for the case of the intra-molecular $COO^- - COO^-$ distance in Figure 3(d). If the conditions are satisfied the coordinates are saved and a new cycle begins, otherwise 4 new arms are generated until the required conditions are met. At this point an interface map is generated in terms of knowing all the x,y,z coordinates of the molecular centers, and their 4 corresponding COO^- groups and now we have to evaluate how many TA molecules are cross-linked by evaluating the probability of reaction based on the relative distances between the carboxylate groups.

In order to calculate the fractional conversion of TA to calcium-naphthenate precipitates, we have evaluated how many possible cross-linked sites exist. This has been done by calculating the distances between the inter-molecular carboxylate groups and evaluating the probability to place a calcium ion between them according to Figure 4. We have used a previously obtained[13] PDF for checking the probability for reaction of two carboxylate groups with one calcium ion. The probability of reaction is constructed to represent the probability of two carboxylate groups to be associated to one calcium ion as a function of the separation distance between them. This probability has been scaled so the highest value is 1. Then we generate random numbers and check if this number is within the probability. If the random number is smaller then the PDF of reaction, the site is marked as cross-linked and if it is larger there is no cross-linking possibility. The fractional conversion $f_p(\Gamma_{TA})$ of calcium naphthenate precipitate is defined as the fraction of tetra carboxylic acid molecules on the interface that are cross-linked by an ionic bond formed by calcium and two carboxylate groups that belong to different tetra acid molecules. The fractional conversion is calculated by:

$$f_p(\Gamma_{TA}) = \frac{\langle N_{cl}(\Gamma_{TA})\rangle}{\Gamma_{max}} \tag{5}$$

$\langle N_{cl}(\Gamma_{TA})\rangle$ is the average number of cross-linked sites for a given Γ_{TA} and Γ_{max} is the maximum interfacial concentration, which was given above and equals Γ_{max}=0.1387 molecules/nm^2. $f_p(\Gamma_{TA})$ is scaled so the highest value equals 1.

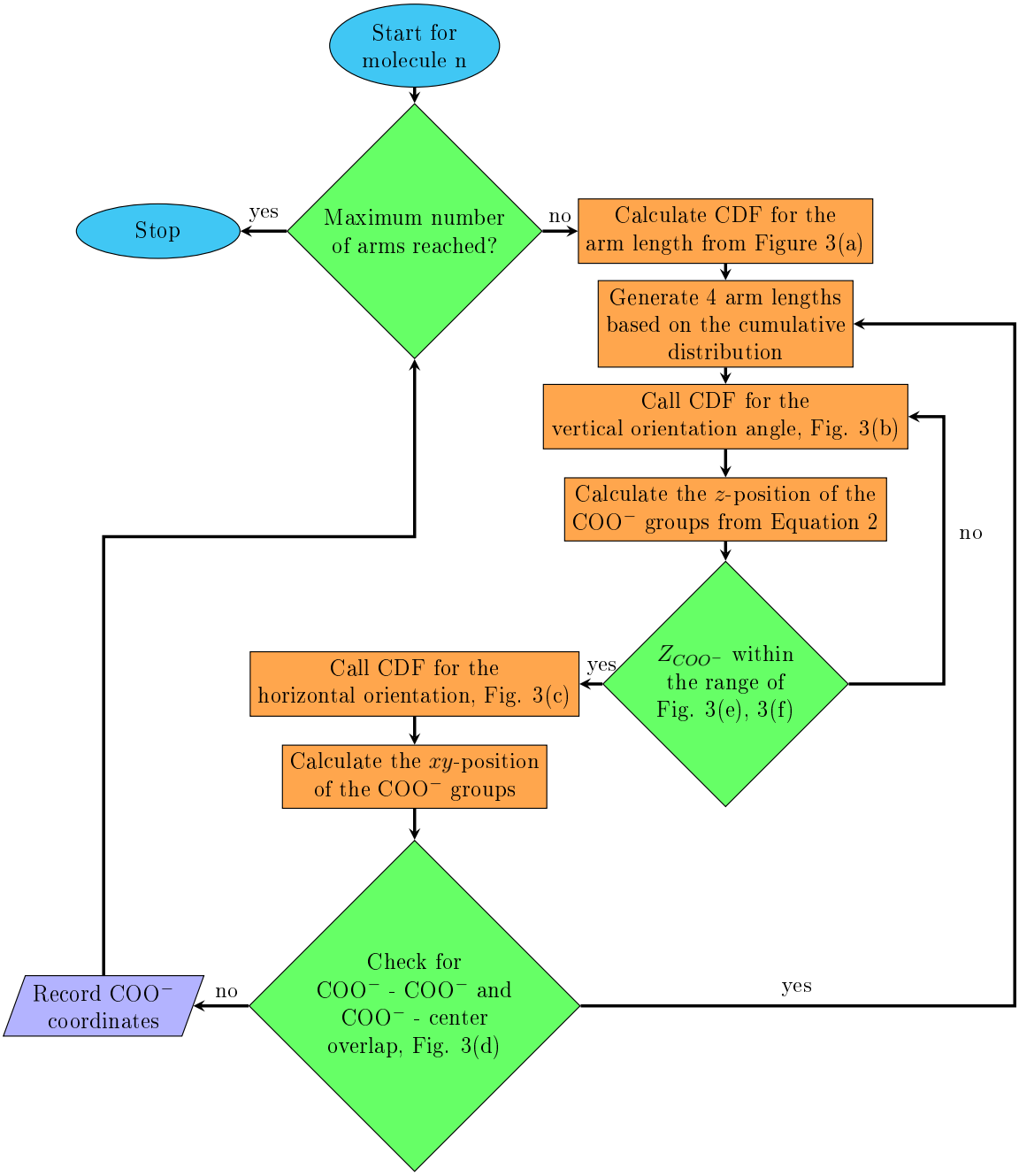

Figure 8: Algorithm for generating the coordinates of the COO^- groups at the terminus of the TA arms.

Results: Coarse-grain Interface Density Maps

In this section the coarse-grain representation ("interface map") of the interface region and the derived fractional conversion of tetra-acids to calcium-naphthenate precipitates is discussed. In the previous section it has been discussed how the interface maps have been built from MD simulation derived probabilities explicitly accounting for the solvents (oil-water interface region) and the calcium ions. Therefore, the interface maps build in a Monte Carlo like approach implicitly include the solvent and the calcium ions effects.

In Figure 9 an example of an interface map created for the ARN molecule is presented for an interfacial concentration of 0.0687 molecules/nm^2 as an example. The molecule centers are depicted in blue and the carboxylate groups in red. In order to analyse the sensitivity of the behavior with respect to the number of interface maps we have generated 50, 100 and 500 interface maps for every concentration and have calculated the fractional conversion for ARN and BP10 based on their average. The results are presented in Figure 10(a) for ARN and Figure 10(b) for BP10. First, it can be noted that the results for ARN and BP10 are very similar to each other, since BP10 has been designed to have similar interfacial properties as ARN. A second observation is that averaging over 50 maps gives fluctuation in $f_p(\Gamma_{TA})$, while generating at least 100 maps provide smoother prediction of $f_p(\Gamma_{TA})$. The fractional conversion appears to increase from 0 to 1 non linearly, but not sigmoidally as assumed by Kovalchuk et al.[12] At 50% surface concentration about 24% of the tetra-acid molecules are converted and the conversion rises to 50% for 70% of surface concentration.

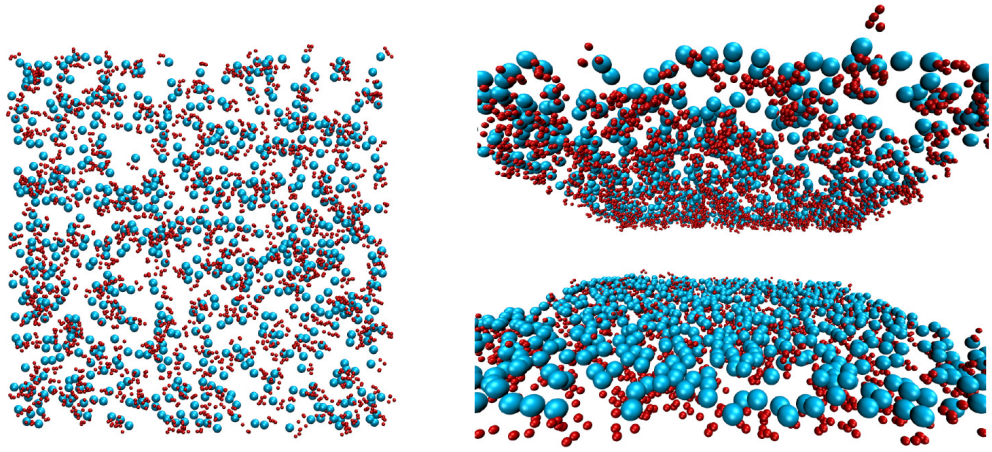

Figure 9: Generated interface density map of ARN with Γ_{TA}=0.0687 mol/nm^2. The molecular centers are depicted in blue and the carboxylate groups in red.

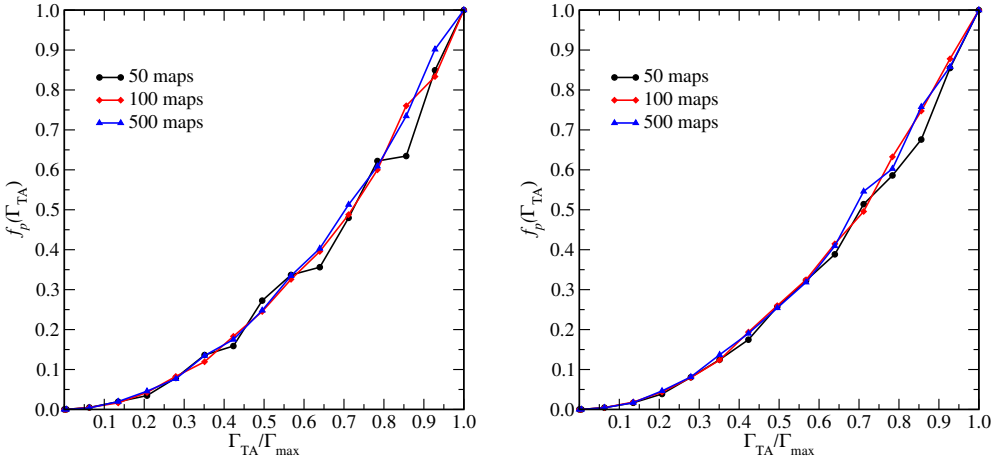

(a) Fractional conversion of ARN

(b) Fractional conversion of BP10

Figure 10: Fractional conversion ($f_p(\Gamma_{TA})$) of a) ARN and b) BP10 to calcium-naphthenate precipitates as a function of the interfacial concentration (Γ_{TA}).

In Figure 11 the number of intra- and inter-molecular cross-linked sites as a function of the interfacial concentration for ARN and BP10 and averaged over 500 maps are presented. BP10 overall has more cross-linked sites, both intra- and inter-molecular. The intra-molecular bonding sites are dominating the inter-molecular bonding sites for both TA molecules. The

increase of intra-molecular bonding sites is linear with the increase of Γ_{TA}, while the inter-molecular sites are increasing non-linearly.

The MD simulations sampled numerous geometric configurations of the tetra acid molecules at the oil water interface and indicate that for any carboxylate group, three of the nearest neighbours will most likely be carboxylate groups from the same tetra acid molecule. Figures 3(f) and 4 clearly indicate that carboxylate groups from the same parent molecule are very likely to be within the mutual displacement range where bonds can form with calcium. The results in Figure 11 clearly show that the bonds between carboxylate groups are predominately between carboxylate groups in the same molecule (e.g., not a cross-linked calcium naphthenate precipitate). The linear trend for the intra-molecular bonds in Figure 11 should be expected since the relative displacement between carboxylate groups within the same tetra carboxylic acid molecule is not strongly affected by the interfacial concentration of all tetra acids.[10,11] Increasing the interfacial concentration of tetra acid molecules increases the probability that the set of nearest carboxylate neighbours within the range necessary to form a bond with a given carboxylate will contain an increasing number of carboxylate groups from other tetra acid molecule in addition to the 3 carboxylates attached to its parent molecule. Thus, as one approaches the upper bound of the interfacial concentration domain, the available sites for cross-linking only increase relative to the 3 intramolecular binding sites. Clearly, this would lead to an increased probability to form cross-linked bonds as one approaches the upper bound of the Γ_{TA}/Γ_{max} domain unless there is a bias to form intramolecular bonds. However, Figure 11 indicates that intramolecular bonding is not biased to increase from its linear trend near the upper bound of the Γ_{TA}/Γ_{max} domain. Consequently, based on the results presented here, one should not expect a sigmoidal shape for the functional form of $f_p(\Gamma_{TA})$ as assumed by Kovalchuk et al.[12] because a sigmoidal functionality for $f_p(\Gamma_{TA})$ would imply that the probability to cross-link two different parent TA molecules would have to steadily decrease from the inflection point of the sigmoid to the upper bound of the Γ_{TA}/Γ_{max} domain.

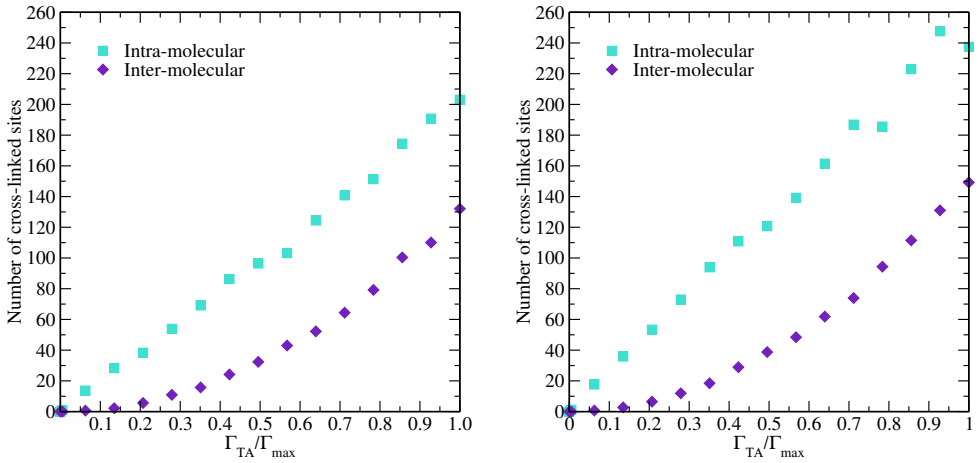

(a) Cross-linked sites of ARN

(b) Cross-linked sites of BP10

Figure 11: Number of cross-linked intra- and inter-molecular sites of a) ARN and b) BP10 as a function of the interfacial concentration (Γ_{TA}).

Conclusions

Molecular dynamics simulations of two different types of tetra-carboxylic acids (TA) at a oil-water interface have been carried out and different geometric probability functions have been obtained in order to describe their structure and orientation in the interfacial region. A coarse-grained Monte Carlo approach based on the MD simulated structural probabilities has been introduced to reconstruct the interfacial density of the TA molecules at the oil-water interface. This approach includes a random positioning of molecular center moieties at the interface in order to represent the specified interfacial concentration. After the molecular centers been placed, the positions of the carboxylate groups are determined according to the MD structural probabilities. More specifically we have used the hydro-carbon chain length probability, z-displacement probability, the normal and tangential angle orientation probabilities of the hydro-carbon chains to calculate the positions of the carboxylate groups. Then we have assessed if the positions of the carboxylate groups match the simulated probabilities for the z-position and the intra-molecular distances between the carboxylate groups. When all the criteria are met a random coarse-grain interface map of all COO^- locations is generated.

The coarse-grain representation of the interface density of the tetra-acid molecules allows one to quickly generate a large amount of these interface maps. That gives the opportunity to explore a significant amount of different possible configurations of the interfacial structure of the tetra-acids. In turn, these maps have been used to determine the fraction of the TA molecules cross-linked to each other through calcium as a function of the interfacial concentration by comparing the COO^- group distances to the probability for binding with calcium. Two molecules are considered cross-linked if the distance between two carboxylate groups from different TA molecules are within a probability of reaction with calcium obtained again from MD and umbrella sampling.[13]

The fractional conversion of TA molecules to calcium-naphthenate precipitates have been calculated for ARN and BP10. The results suggested similar behaviour of the two tetra-

acids as a function of increasing interfacial concentration, where 50% of the TA molecules are cross-linked when the interfacial coverage is around 70%. The fractional conversion increases non linearly with the increase of the surface coverage, but did not demonstrate the sigmoidal shape assumed by Kovalchuk et al.[12] Thus, the $f_p(\Gamma_{TA})$ calculated in this work should be employed into the process model of Kovalchuk[12] to properly characterize the cross-linking mechanism in the multi-scale framework. The analysis of the intra- and inter-molecular cross-linked sites demonstrated that the intra-molecular sites are dominating and are increasing linearly with the increase of the surface concentration. The inter-molecular sites are increasing non-linearly with the increase of the interfacial concentration.

Acknowledgement

The authors acknowledge The Research Council of Norway NFR project 209337 and The Faculty of Natural Science and Technology, Norwegian University of Science and Technology (NTNU) for financial support.

References

1. Sjöblom, J.; Simon, S.; Xu, Z. The chemistry of tetrameric acids in petroleum. *Adv. Colloid Interface Sci.* **2014**, *205*, 319–338.

2. Baugh, T.; Grande, K. V.; Vindstad, J. E.; Wolf, N. O. The Discovery of high Molecular Weight Naphthenic Acids (ARN Acid) Responsible for Calcium Naphthenate Deposits. SPE Seventh International Symposium on Oilfield Scale, Aberdeen, U.K., May 11-12, 2005; SPE 93011; Curran Associates, Inc.: Red Hook, NY, 2006; pp 9-15.

3. Lutnaes, B. F.; Brandal, Ø.; Sjöblom, J.; Krane, J. Archaeal C80 isoprenoid tetraacids responsible for naphthenate deposition in crude oil processing. *Org. Biomol. Chem.* **2006**, *4*, 616–620.

4. Hemmingsen, P. V.; Kim, S.; Pettersen, H. E.; Rodgers, R. P.; Sjöblom, J.; Marshall, A. G. Structural Characterization and Interfacial Behavior of Acidic Compounds Extracted from a North Sea Oil. *Energy Fuels* **2006**, *20*, 1980–1987.

5. Lutnaes, B. F.; Krane, J.; Smith, B. E.; Rowland, S. J. Structure elucidation of C 80 , C 81 and C 82 isoprenoid tetraacids responsible for naphthenate deposition in crude oil production. *Org. Biomol. Chem.* **2007**, *5*, 1873–1877.

6. Nordgård, E. L.; Magnusson, H.; Ann-Mari D. Hanneseth, J. S. Model compounds for C 80 isoprenoid tetraacids Part II. Interfacial reactions, physicochemical properties and comparison with indigenous tetraacids. *Colloids and Surfaces A: Physicochem. Eng. Aspects* **2009**, *340*, 99–108.

7. Nordgård, E.; Sjöblom, J. Model Compounds for Asphaltenes and C 80 Isoprenoid Tetraacids. Part I: Synthesis and Interfacial Activities. *J. Dispersion Sci. Technol.* **2008**, *29*, 1114–1122.

8. Simon, S.; Reisen, C.; Bersås, A.; Sjöblom, J. Reaction Between Tetrameric Acids and Ca2+ in Oil/Water System. *Ind. Eng. Chem. Res.* **2012**, *51*, 5669–5676.

9. Sundman, O.; Simon, S.; Nordgård, E. L.; Sjöblom, J. Study of the Aqueous Chemical Interactions between a Synthetic Tetra-acid and Divalent Cations as a Model for the Formation of Metal Naphthenate Deposits. *Energy Fuels* **2010**, *24*, 6054–6060.

10. Riccardi, E.; Kovalchuk, K.; Mehandzhiyski, A. Y.; Grimes, B. A. Structure and Orientation of Tetracarboxylic Acids at Oil-Water Interfaces. *J. Dispersion Sci. Technol.* **2014**, *35*, 1018–1030.

11. Kovalchuk, K.; Riccardi, E.; Grimes, B. A. Multiscale Modeling of Mass Transfer and Adsorption in Liquid-Liquid Dispersions. 1. Molecular Dynamics Simulations and Interfacial Tension Prediction for a Mixed Monolayer of Mono- and Tetracarboxylic Acids. *Ind. Eng. Chem. Res.* **2014**, *53*, 11691–11703.

12. Kovalchuk, K.; Riccardi, E.; Grimes, B. A. Multiscale Modeling of Mass Transfer and Adsorption in Liquid-Liquid Dispersions. 2. Application to Calcium Naphthenate Precipitation in Oils Containing Mono- and Tetracarboxylic Acids. *Ind. Eng. Chem. Res.* **2014**, *53*, 11704–11719.

13. Mehandzhiyski, A. Y.; Grimes, B. A. Calculation of the Probability for Ionic Association and Dissociation Reactions by Molecular Dynamics and Umbrella sampling. *Submitted for publication* **November 2015**,

14. Jorgensen, W. L.; Maxwell, D. S.; Tirado-Rives, J. Development and Testing of the OPLS All-Atom Force Field on Conformational Energetics and Properties of Organic Liquids. *J. Am. Chem. Soc.* **1996**, *118*, 11225–11236.

15. Abascal, J. L. F.; Vega, C. A General Purpose Model for the Condensed Phases of Water: TIP4P/2005. *Journal of Chemical Physics* **2005**, *123*.

16. Hess, B.; Kutzner, C.; van der Spoel, D.; Lindahl, E. GROMACS 4 Algorithms for Highly Efficient, Load-Balanced, and Scalable Molecular Simulation. *J. Chem. Theory Comput* **2008**, *4*, 435–447.

17. Berendsen, H. J. C.; Postma, J. P. M.; van Gunsteren, W. F.; DiNola, A.; Haak, J. R. Molecular Dynamics with Coupling to an External Bath. *J. Chem. Phys.* **1984**, *81*, 3684–3690.

18. Parrinello, M.; Rahman, A. Polymorphic Transitions in Single Crystals: A New Molecular Dynamics Method. *J. Appl. Phys.* **1981**, *52*, 7182–7190.

19. Bussi, G.; Donadio, D.; Parrinello, M. Canonical Sampling through Velocity Rescaling. *J. Chem. Phys.* **2007**, *126*, 014101–01407.

20. Essmann, U.; Perera, L.; Berkowitz, M. L.; Darden, T.; Lee, H.; Pedersen, L. G. A Smooth Particle Mesh Ewald Method. *J. Chem. Phys.* **1995**, *103*, 8577–8593.